HIGH VELOCITY IMPACT OF DYNEEMA

LAMINATES OF VARYING SIZE

by

Jeffrey Rockwell

A thesis submitted to the Faculty of the University of Delaware in partial fulfillment of the requirements for the degree of Master of Civil Engineering

Summer 2014

HIGH VELOCITY IMPACT OF DYNEEMA

LAMINATES OF VARYING SIZE

by

Jeffrey Rockwell

Approved: ____
John W. Gillespie, Jr., Ph.D.
Professor in charge of thesis on behalf of the Advisory Committee

Approved: ____
Harry W. Shenton III, Ph.D.
Chair of the Department of Civil and Environmental Engineering

Approved: ____
Babatunde A. Ogunnaike, Ph.D.
Dean of the College of Engineering

Approved: ____
James G. Richards, Ph.D.
Vice Provost for Graduate and Professional Education

ACKNOWLEDGMENTS

I would like to thank the Department of Defense, Office of Naval Research for providing the funding for this research. I would also like to thank my advisors Dr. John Gillespie, Jr. and Dr. Shridhar Yarlagadda for their direction, support, and giving me the opportunity to do this work for them. Additional assistance was given by members of the CCM community including Dr. Bazle Haque, Dr. Joseph Deitzel, and Ray McCauley. Lastly, I would like to thank all of my friends and family for their support.

TABLE OF CONTENTS

LIST OF TABLES

LIST OF FIGURES

ABSTRACT

This research focuses on the high velocity impact response of Dyneema HB-26 panels consisting of a unidirectional UHMWPE fiber reinforced polyurethane matrix in a cross-ply laminate. During high velocity impact by a penetrator, significant energy absorption occurs through various deformation mechanisms related to penetration, delamination, and tensile failure of the layers that undergo large transverse deformation and often extends to the panel boundaries. The influence of panel size on ballistic resistance and associated damages studied for a range of areal densities. The test matrix consisted of impacting 1.5 and 2.5 psf laminates with panel dimensions of 24x24 inches, 14x14 inches, 8x8 inches with a hardened steel 30 caliber fragment simulation projectile. The V_{50} or ballistic limit was calculated for each combination of areal density and panel size. Ballistic limit was found to increase approximately 50% with areal density for all panel sizes. Ballistic limit was also found to increase approximately 6-8% as panel size decreased from 24 x 24 inches to 8 x 8 inch for both areal densities.

Detailed damage analysis included measuring the panel transverse back-surface deflection during impact, C-scan analysis to determine size and shape of delamination patterns, cross sectioning of the panels to show through thickness damage mechanisms, and SEM imaging to show fiber-matrix level failure modes. Characteristic damage consisted of a center hole at the point of impact surrounded by circular pattern of delamination with four localized and orthogonal strip delamination oriented in the fiber direction extending outward. The back surface deflection formed

a cone with a characteristic angle. The damage analysis of the various panel sizes showed that the strip delaminations in the primary fiber direction reached the free edges in the smallest panels. In these panels, material undergoes localized deformation through edge pull in which dissipated additional energy through frictional sliding between layers. This also resulted in larger back surface deflections during impact that slowed the projectile over a longer time and distance and prevented the projectile from fully perforating the material. This effect was most prevalent in the smallest and thickest panels (i.e. 8x8inch/ 2.5 psf panels).

Chapter 1

INTRODUCTION

1.1 Motivation for Research

Composite materials have been widely used as a means to stop high velocity projectiles. Some of the major composite materials that are used in impact loading scenarios are aramid (Kevlar), glass, and ultra-high molecular weight polyethylene (UHMWPE) fibers. These types of fibers are used because of their high specific tensile strength and toughness. Aramid and UHMWPE composites have been used more in high performance applications because of their low weight compared to glass. (N.K. Naik, 2005)

Table 1 shows a number of fibers that are commonly used in many different applications. Depending on the required stiffness, density, elongation to failure, and cost each of these fibers could be ideal for a specific application. Materials that perform well during high velocity impact events generally have a high specific tensile strength and elongation to failure which is why Dyneema, Spectra, Aramid 29, and S-Glass are commonly used. In most applications additional weight savings is beneficial so materials with high specific strength and stiffness are desired. Dyneema's low density yet similar tensile strength and stiffness make it a valuable material when reducing weight yet keeping the same performance as other materials.

Table 1 General properties of major composite fibers

	Dyneema SK60	Spectra 900	Aramid 29	Aramid 49	Carbon HS	E-Glass
Density (g/cm3)	0.97	0.97	1.44	1.45	1.78	2.55
Tensile Strength (GPa)	2.7	2.5	2.7	2.7	3.4	2.0
Tenacity (g/den)	30	-	22	22	22	9
Modulus (GPa)	87	-	58	120	240	73
Specific Modulus (g/den)	1000	-	450	940	1500	310
Elongation at break (%)	3.5	3.0	3.7	1.9	1.4	2.0

(Dingenen, 1989) (Russell, 2013)

During impact the projectile's momentum and kinetic energy are transferred to the composite panel. The projectile will typically penetrate through the panel thickness until arrest or complete perforation. During short time scales, complex wave propagation through the thickness and in the plane of the panel is generated by the impact event. At longer time scales the panel will undergo large dynamic deformation. The net result is extensive localized damage that varies through the thickness and laterally where delamination between layers of the composite is created. In materials that have a weak interlaminar bond strength or low fiber stiffness, delamination may propagate to panel boundaries.

It is well known that the areal density, or weight of material over a unit area, plays an important role in the penetration resistance. Generally the heavier and thicker the material is, the more energy it can dissipate. The influence of the in-plane dimensions of a panel on penetration resistance, extent of damage, and the magnitude of dynamic deflection are not as well understood. Two common high velocity impact testing standards NIJ 0108.01 and UL 752 clearly define how materials should be impacted with different projectiles of varying velocity, mass, projectile material, and shape. It is not addressed how the size of the in-plane dimensions of the impacted material may change the results. UL 752 calls out that every sample must be 12” x 12” and NIJ 0108.01 calls out that the sample must be at least 12” x 12”. The only regulations are that the material is supported and that if results indicate that if a larger test sample would result in penetration than the larger sample should be used. (NIJ 0108.01, 1985) (UL 752, 2006)

It is assumed by these standards that a panel size does not have an effect on the ballistic resistance of a material. Depending on the material, this may cause major differences in the impact performance and damage propagation. For example, when impacted with a 30 caliber FSP at its ballistic limit a structural composite such as S-glass/epoxy may have localized damage from a ballistic impact that arrests within a 4 inch diameter around the impact location. Conversely a panel fabricated with UHMWPE can have damage that propagates 12inches across, as shown in Figure 1-1. If the damage size extends to the panel boundaries there may be an effect of panel size on ballistic resistance.

(a) 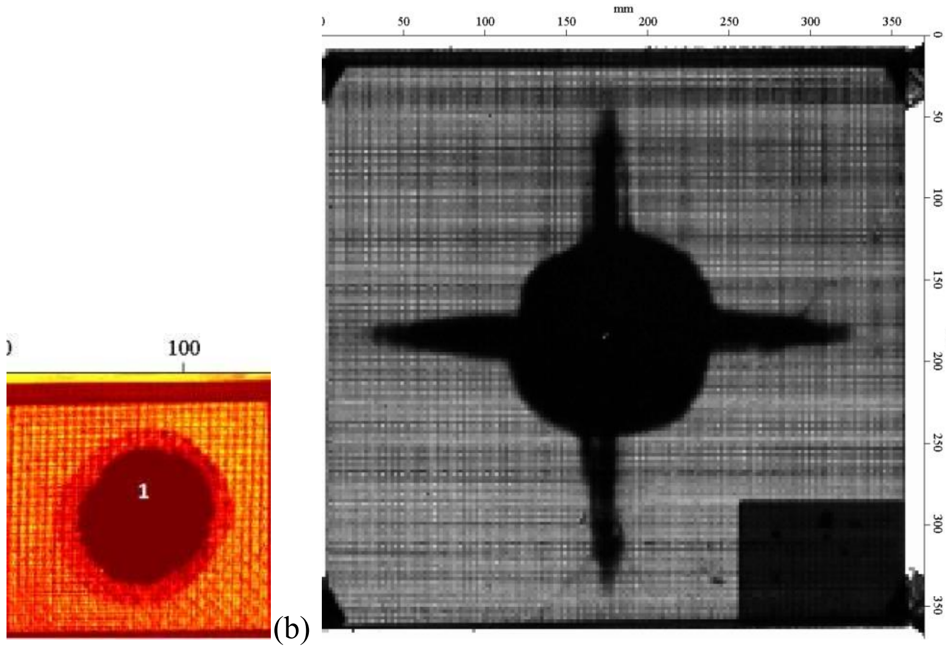 (b)

Figure 1-1 Example of internal damage propagation in a thin, 0.3in, (a) 6x6inch Sglass/epoxy and (b) 14x14inch UHMWPE laminate both impacted with a 30 caliber FSP

This research specifically looks at UHMWPE laminates (Dyneema HB-26) during high velocity impacts of 30 caliber FSPs to see if damage propagation and ballistic resistance are affected by panel size. Dyneema laminates utilize fibers with high tensile strength combined with a compliant matrix to allow for large delaminations and deflections to dissipate the energy from the projectile. Given these attributes, Dyneema is a material that could potentially susceptible to the effects of panel size on impact response.

1.2 Scope of Research

The initial phase of this research was to understand how composites react under high velocity impact events. During these events different mechanisms occur and it was crucial to understand the differences before conducting actual testing. Additionally it is useful to understand how the Dyneema material differs from other materials and how this could affect testing and damage analysis.

The experimental part of this work breaks down into two different categories; ballistic testing and damage analysis. Ballistic testing consisted of panels of two different thicknesses (i.e. areal density) and three different panel sizes. The different thicknesses were to represent a thin (1.5 psf) and thick (2.5 psf) laminate and the different panel sizes allowed for different amounts of interlaminar delamination to occur. The method for analyzing ballistic performance was based on the Military Standard 662F that considers the probability of penetration. Curve fitting of the velocity data used both the Lambert and Gama/Gillespie penetration equations to determine the ballistic limit of the panel.

The damage analysis portion of the research includes both nondestructive evaluation and destructive evaluation included C-scanning, cross sectioning, optical microscopy, and scanning electron microscope imaging. This was done to determine the extent of the damage that occurred from testing and what modes of failure took place during the impact. Through the testing and damage analysis there were noticeable differences that could be seen and conclusions were made based on this information.

1.3 Thesis Organization

Chapter 2 lays out important background information about the mechanics behind an impact event and the specific mechanisms that are affected by the size of the Dyneema panels. Details are given for all of the different calculation methods that are used to categorize the ballistic resistance of the materials in later chapters. The methods for observing and quantifying the damage sustained to the panels during impact are also covered in this chapter.

Chapter 3 shows information about the Dyneema used in this research and the details on the projectile that it was impacted with. This chapter also defines the naming convention for the test data used throughout this paper.

Chapters 4 covers the procedures used for all of the processes that were part of this research. This includes all of the methods for measuring ballistic resistance and the methods for analyzing damage. These included C-scanning, cross sectioning, measuring edge pull-in, measuring witness plate deformation, microscopy, and SEM imaging.

Chapter 5 includes all of the results found from all of the testing that was explained in Chapter 4. These include both the physical testing and the damage analysis performed. Each section draws preliminary conclusions on what was found and how it relates to earlier work.

Chapter 6 gives the resulting conclusions that were made when all aspects of testing and analysis were completed. This section also gives thoughts on how to use and analyze this material for future researchers based on what was found in this study. Ideas for future work are also covered in this chapter.

Chapter 2

BACKGROUND INFORMATION

2.1 High Speed Penetration Mechanics in Composites

There are many different types of loading conditions that exist in the field of structural analysis of materials. The common types include point loads, distributed loads, and dynamic loads. High speed impact loads count as dynamic loads but are unique because of the high rate of loading. During a ballistic impact event the momentum from the projectile is transferred into the target material while energy is dissipated through multiple mechanisms. These mechanisms include deformation of the projectile, strain energy in the laminate, and kinetic energy of the laminate. The remaining energy is dissipated through damage mechanisms that occur during the impact event. Some examples of these damage mechanisms are matrix damage, delamination, fiber-shear, fiber-crush, and tensile fiber fracture. If the total momentum and kinetic energy from the projectile is transferred into the panel and the energy is converted into the kinetic and strain energy of the panel or absorbed through damage mechanisms then the projectile will be stopped. If the projectile has more energy than can be captured through these mechanisms then the projectile will completely penetrate the material and have a residual velocity and kinetic energy.

As the projectile moves through a structural composite material there are a number of phases that occur. A paper by Gama and Gillespie (B. A. Gama, 2008) separates these phases as Phase I – Impact-contact and stress wave propagation, Phase II – Hydrostatic compression and local punch shear, Phase III – Shear plug formation under compress-shear, Phase IV - Large deformation under tension-shear, and Phase V – End of penetration and structural vibration. These phases can be seen in Figure 2-1. During these phases the projectile moves through the material which fails through the different failure mechanisms mentioned above.

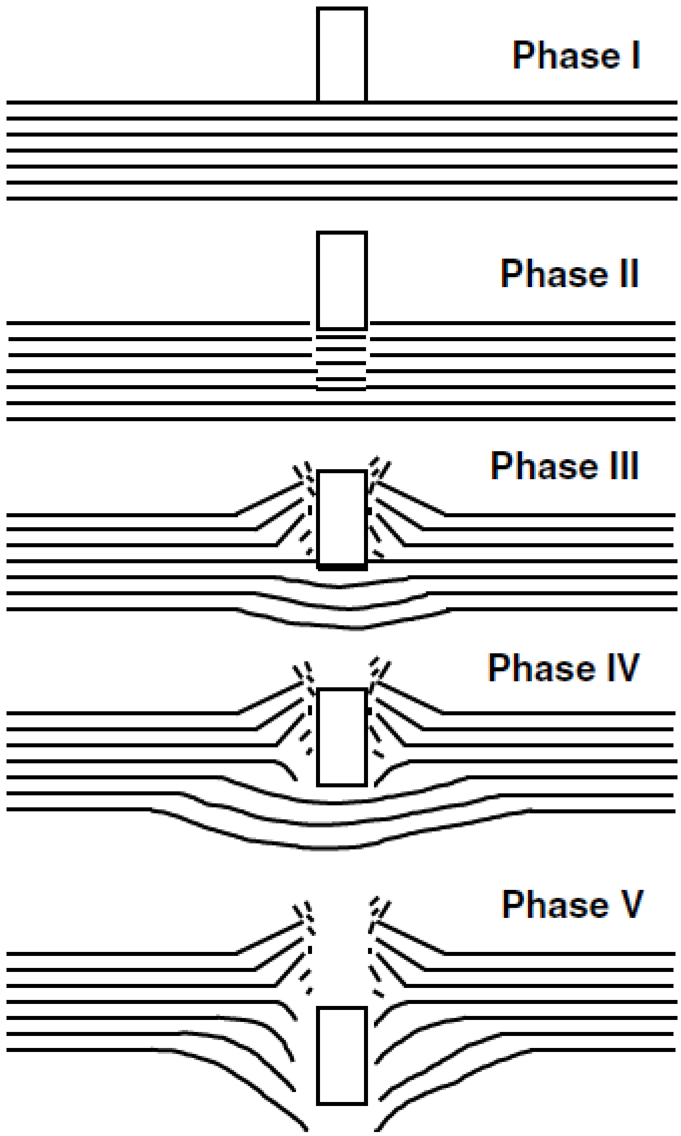

Figure 2-1 Phases of ballistic penetration (B. A. Gama, 2008)

Early modes of failure starting on the impact side of the panel consist of fiber-crush and fiber-shear. Once the stress wave from the projectile reaches the backside of the material deflection can occur in the backface of the material, starting in Phase III. While the backface is deforming elastic energy from the projectile is reacted as tension in the elongated fibers. As the projectile continues to move damage will occur not as just fiber-shear but as a combination of fiber-shear and tensile fracture in fiber yarns under the projectile and the area of affected fibers becomes larger. This results in a trapezoidal damage cone in thin laminates and an hourglass shape in thick composites. As the backface deforms under the decelerating force of the projectile, laminas separate and interlaminar delamination propagate laterally. Once the projectile reaches the last few laminas near the back surface, the fibers fail in tension and the projectile will exit with a residual velocity. Then the fibers will relax and vibration of the material will occur until the energy is stored elastic energy is dissipated. Some permanent back face deflection will remain from inelastic deformation. This sequence is nearly identical incomplete penetrations with the only difference being that the some layers on the backside of the panel have not been perforated. If the projectile velocity is high enough the different Phases may occur to different depths through the panel thickness (B. A. Gama, 2008)

2.1.1 Structural vs. Dry Fabric Composites

The above mechanisms are those that occur in structural composite armor. Dry fabric systems do not have a resin and are flexible. Impact loading of a textile fabric by an FSP typically loads the yarns under the projectile in tension. Load transfer to adjacent yarns occurs through fiber-fiber contact and friction. Fiber failure is typically dominated by tension loading.

The behavior of thick section Dyneema laminates consisting of continuous UHMPE fibers impregnated with a low modulus polyurethane laminated in a cross-ply configuration have a combination of deformation modes characteristic of both the structural composite and the flexible composite.

The main distinction that dry fibers have is that stress waves travel faster and transfer more load in the direction of the yarns or fibers. When a fabric deflects from an impact, tension is distributed along the yarns that are directly under the projectile and stress follows along the yarn's length away from the impact site. These yarns are referred to as primary yarns because they are loaded directly by the projectile. The surrounding yarns are referred to as secondary yarns because they are loaded during an impact but only from stress waves that have been transferred from the primary yarns through friction. Regions in the material are referred to as region 1 and 2 depending on if they are directly under the projectile or not, as in Figure 2-2. As will be shown in later chapters, one can also define primary and secondary yarns in the case of Dyneema laminates.

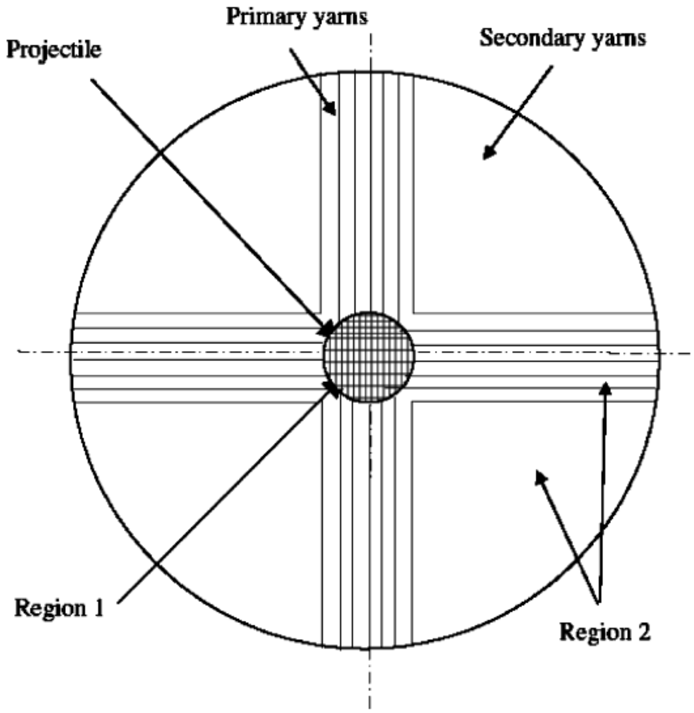

Figure 2-2 Front view of a target fabric material under impact loading (N.K. Naik, 2005)

2.1.2 Dyneema Laminate Structure

Dyneema HB-26 is interesting because it both has attributes that resemble dry fabrics and structural composites. This creates a set of damage mechanisms that take from both types of materials. To understand how Dyneema reacts under high velocity impact loads the structure of the composite laminates much be understood first.

The Dyneema HB-26 material is shipped by DSM as sheets of SK76 Dyneema fibers bonded by a polyurethane resin with a fiber volume fraction of 87%. Each sheet is composed of 2 layers of 0° fibers and 2 layers of 90° fibers alternating in a 0/90/0/90° unsymmetrical configuration. The shipped sheet of HB-26 has a thickness of approximately 240 μm. Thicker laminates can be made by stacking multiple sheets on top of each other. While stacking, the sheets are not rotated to make sure that the 0/90° configuration continues throughout the laminate. The resulting laminates are also not symmetric about the mid-plane. (Tao Xu, 2007) (Russell, 2013)

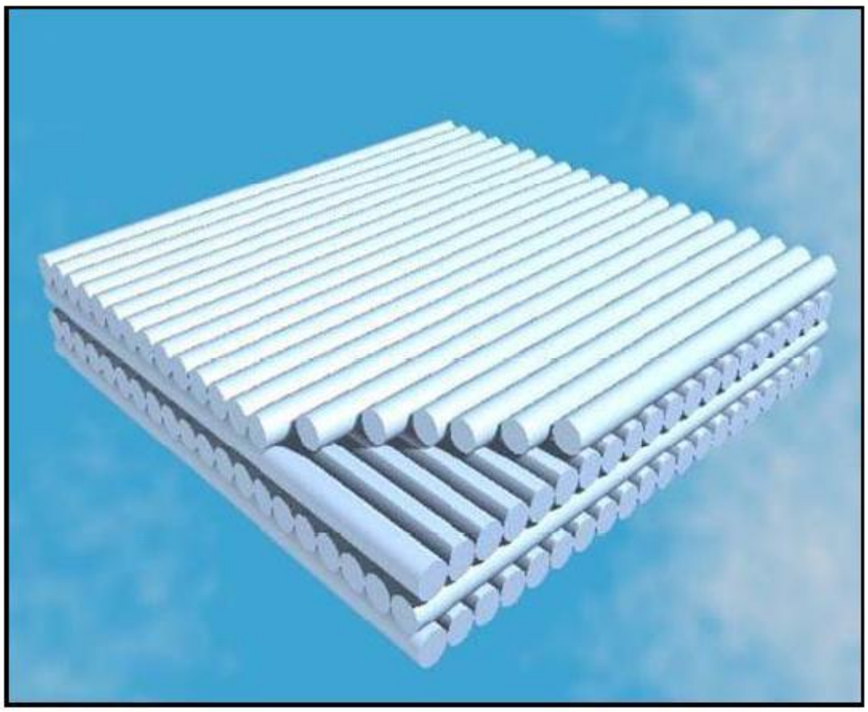

Figure 2-3 Diagram of 0/90/0/90° lamina stacking sequence (Marissen, 2011)

Many times composites use woven bundles of fibers, or yarns, instead of unidirectional fiber layups. Dyneema HB-26 is non-woven to gain performance during high velocity impacts. During an impact the stress wave will propagate outward from the impact site. Woven fabrics have more give due to the undulations in the fibers and will have to stretch out before the stiffness of the material can be fully utilized. Unidirectional fibers are already aligned so they are immediately available to transfer loads at the maximum rate. (V. B. C. Tan, 2005)

Dyneema laminates gain most of their energy dissipating ability from the fiber structure. The polyurethane matrix is there to loosely bind the fibers together. Because of the low stiffness of the matrix and low compression and shear properties of the fiber, there is little structural rigidity except in inplane tension that is dominated by the fiber properties. Typically resins are useful to help the composite resist compressive loads. Instead the low modulus and high strain to failure available from the matrix allows for deflections and delaminations to occur in the material to fully utilize the strength of the Dyneema fibers. For polyurethane resins the modulus is approximately 0.586GPa and the strain to failure is 32%. The polyurethane resin also is very effective in absorbing significant amounts of energy during delamination between layers. (Roman, 2005)

2.1.3 Mechanisms in Dyneema Laminates Affected by Panel Size

The energy dissipating mechanisms that occur in Dyneema are a combination of both rigid structural and dry fabric armor due to its structure. As will be shown, localized damage at the point of impact and penetration is seen analogous to the structural laminate (see Phase I-V in Figure 2-1). Dyneema also undergoes extensive delamination around the point of impact but can be typically much larger in diameter than the structural composite. Large cone of permanently deformed layers are seen on the back surface with base diameters that can approach panel sizes. Unique to Dyneema is the presence of the primary yarns that delaminate and are pulled into the impact site which is analogous to the deformation mechanism for dry fabrics shown in Figure 2-2. These delaminations associated with the primary yarns can extend very large distances and reach panel boundaries. Consequently, the choice of panel size and thickness may affect the deformation and damage modes and associated ballistic limit. These types of interactions are discussed below in more detail.

2.1.3.1 Interlaminar Delamination

During the impact as the stress wave travels through Dyneema there are different stresses induced in the fibers and between laminas. This difference in stresses can cause the matrix to debond from the fiber, stretch, and break which delaminates the laminas from each other. The energy dissipated in the stretching and then breaking the matrix adds to the overall energy dissipated by the panel.

Interlaminar delamination can occur in two different modes. The laminas can be separated either by interlaminar tension, interlaminar shear, or a mixed-mode loading that acts to separate the layers. These interlaminar failures are described as mode I and mode II delaminations respectively. Mode I delamination can occur during Phase I where the compression wave reflects off the back surface as a tension wave or during Phase III-IV where the projectile is arresting and peeling the layers from the top portion of the panel. As this delamination grows the crack growth becomes mixed mode with increasing level of mode II. During Phase II-III, the penetration phase has a significant amount of mode II shear loading near the impact site. The delamination of the primary yarns over large distances is Mode II dominated as well.

On large panels the primary yarn delaminations that extend the farthest can arrest before reaching the free edge. If a panel is small enough delamination not only the primary yarns but also the delamination's that form around the impact site can propagate to the free edge. These differing types of delamination are discussed later in depth in section 4.2.

2.1.3.2 Friction

Friction is a major method of energy dissipation mostly as the projectile slides against broken fibers as it moves through the material. This type of friction is not dependent on the panel size because it is only concerned with the projectile and the fibers directly next to it. Additional frictional energy occurs as laminas slide between each other after they have delaminated. This is especially the case in Dyneema because of the weak bonding between laminas creates many sliding planes. The high elongation to failure of the polyurethane matrix dissipates a large amount of energy prior to failure. If more laminas are delaminated the potential energy dissipation could be noticeable. (N.K. Naik, 2005)

2.1.3.3 Elastic Deformation of Secondary Fibers

In addition to the energy dissipated by the primary fibers, the deformation in the secondary fibers can also store energy. Stress is transferred from the primary fibers to the secondary fibers through the matrix and friction between the fibers. If the panel size is reduced there will be less secondary fibers that can be activated which could affect the energy dissipation of the panel.

2.1.3.4 Dynamic Cone Formation

Also referred to as “bulge formation of the backface”, dynamic cone formation occurs on the backface of the material (as seen in Figure 2-4). As the decelerating force from the projectile acts on the delaminated plies in the backface, these plies will stretch in tension and move away from the rest of the material. This movement puts the material near the back face in tension until either the projectile is stopped or the projectile breaks through the fibers and exits the material. (N.K. Naik, 2005)

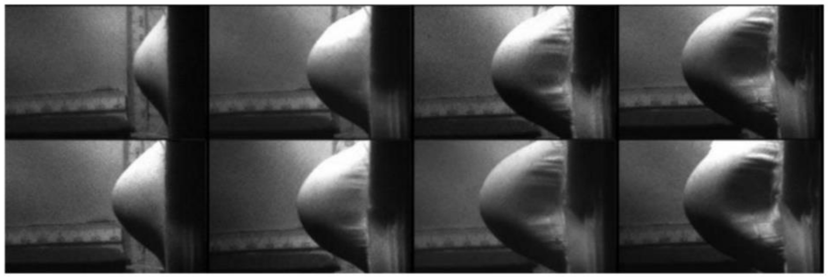

Figure 2-4 Dynamic Deflection/Bulge during Ballistic Impact on Soft Laminate (Kevin M. Ayotte, 2011)

The compliant polyurethane matrix in HB-26 allows for large deformation through fiber stretching, delamination and sliding of the layers resulting in formation of a dynamic cone with higher amplitude and base diameter on the backface (compared to most structural composites). Allowing more material to move and moving it farther away from its original position increases the amount of energy that can be transferred from the projectile to the material. As the dynamic cone moves farther away from its origin it will be gaining elastic energy being stored in the fibers in addition to kinetic energy. Once the dynamic cone and projectile reach a maximum deflection, the material will then retract back due to the stored elastic energy. This vibration period will continue until all of the energy is dissipated into the materials and supports.

By creating a large dynamic cone with a large maximum deflection the projectile can be slowed over a longer period of time allowing more stress to be transferred to the material farther away from the impact site. Changing the panel size of the impacted material may change the ballistic limit because less material could be available to take the transferred energy and higher deflections could occur due to more freedom of material movement. Clearly the panel size may have an important impact of the conformation and overall size. (B. A. Gama, 2008)

2.1.3.5 Tensile Fracture of Primary Fibers

When a projectile impacts a Dyneema panel the primary damage mechanisms changes from fiber-shear to tension-shear as the projectile penetrates the panel. This occurs later in thick Dyneema panels when the projectile is getting closer to the backside of the material. The fibers that are activated the most in tension are the primary fibers because they are directly under the projectile. This force is transferred along the length of the fibers until the projectile has overcome the tensile strength of the fibers, the energy of the projectile has been dissipated, or the edge of the panel is reached.

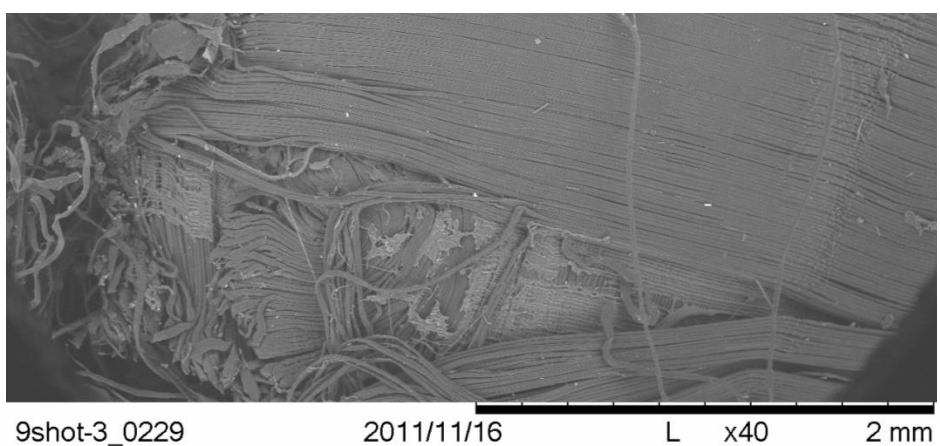

Figure 2-5 SEM imaging of Dyneema fibers breaking from tensile failure during impact event

If a test panel is small enough the stress wave that reaches the edge of the panel will have enough force to debond the fibers from the matrix in mode II shear. This results in a pull-in of the fibers along the free edge. The size of the panel may affect how the primary fibers react under tension during Phase IV loading. (Kevin M. Ayotte, 2011)

2.2 Ballistic V_{50} Calculation Methods

Ballistic testing is the most exact way to quantify the ballistic performance of a material. This is simply firing a projectile at a target sample while measuring the initial velocity and residual velocity of the projectile before and after impacting the sample. By changing the velocity of the projectile and observing partial or complete penetrations of the sample a ballistic limit of the sample can be determined for that specific sample and projectile.

To gauge how the Dyneema samples of different sizes react to impact events a method of analysis needed to be chosen. It is common practice in the industry to categorize materials by their ballistic limit or V_{50}. The V_{50} is defined as the velocity where there is a 50% chance that a projectile will be captured during impact and a 50% chance that the projectile would fully exit the material. Similar velocity terminology includes V_0 and V_{100} where there is a 0% or 100% chance of penetration respectively. Because the V_{50} of a material is probabilistic it should be reminded that the resulting calculated V_{50} may have some variability.

In a ballistic event the initial and residual velocities can be recorded. The initial velocity, V_I, is the velocity that the projectile is traveling right before impacting the material and the residual velocity, V_R, is the final velocity after the projectile exits the material. If the projectile does not exit the material then the V_R is 0. Once tested, the combination of V_I and V_R data from each sample impact can be used by different methods to calculate an estimated V_{50}.

2.2.1 Calculation of V_{50}

The V_{50} for each test was calculated through three different methods. The first was the MIL-STD-662F, the Department of Defense Test Methods Standard V_{50} Ballistic Test for Armor. The second was a technique of fitting different ballistic equations to the initial and residual velocity data. The third was a technique called probability of penetration. This was mainly done to show the range where the results from the other two techniques should fall. These three methods were used to calculate V_{50}s and then these were compared with each other.

2.2.1.1 Military 662F Standard

The 662F method does have regulations on the chosen initial velocities of the projectiles. These were not done in exactly the same way because the primary method for V_{50} calculation was from fitting the V_I/V_R curves. For this reason only the method of calculating the V_{50} was used. The 662F method is to calculate the arithmetic mean of an equal number of the highest partial and lowest complete impacts. An allowable velocity span is defined by the contracting officer. This was taken as 6 impacts; the 3 highest partial and 3 lowest complete impacts. (DOD-USA, 1987)

2.2.1.2 V_I/V_R curve fitting

The other method used to calculate the V_{50}s was from fitting curves to the V_I/V_R data using different ballistic equations. Two equations were used for fitting purposes because in some cases one would create a better fit than the other.

The first equation used for curve fitting was the Lambert Equation. This equation was developed by the USA Ballistic Research Laboratory at Aberdeen Proving Ground.

Equation 1 Lambert Equation (Misey, 1978)

$$V_R = \beta * (V_I{}^p - V_{BL}{}^p)^{(1/p)}$$

For some cases the Lambert Equation did not result in curves that fit the data or would return an error. This generally happened in cases when there was a large deviation between data points. For these cases another equation was used. This equation was developed for determining the ballistic limit of thick section composite materials, similarly to the Lambert equation. This equation assumes that the projectile and the impacted material have the same velocity during impact and moves at a velocity of $V^{max}{}_{A,R}$. β and ς are fitting parameters.

Equation 2 Gama & Gillespie penetration equation (Kevin M. Ayotte, 2011)

$$V_{P,R} = \left[\left(V_{A,R}^{\max} \right)^2 + \beta^2 \left(\varsigma V_I^2 - V_{BL}^2 \right) \right]^{\frac{1}{2}}$$

The resulting plot of the velocity data and the fitted curve result gives a theoretical V_{50} for a specific material thickness and panel size. Figure 2-4 gives the resulting curves calculated from the Lambert and Gama & Gillespie Equations. The location at where the curves cross the V_I axis is the resulting calculated V_{50} for each equation. In cases where both equations resulted in well fit curves both curves were very similar, see Figure 2-6. In this case the Lambert equation was used as the default.

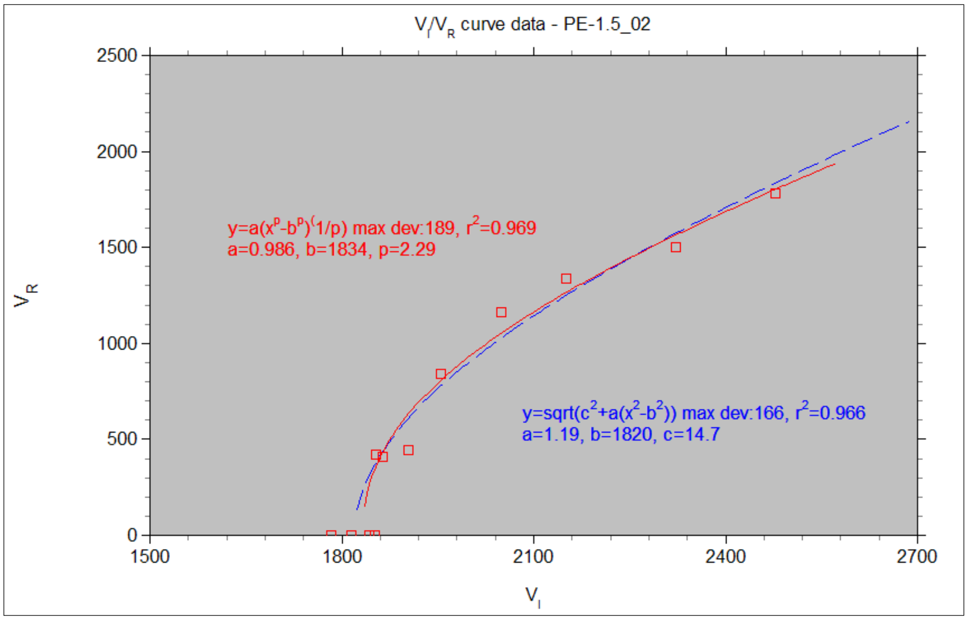

Figure 2-6 Example plot of the different curve techniques to calcualte a V_{50} (1.5 psf 14x14inch Dyneema sample, red curve is Lambert equation, blue curve Gama/Gillespie equation)

2.2.1.3 Probability of Penetration

The third method to confirm the data found from the first two cases was looking at the probability of penetration. This technique involves matching the highest partial with the lowest complete, then the next highest partial with the next highest complete and so on. A complete penetration is represented by a 1 while a partial penetration is represented by a 0. A line is then connected between these two points. The data points that can be used for this are only the ones near the V_{50} so only three sets of data points were used per data set. Using velocities too far away from the V_{50} would not give with accurate results. In a perfect scenario the three lines would all cross each other along the 0.5 mark. The corresponding initial velocity at this point would be the exact V_{50} from the test. The V_{50} calculated from the 662F standard and V_I/V_R curve fitting method were also plotted to see if they are in the range of the expected V_{50}. Figure 2-7 is an example result for the Probability of Penetration method.

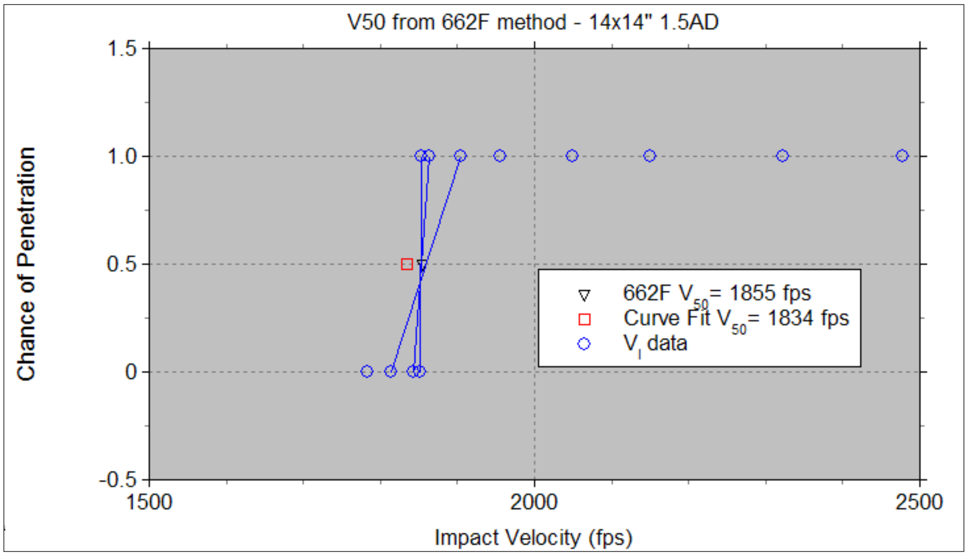

Figure 2-7 Example of probability of penetration chart (1.5 psf 14x14inch Dyneema sample)

These different methods for calculating the V_{50} from the test data gathered on samples. The results from these different methods are compared to see how similar the results were. Any difference in V_{50} between panels of different sizes should be noticeable using these methods.

2.2.2 Energy Dissipation

Once the V_{50} was determined the amount of energy that was dissipated during an impact at the calculated V_{50} was also determined. This was simply done by using classical mechanics. Knowing the amount of energy dissipated can be useful when drawing comparisons between different projectiles because then a direct velocity comparison would not be conclusive.

Equation 3 Energy Dissipation at V_{BL}/V_{50} (Kevin M. Ayotte, 2011)

$$E_{BL} = \frac{1}{2} m_P V_{BL}^2$$

2.3 Damage Analysis Methods

In addition to the V_{50}s being compared, the damage modes and damage propagation was a major subject of interest for this study. Many different techniques were used to quantify and understand what damage would form depending on changing the panel size of the Dyneema samples. The analysis techniques included both destructive (DE) and non-destructive (NDE) methods. The NDE methods were performed prior to the DE methods so that the entire undamaged panel would be observable. The descriptions of the techniques are described below in the same order that they were performed.

2.3.1 Witness Plates

Witness plates were attached flush to the backside of select samples during testing. They were used to measure the shape of the deflected panel at its maximum deflection. This includes the shape of the dynamic cone along with any additional global deformations in the panel. Only the witness plates of partial penetrations were of interest because if there was a complete penetration the projectile would have exited the witness plate and damaged the captured shape of the dynamic cone. During testing after a few samples were impacted it was generally realized what velocities would return partials or completes. Only panels that were expected to be partials incorporated the witness plates. In some cases these turned out to be a complete penetration and the witness plate was discarded. This process allowed a high partial to be captured without using too many witness plates. The witness plates were made from aluminum alloy 1100 with a thickness of 0.020in and yield strength of 5000psi.

Measurements included the maximum displacement of a witness plate, the widths/diameter of the dynamic cone that was formed, and the angle that the dynamic cone formed. In many cases the widths of the dynamic cone were very difficult to measure so the angles of the dynamic cone were used to display trends.

2.3.2 C-scanning

To obtain an initial idea of what the internal damage of the samples looks like ultrasonic C-scanning was used to measure the maximum extent of interlaminar delaminations through the sample thickness. This NDE technique requires the part to be submerged into a tank of water and clamped into position so it is immobile. A signal is then transmitted from one transducer through the water and sample to another at a fixed distance. The intensity of the signal can be increased or decreased depending on the attenuation of the sample. The resulting amplitude of the signal that the second transducer receives is then recorded as a number. This technique is called "Pitch-Catch" or "through transmission". The intensity of the signal was set so that when looking at an undamaged sample the retrieved signal was in a collectable range. When the transducers move to a damaged area the amplitude of the signal drops off dramatically. This is due to air, internal voids and delaminations that attenuate or reflect the input signal, thus reducing the transmitted signal strength. The transducers then scan back and forth recording the peak amplitude at each point. This data can be then plotted as a 2D image where the amplitude from 0% to 100% and plotted in a grey scale. This shows the undamaged regions of the sample as white or gray and damaged regions as black.

(a) (b)

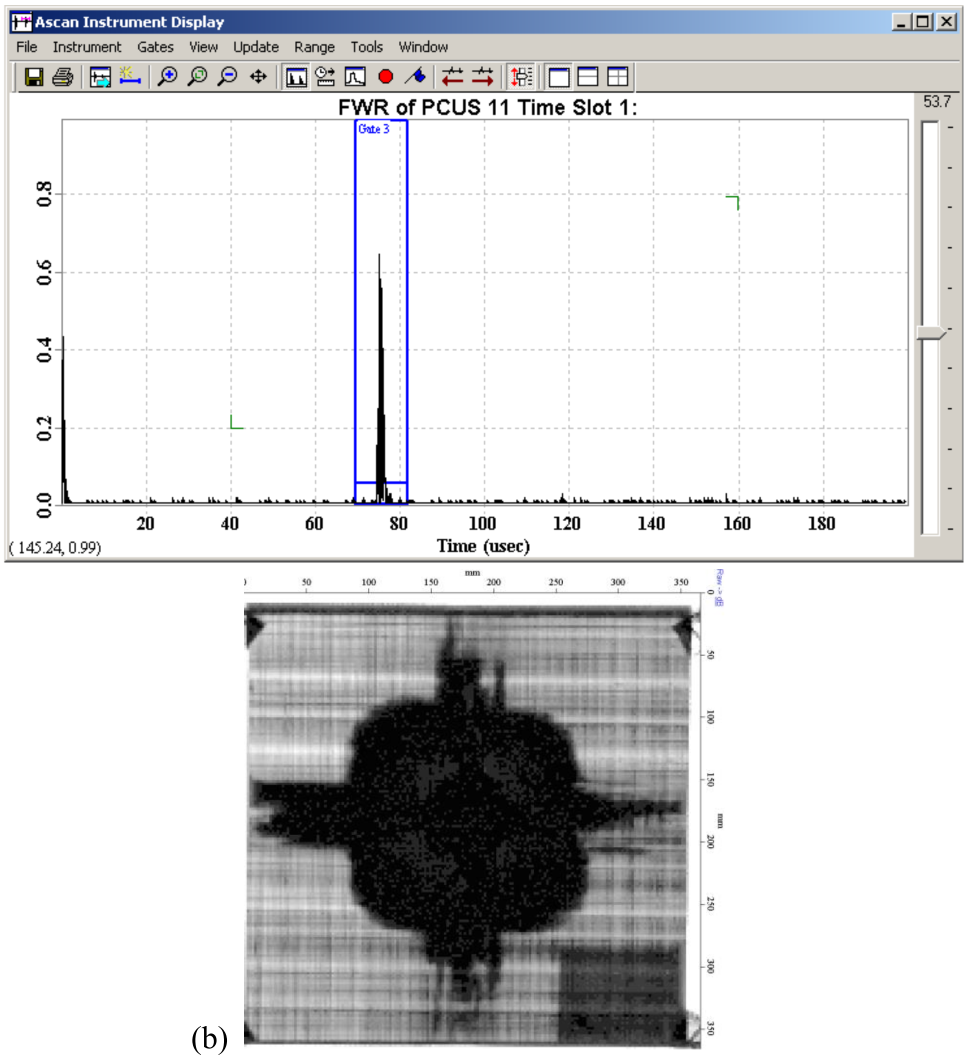

Figure 2-8 Pitch Catch scan (a) with an amplitude of signal for 2.5 psf Dyneema samples, over an undamaged section of material, and (b) a resulting 2D image from the plotted amplitude measurements

The Pitch-Catch scanning is useful in knowing how far the damage in the sample spreads but does not show where in the through thickness the damage occurred. Because the signal only works off of signal strength, there is only data for how much of the signal is lost, not where in the thickness of the sample that the delamination has occurred. In order to determine where in the through thickness the delamination has occurred Pulse-Echo scanning can be used. The Pulse-Echo technique uses only one transducer which sends out a signal and then captures the reflected signal.

The resulting plot of this information (as seen in Figure 2-9) is a chart showing the signal strength and the time that it took for the signal to reach the transducer, or "time of flight (TOF)" which requires the signal to pass through the material twice. Peaks develop depending at different TOF locations. A defect free panel of known thickness is used to determine the wave speed. The largest and first peak is the signal reflected off of the surface of the material, while others can be caused from reflections off of the backside of the material. In the case of panels with defects, each delamination will generate a reflection that is picked up by the transducer. By recording the amplitude on a specific TOF region images can be isolated to display damage at a specific depth within the laminate since the wave speed is known. The longer the TOF, the deeper within the panel the damage has occurred. Similar to the Pitch Catch method, the resulting amplitudes can be recorded as a percent and then plotted into a 2D image showing damage at a specific depth. (Shen, 2012) a)

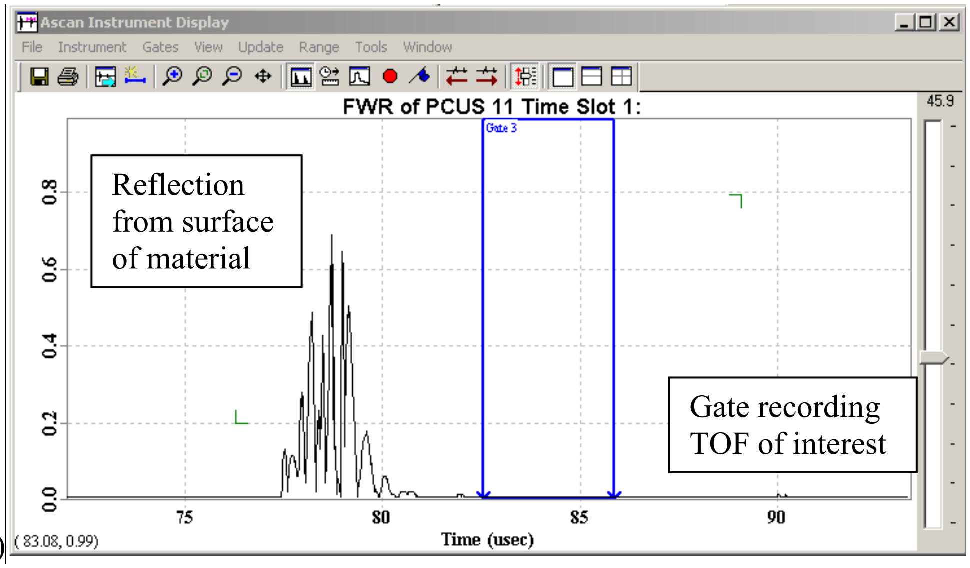

Ascan Instrument Display
File Instrument Gates View Update Range Tools Window
FWR of PCUS 11 Time Slot 1:
45.9
Gate 3
Reflection from surface of material
Gate recording TOF of interest
0.0
0.2
0.4
0.6
0.8
75
80
85
90
Time (usec)
(83.08, 0.99)

b)

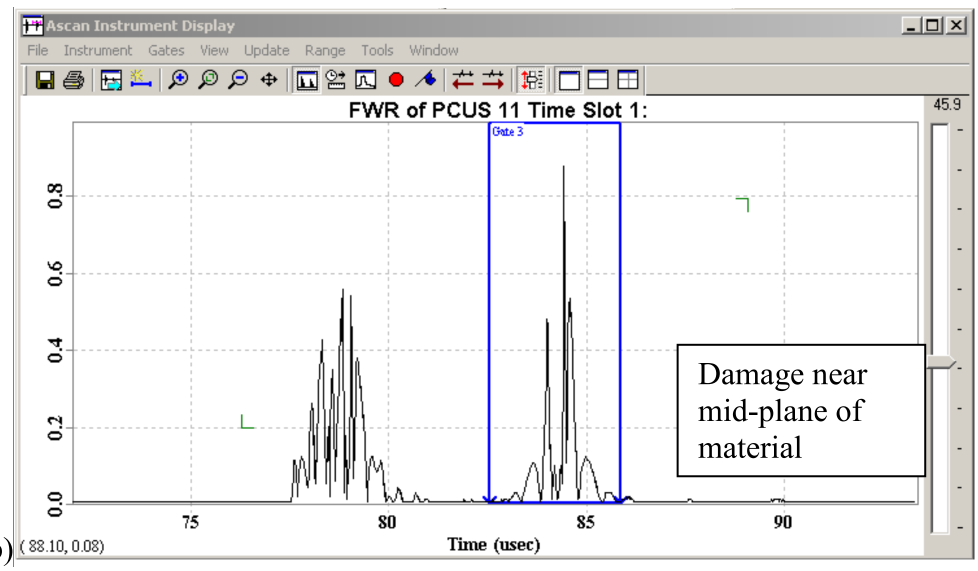

Ascan Instrument Display
File Instrument Gates View Update Range Tools Window
FWR of PCUS 11 Time Slot 1:
45.9
Gate 3
Damage near mid-plane of material
0.0
0.2
0.4
0.6
0.8
75
80
85
90
Time (usec)
(88.10, 0.08)

c) 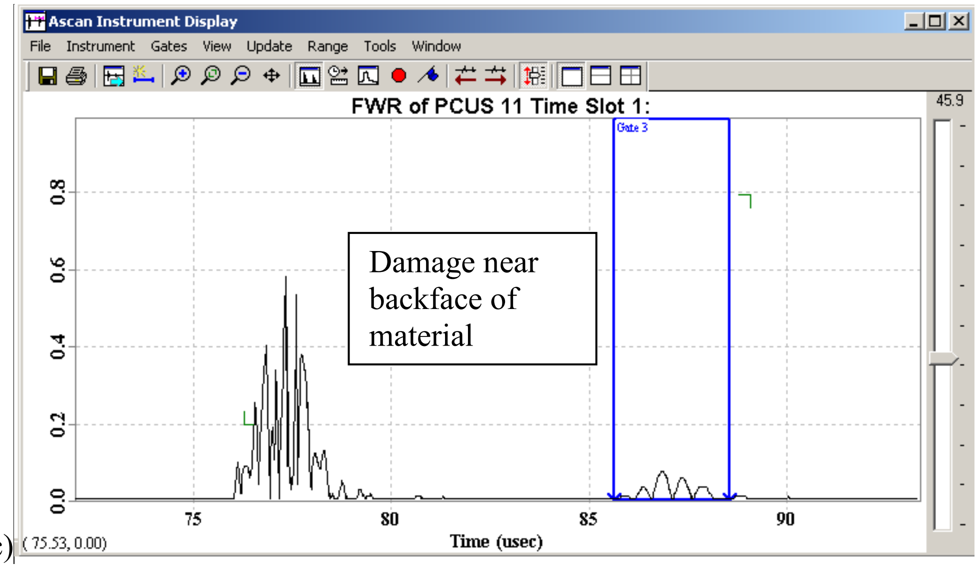

Figure 2-9 Pulse Echo scan resulting amplitude of signal for 2.5 psf Dyneema samples over a) an undamaged region, b) a region of mid-plane damage, c) and a region of backface damage

The work done in this thesis focused on Pitch Catch scanning as it was enough to show the extent on damage throughout the test panels. The images produced showed well enough damage caused by delamination in the primary fibers and dynamic cone formation. For categorizing damage in the through thickness destructive cross sectioning of the panels was done because the degree of accuracy from location damage in the through thickness in Pulse-Echo scanning was low.

2.3.3 Cross Sectioning

The damage that was sustained in the material to this point was analyzed using macroscopic techniques. In addition to macroscopic damage, microscopic damage observations were also recorded. The first way that this was accomplished was with microscopy. This allowed for looking at cross sections of the through thickness of the

Dyneema material. Being able to look at the microstructure of a laminate from the side allows seeing which layers the interlaminar delamination occurs and the cracking propagates between laminas. One point of interest was if delaminations would occur between all of the laminas or would be localized only between the 4 lamina plies that the original Dyneema HB-26 was shipped in. Specifics on the sample preparation process are discussed in Chapter 4.

2.3.4 SEM Imaging

To observe microscopic damage in the material Scanning Electron Microscope (SEM) imaging was used in addition to Microscopy. This technique was used to analyze the surfaces of delamination planes in the laminate. Observations could be made involving fiber/matrix interactions and failures during the impact. Another interest was seeing if there were major differences between delaminations close to the impact site or near the far edges of the delaminations.

The SEM imaging could only be used for making observations perpendicular to the lamina instead of in the through thickness view obtained from the Microscopy samples. Any lamina of interest could be visible but the laminate would have to be pulled apart to expose the viewing surface. This could potentially alter the material and so it was done carefully and the material was allowed to separate on its natural delamination planes. One benefit to using SEM was that the sample materials did not have to be processed like the Microscopy samples. This reduced the damage that could be induced by sample processing which resulted with much higher image quality.

This covers all of the information regarding the important failure mechanism in Dyneema, the background of the testing, and the background of the damage analysis techniques. The next section is dedicated to detailed information about the Dyneema material and the projectile used for this research.

Chapter 3

MATERIAL INFORMATION

The material that was used for this research was Dyneema HB-26. Dyneema is a UHMWPE fiber created by DSM that is lightweight, flexible, tough, and has a high tensile strength. Dyneema is used in products ranging from gloves, fishing line, shipping ropes, to body armor. The specific brand that was used in this research was Dyneema HB-26 which is primarily used for hard armor systems to be used on ships, aircraft, and land vehicles. Other benefits of Dyneema HB-26 are its multi-hit capabilities, flame retardancy, and heat resistance. For these reasons Dyneema HB-26 is currently being used as spall liners for protection against AK47 bullets and IEDs. The purpose of this research was to study a high performance UHMWPE laminate that was currently being used so Dyneema HB-26 was determined to be a perfect candidate. (Dyneema, DSM Dyneema Press Release, 2006)

3.1 Dyneema Properties

Dyneema fibers are composed of polyethylene chains that are usually between 2 and 6 million molecules long. This gives Dyneema a very high tensile strength and modulus with a relatively low weight. These fibers are produced using a technique called gel spinning. Although Dyneema performs well in tension it is extremely prone to molecular buckling and therefore performs poorly in compression. Dyneema has a very low yield compression stress compared to its ultimate tensile strength. A Dyneema fiber will begin yielding in compression at around 1% of its ultimate tensile strength. This drawback has reduced the use of Dyneema fibers in many applications. Given their high chance of molecular buckling cutting Dyneema fibers is also difficult. The fibers generally try and spread out instead of breaking. This can be useful for anti-shear applications but caused issues for the necessary damage analysis for this research that will be discussed later. (Marissen, 2011)

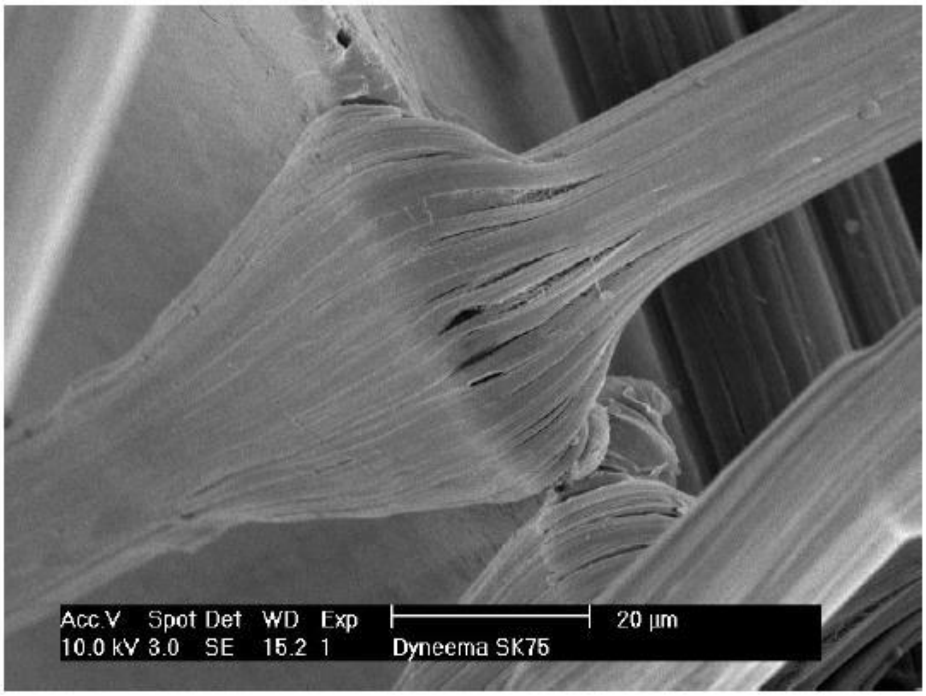

Figure 3-1 SEM of a single Dyneema fiber attempted to being cut by a razor (Marissen, 2011)

Dyneema fibers are 15 times stronger than steel and 40% stronger than aramid fibers by weight. (Dyneema, DSM Dyneema Press Release, 2006) Dyneema is less dense than water making it an ideal material for marine applications. Another benefit is that they are resistant to many chemicals, UV rays, and water resistant which makes storage and use simple. A drawback to the chemical resistance of Dyneema is that it is difficult to bond resins to the fibers because the fiber will not chemically bond to the resign which creates a weak fiber matrix interface. (Marissen, 2011)

The specific properties for the Dyneema material used for this project were not obtained through additional small scale testing. It was felt that the exact material properties would not be absolutely necessary when it came to the reaction of the material under high velocity impact testing. General knowledge would be useful for testing which is why other sources are cited for similar UHMWPE materials even though they might not be exactly the same for the material used in this research. General Dyneema fiber properties are included in Table 1.

3.2 Processing of Dyneema

Like many laminate composites, the recommended treatment of Dyneema HB-26 is similar to many pre-impregnated fiber systems. The laminates are produced by pressing the material at a raised temperature and high pressure to bond the laminas together. One difference is that the matrix and fiber are both made of thermoplastics. The fiber is an UHMWPE and the matrix being polyurethane. Temperatures for processing need to be high enough to get the matrix moving but not high enough to break down the polymer chains of the Dyneema. For this reason the processing temperature is not to rise above 125° C. Additionally, to assist the resin to penetrate the fibers a high pressure is required. The suggested processing pressure recommended by Dyneema is at 165 bar (1240 psi). Figure 3-3 shows the exact recommended processing cycle for Dyneema.

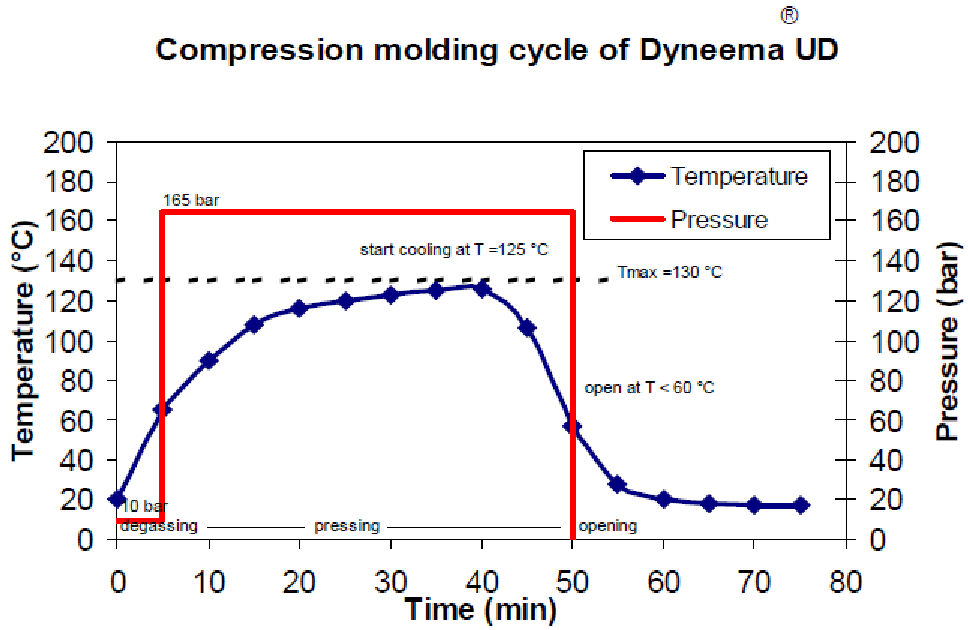

Figure 3-2 Recommended processing cycle for Dyneema HB-26 (Dyneema, 2004)

The melting point for Dyneema HB-26 is fairly low (between 150 and 200 °C).(DSM, 2011) This could cause an issue during an impact because if the fibers were elongated fast enough there could be enough heat generated to melt or deform the fiber thus lowering the properties of the material. UHMWPE has been shown to switch between brittle failure to a plastic yielding when heat is applied. This could allow for lower strengths but higher fiber elongation. Research has shown that in fact the temperature change that occurs during high velocity loading does not result in significant temperature change (less than 1 °C). This would mean that any property changes that would develop due to temperature change would be negligible. (V. B. C. Tan, 2005)

3.2.1 Fiber Denting

During the SEM analysis of the Dyneema laminates it was noticed that there were marking on the fibers of the untested samples. They were evenly spaced and circular in shape. These markings were noticeable in both the impacted and not impacted samples. It was concluded that these were dents in the fibers caused due to the high pressure pressing required for Dyneema processing. The Dyneema fibers become pliable due to heating and when pressed at high pressures the 0° and 90° fibers will create dents in each other where they make contact. Figure 3-4 shows denting in both samples that were not impacted and those that were impacted. Additionally it shows a shot of a UHMWPE fiber from Marissen's research that has not been pressed at all. In this case there is no denting present.

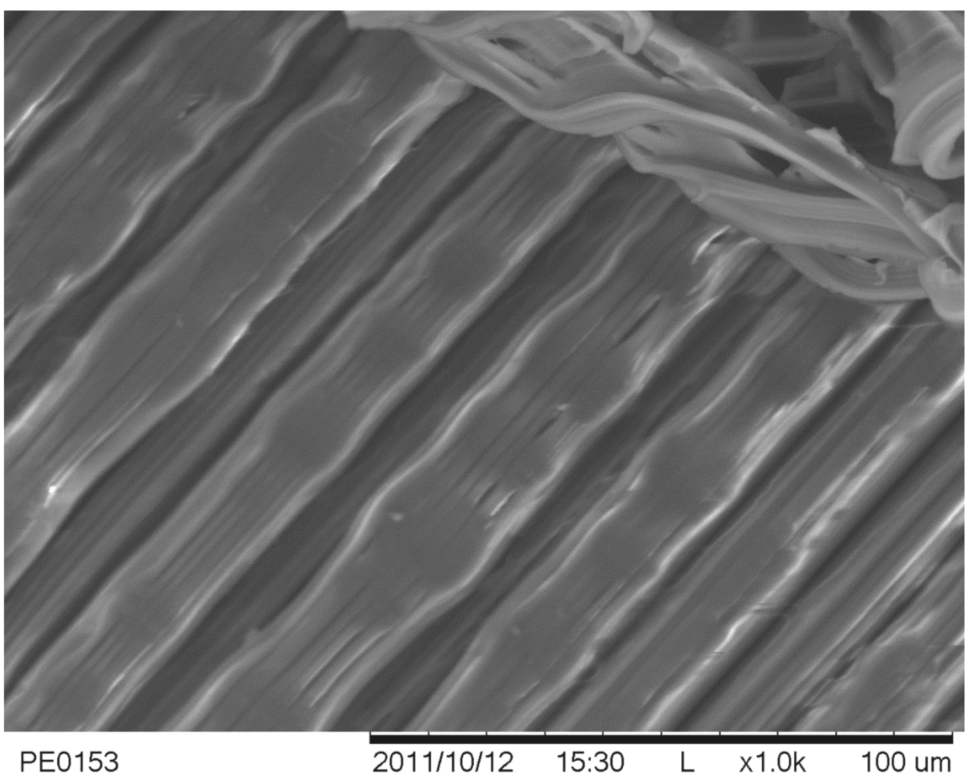

(a)

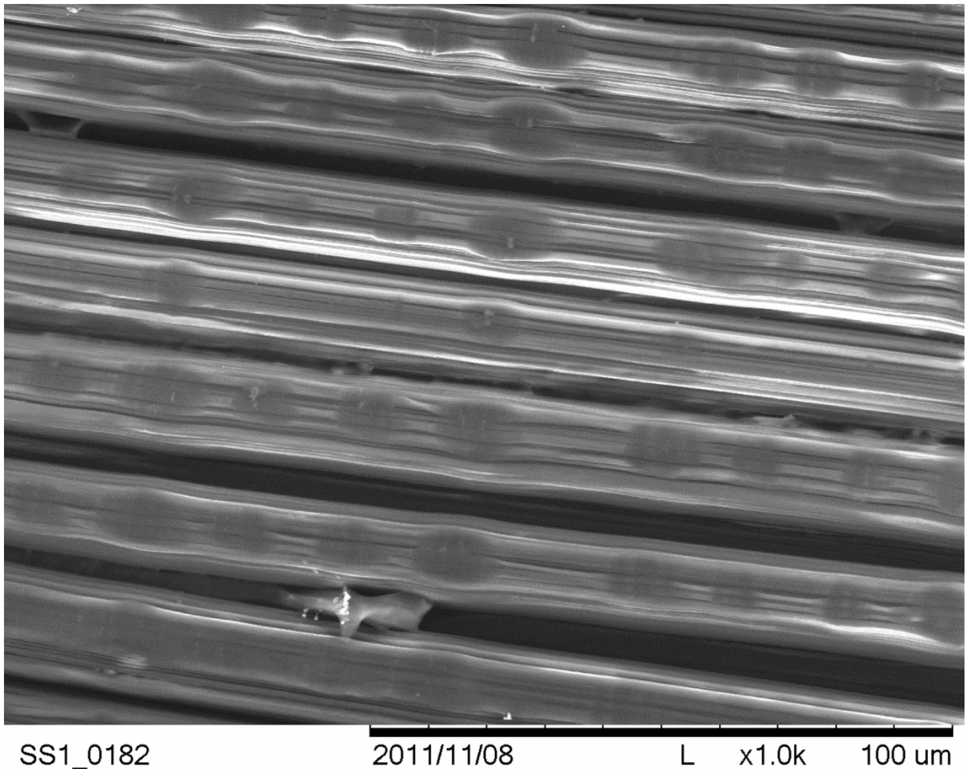
SS1_0182
2011/11/08
L
x1.0k
100 um

(b)

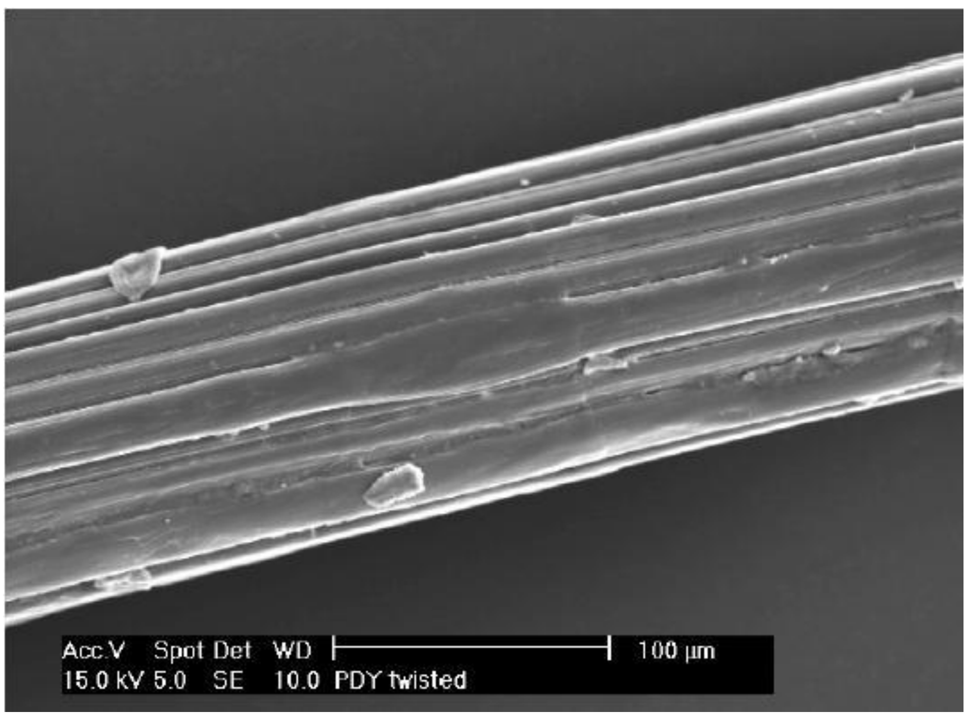
Acc.V Spot Det WD
100 µm
15.0 kV 5.0 SE 10.0 PDY twisted

(c)

Figure 3-3 Fiber denting in both an (a) undamaged (b) impacted sample and (c) an unprocessed fiber (Marissen, 2011)

3.3 Panel Property Selection

Given that the motivation for this research was to determine if there was a relationship between energy dissipation and panel dimensions, the size of the tested panels needed to be defined. These sizes were chosen to isolate different types of damage propagation. The amount of samples used for each test condition that were to be used was decided based on the data analysis that was used after testing. This method of data analysis requires a large amount of samples to fully understand how the material reacts while loaded. Generally, for this method 16 samples are used but for convenience of manufacturing it was decided that each test set would consist of 12 samples.

3.3.1 Thickness Selection

The thickness of the material was chosen as two thicknesses to address any differences that may occur due to the material thickness. Material of varying thicknesses will undergo different amounts of the five impact phases. (B. A. Gama, 2008) The samples were chosen as a representation of the weight of the material per unit area (pounds per square inch). The thicknesses for panels of area density of 1.5 psf and 2.5 psf are 0.30in and 0.50in, respectively.

3.3.2 Panel Size Selection

The size of the test samples were chosen to represent three different damage scenarios. The largest panel size was 24x24in which represented an infinitely large sample where no damage reached a free edge. The second was a 14x14in sample that allowed interlaminar delamination along the primary fiber direction to reach a free edge. The smallest sample was 8x8in to allow a situation where the dynamic cone formation could interact with the support conditions (more details given in Chapter 4.1.2). Figure 3-4 shows how the different panel sizes were chosen to fit the different damage scenarios.

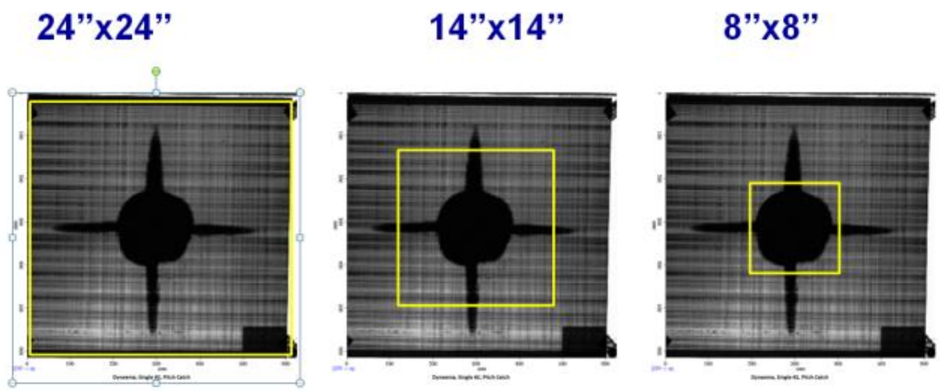

Figure 3-4 Material size selection to represent different damage scenarios

3.4 Projectile Selection and Details

For this testing the projectile used was a .30 caliber fragment simulation projectile (FSP). The FSP round is made from hardened steel and weighs 44-grains (2.85 grams). The tip of the FSP projectile is flat in some regions and has sloped edged on others. This allows the projectile to act like a flat headed projectile while being much more controllable at higher firing speeds. Flat tipped projectiles have shown to cause larger delaminations because more fibers are being directly loaded rather than pushed out of the way. (V. B. C. Tan, 2005) This maximized the damage that would be sustained without increasing the caliber size. The .30 caliber size was chosen because .30 caliber rounds are a common threat size and would result in testable velocities ranges for the sample panels.

Figure 3-5 .30 caliber FSP

3.5 Sample Naming

With this information considered, the naming of materials and testing was done. The names of samples will be used as indicated for the rest of this thesis.

PE_ (areal density) _ (test group) _ (impact number)

Where:

Areal density = 1.5 or 2.5 psf

Test groups = each set of 12 samples of different thickness and dimensions as in Table 2.

Table 2 Sample naming

Test Group	Areal Density (psf)	Panel Size (in)
01	1.5	24x24
02	1.5	14x14
03	1.5	8x8
04	2.5	24x24
05	2.5	14x14
06	2.5	8x8

Impact number = the order in which samples were impacted during testing

Now that the materials and properties for the test samples are explained the testing procedure is detailed below.

Chapter 4

PROCEDURE

4.1 High Velocity Impact Testing

In order to calculate the V_{50} using either the Lambert or Gama & Gillespie equation first the initial and residual velocity data had to be obtained. This was done by the following procedure which was identical for each set of samples. All ballistic testing was performed at Chesapeake Testing in Belcamp Maryland.

4.1.1 Velocity Selection

To build a set of data that could be easily fit to either equation some data points had to be just below the V_{50} and the rest needed to be either just above or much higher. The initial velocity of the projectile could be adjusted slightly by changing the amount of powder that was put inside of the cartridge. This would not give an exact resulting projectile velocity but it would usually was within 50fps. By gathering multiple impacts near the ballistic limit this would help locate the exact V_{50}.

The initial impact was set to be higher than the expected V_{50} of the material so that the residual velocity could be measured. Then the initial velocity was dropped until a partial penetration occurred. The higher initial velocities were added to build the tail end of the curve and the remaining shots were done as close to the ballistic limit as possible. The resulting 12 data points were enough to generate curves using either of the ballistic equations outline earlier. The raw velocity data can be found in Appendix A.

4.1.2 Support Conditions

The support conditions used for testing can have an effect on how the material moves during an impact events. If material is held rigid less dynamic deflection could occur and also prevent delamination propagation. For this testing it was preferred that the maximum movement of the material should be allowed. This meant that all of the edges of the material were free with no constraints. This would allow for maximum deflection and damage to propagate to all of the edges. Corner clamping was put into place just as a means to keep the samples in place.

4.1.2.1 Clamping in Corners

The samples that were tested were held against a steel frame with four C-clamps in each corner. The clamps were hand tightened so that the region under the clamp would not move during the impact. In all of the tests at no time did the clamps fall off due to a lack of grip on the sample. In some tests delamination did occur in layers that were under the clamp. This showed that damage did occur but material movement in this region was still relatively low.

The samples were clamped into a steel frame offset with steel pucks. There were a total of four pucks placed behind the corners where the clamps were placed. The pucks allowed for free movement around all the edges of the material. The locations of the pucks were the only points that were fixed; the rest of the material was allowed to move freely. The pucks were 0.75 inches deep, had a diameter of 2 inches with an inside diameter of 0.75 inches.

Figure 4-1 The four pucks used for backface corner support

Figure 4-2 Puck in conjunction with clamp used on 2.5 psf 24x24inch Dyneema)

4.1.2.2 Sample Perpendicular to Impact

The sample was placed so that the projectile was impacted perpendicular to the surface of the sample. This defined the impact as having a 0° obliquity. An impact with 0° obliquity is generally thought as the worst case scenario in high velocity impacts. With an obliquity higher than 0° the projectile can move through more material thus increasing the ballistic limit. With a relatively high obliquity there is an increased chance for the projectile to reflect off the panel and not penetrate at all.

4.1.2.3 Impact in Center of Material

The impact site on the panel occurred directly in the center of the panel. Given that the panels were square this allowed an equal distance between the impact site and the four free edges. This attempted to get symmetrical damage in the horizontal and vertical directions. The distance from the free edge to the impact site for the 24x24in, 14x14in, and 8x8in cases were 12in, 7in, and 4in respectively.

4.1.2.4 Weapon Specifics

The weapon used for this testing consisted of a universal receiver that fired the projectile through an appropriately sized barrel for the .30-cal FSP. The weapon was placed 15 feet away from the target. To achieve high velocities different amounts of gunpowder were used as propellant. Powder was placed into a .30-cal cartridge, then wadding, and lastly the projectile.

Figure 4-3 Weapon used for impact testing (courtesy of Chesapeake Testing)

4.1.3 Data Collection

The data collected from testing were from a number of variables. The velocity data was measured to know the velocity of the projectile before and after it impacted the sample. This velocity data was used to calculate the energy dissipated by the sample and to calculate the V_{50}.

4.1.3.1 Detectors

Two methods were used for measuring the velocity of the projectile. To measure the initial velocity of the projectile a set of two Oehler Research model No. 57 infrared screens were used. Once the projectile trips the optical sensor the time was recorded using a Hewlett-Packard counter chronograph (universal counters, HP model No. 53131A). This was done for both sensors to get to get a time difference between the two screens. Given a fixed distance between the screens the initial velocity of the projectile was calculated.

The residual velocity was measured using a different system which used paper screens instead of optical screens. The paper was printed with a conductive silver pattern on one side. An electrical current was run through the silver and when the projectile punctured the paper the current was broken. This triggered a chronograph which recorded the time interval. Similarly as the initial velocity there were two screens so a time and distance difference was used to calculate the residual velocity of the projectile.

Figure 4-4 Initial velocity screens (courtesy of Chesapeake Tesing)

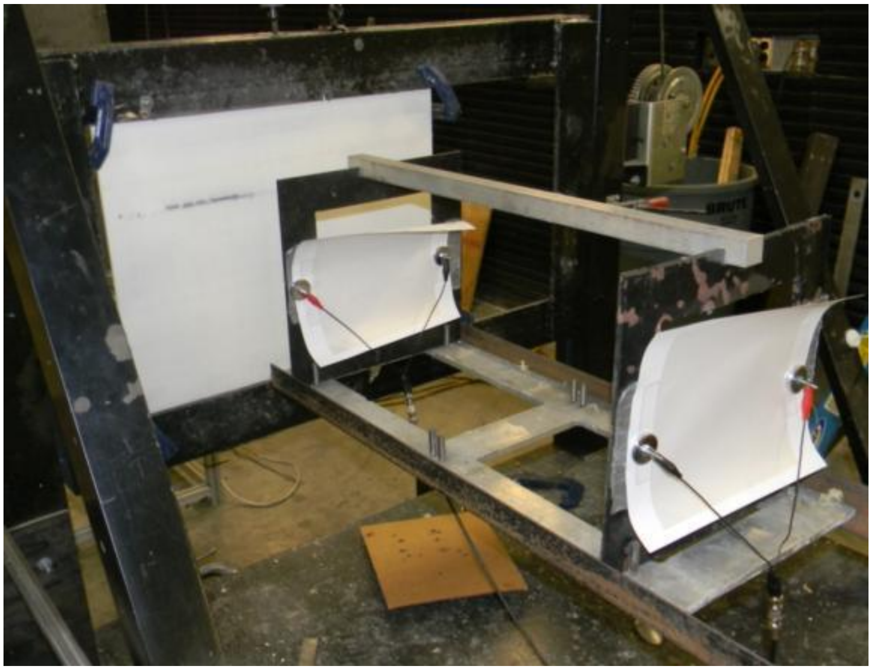

Figure 4-5 Residual velocity screens (courtesy of Chesapeake Tesing)

4.1.3.2 Complete and Partial Penetrations

The distinction between complete and partial penetrations was dependent on whether the projectile fully exited the sample. If the projectile exited the backface of the material then the shot was counted as a complete. In this case the projectile should trip the rear sensors and the residual velocity would be recorded as well as the initial velocity.

In the case where the projectile fully exited the material but did not exit the witness plate that was behind it, the test would still be counted as a complete penetration. During the testing involved for this research there were no cases where this occurred. Therefore for all cases of complete penetrations the projectile exited both the sample and the witness plate.

4.2 Damage Analysis

Different analysis techniques were used categorize and quantify the damage that was sustained to the samples after being impacted. This section outlines the procedures used for each of these damage analysis techniques. Special care was taken to make sure that the viewing surfaces of the materials were not damaged as to not compromise the damage that was sustained due to testing. A number of techniques involve measurements using images generated from cameras or other equipment. All of the measurements were made using the software ImageJ and were done by adjusting the scale to known distances within each picture. An important note is that the material is deflected more during the impact event than can be witnessed in the material after the event. For this reason the measurements taken were to be compared against each other and not to reflect the exact measurements that occurred during the dynamic impact event.

4.2.1 Witness Plate Measuring

The witness plates were the exact same size as the sample panels and were flush up against the samples as they were being tested. This would ensure that as the material deflected during the impact, the shape of the deflection would be captured in the witness plate. The witness plate was held in place by the same clamps that also held the sample panel in place.

It should be noted that the way the witness plate captures the dynamic cone shape was through the yielding of the aluminum. Aluminum allows for large plastic deformations with minimal elastic recovery so when the witness plate deforms during impact it will retain its shape after the Dyneema has returned to its original shape. This deformed aluminum shape therefore shows the shape that the dynamic cone at its maximum deflection. There would be a small amount of elastic deformation that occurred in the aluminum plate and this could not be captured by measuring the witness plate after the impact. It was assumed that this elastic deformation was relatively small and therefore negligible for this research. Figure 4-6 shows the aluminum witness plate on a Dyneema panel after an impact has occurred.

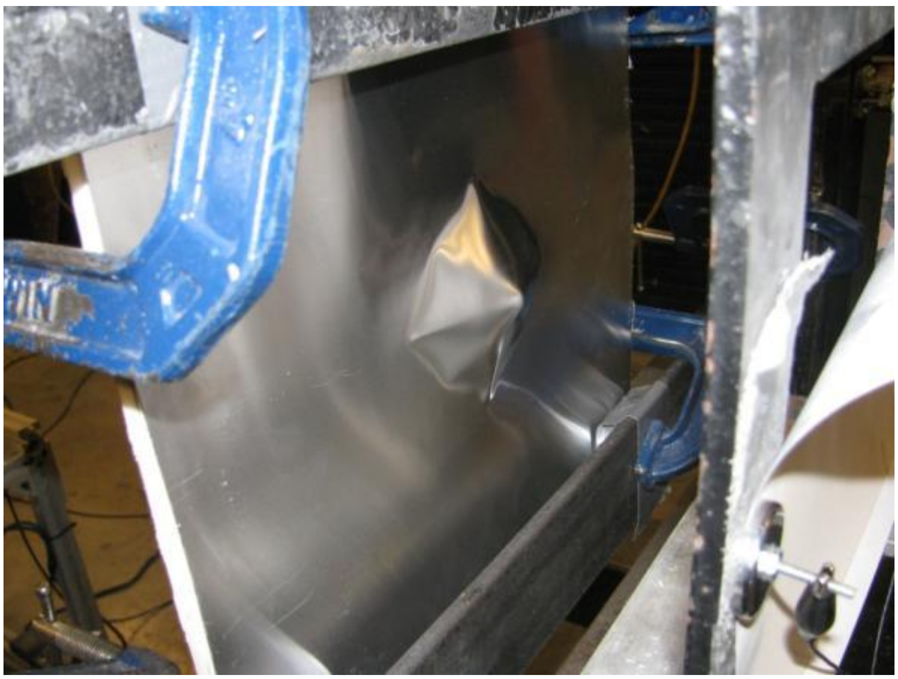

Figure 4-6 Witness plate deflection of a partial penetration

The specific aluminum used was the alloy 1100 with a thickness of 0.020in and yield strength of 5000psi. The in-plane dimensions of the witness plates were all the same as the Dyneema panels (i.e. 24x24in, 14x14in, 8x8in. (McMaster-Carr). Given that the aluminum was thin with a low yield stress it was assumed that the additional energy dissipation gained from the witness plates were negligible allowing direct comparisons between panels with witness plates and without to be made.

The maximum displacement of the witness plates was measured by using photography. This process involved placing the witness plate flat on a table centered over a point and taking a picture from a fixed position. The corners of the witness plates were weighted because during testing the corner clamping produced the same effect. This was done for all of the samples and also with a shot of a ruler at the same point that the witness plates were placed. The image of the ruler was then overlaid on the sample pictures so that measurements would be able to be made. This method both captures the depth of the dynamic cone and the added global deformations that were captured by the witness plate. Earlier methods were used to record the maximum deflections but they did not include the global deflections so they were deemed inaccurate. Figure 4-7 gives an example of the photography process.

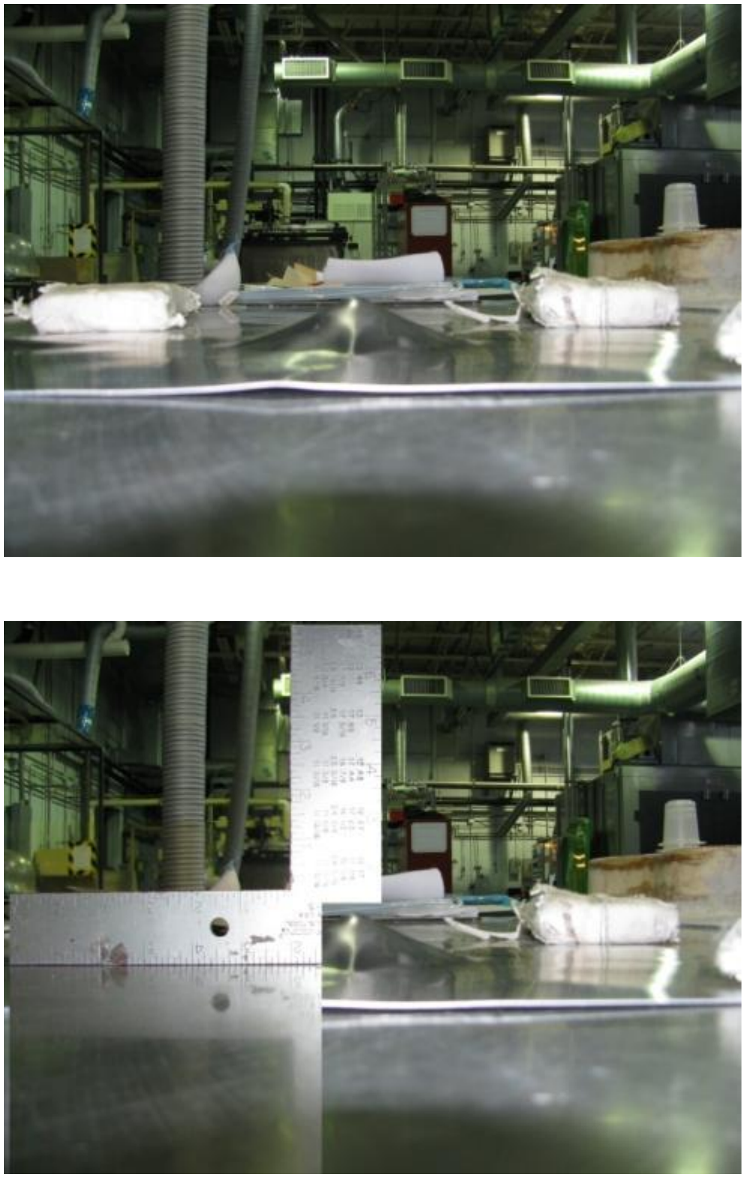

Figure 4-7 Example of how the photography method was used to measure maximum displacement in witness plates

In addition to measuring the maximum deflection the widths or diameter of the formed dynamic cone were also measured. This was done by using calipers and measuring the distance between opposite ends of the cone. The w1 and w3 measurements were taken along the primary fiber direction while the w2 and w4 measurements were along the secondary fiber direction. In some cases this was difficult to do because it was not obvious where he bend in the witness plate started. If the initial portion of the dynamic cone was not obvious within a ½ inch then it was assumed that the resulting measurement was not satisfactory. This was especially evident in samples PE-2.5_04, in which no measurements were taken at all. Figure 4-8 shows the naming and measuring order for all of the witness plate widths.

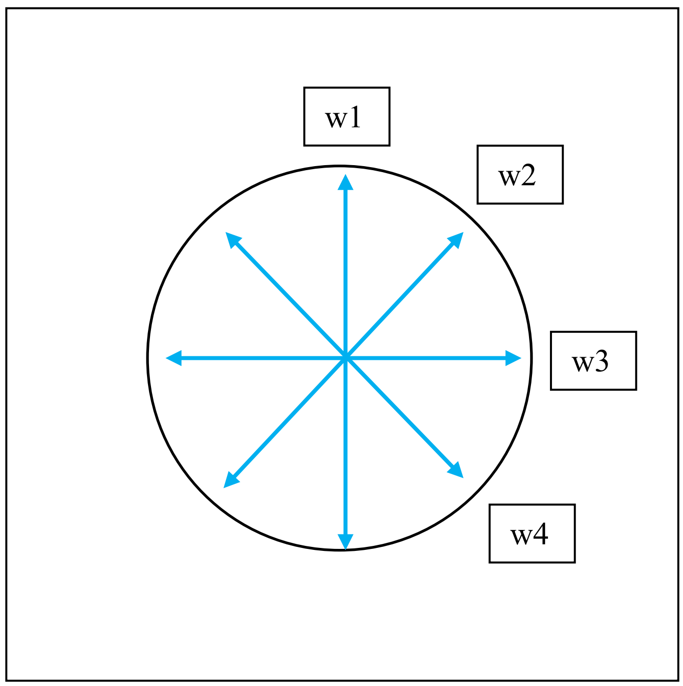

Figure 4-8 Measuring technique for witness plate widths

The shape of the profile of the witness plate was also recorded in a similar way to the photography method that was used to measure the maximum deflection. The witness plates were set up the same way and the camera was used to take a picture of the witness plate from the edge. Then the deformed shape of the witness plate was traced and drawn again on a blank background. This gave the shape of the deformed witness plate. From this the angle of the deformed shape could be recorded. This was done in only the w3 direction due to the orientation of the camera.

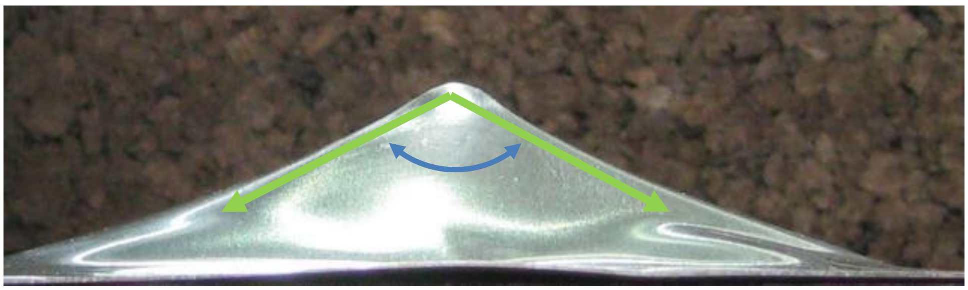

Figure 4-9 Method for measuring the angle of the dynamic cone

4.2.2 C-scanning

The Pitch-Catch method of C-scanning was used for the majority of C-scanning. This method gave consistent results of where the damaged regions occurred in the impacted sample. The method used for this research only captured the maximum amplitude of the received signal. This only showed that damage occurred somewhere within the panel, it does not show where in the through thickness the damage occurred. Other methods were used to determine this and will be discussed later.

Figure 4-10 shows what a C-scan of undamaged Dyneema HB-26 looks like. The signal fully goes through the material and the 0/90 fiber orientation can be clearly seen. This image is useful when comparing to images of samples that have been damaged due to testing. It should be noted that the dark rectangle in the lower right corner was due to an identification label adhered to the panels which trapped small air bubbles. It should be noted that all images with a dark region in this location have not been damaged there; it was just the identification label.

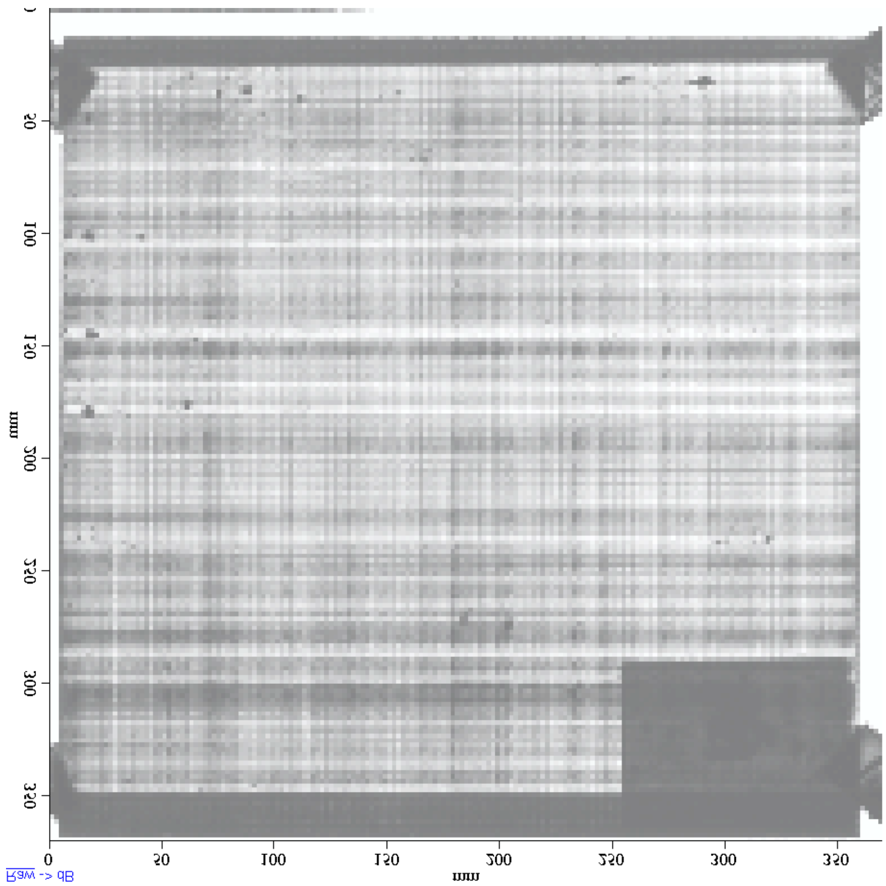

Figure 4-10 Example C-scan of undamaged Dyneema HB-26

All of the 1.5 psf samples were scanned using the Pitch-Catch method. The samples were scanned using 5MHz transducers at amplitude of 50.7dB. This allowed one to see details in the panel while showing complete signal loss when a observing a defect. All of the 2.5 samples were scanned using 5MHz transducers at amplitude 54.1dB.

The Pulse-Echo technique was used for determining damage at specific depths of materials. For these cases all of the samples were observed from the impact side with 5MHz transducers at amplitude of 45.9dB. The Pulse-Echo technique was just used to gauge the different damage regions within the material so extensive measuring of the images was not performed. Example Pulse-Echo images can be found in Figure 5-15.

Once the C-scan images were gathered a number of measurements were used using the software ImageJ. By using the scale on the side of the images distances could be measured. The measurements for the samples included the area of damaged region, the area of just the dynamic region (circular damage), the area of cross damage region (only the legs not in the dynamic region), the diameter of the dynamic damage region, the widths of the cross damage (w#), the widths of the cross legs themselves (wc#), and the angle of the cross damage. The naming convention for the cross damage (w#) is the same as for the witness plate measurements because the measured lengths are in the same direction and plane. The location of these measurements is shown in Figure 4-12. In Figure 4-11 the different regions of damage are shown. The area of the dynamic region is just the circular area and the area of the cross damage is the region of the legs in the 0/90° directions.

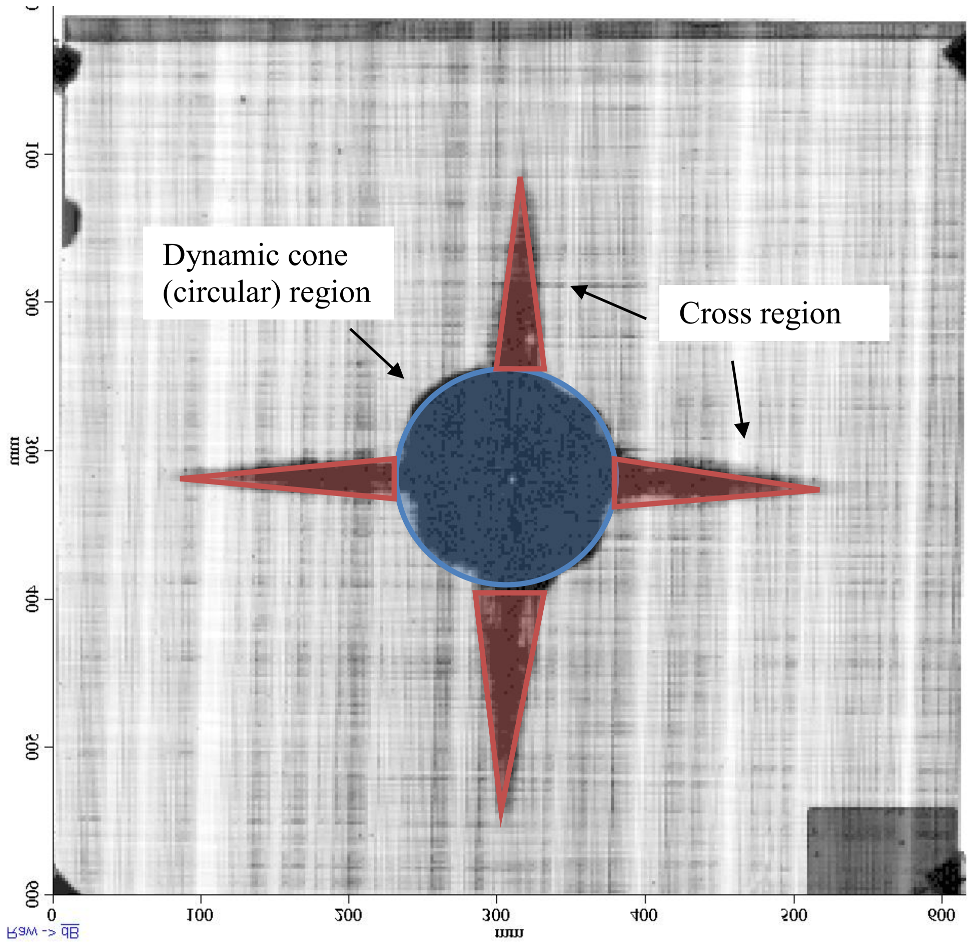

Figure 4-11 Dynamic cone region and Cross region

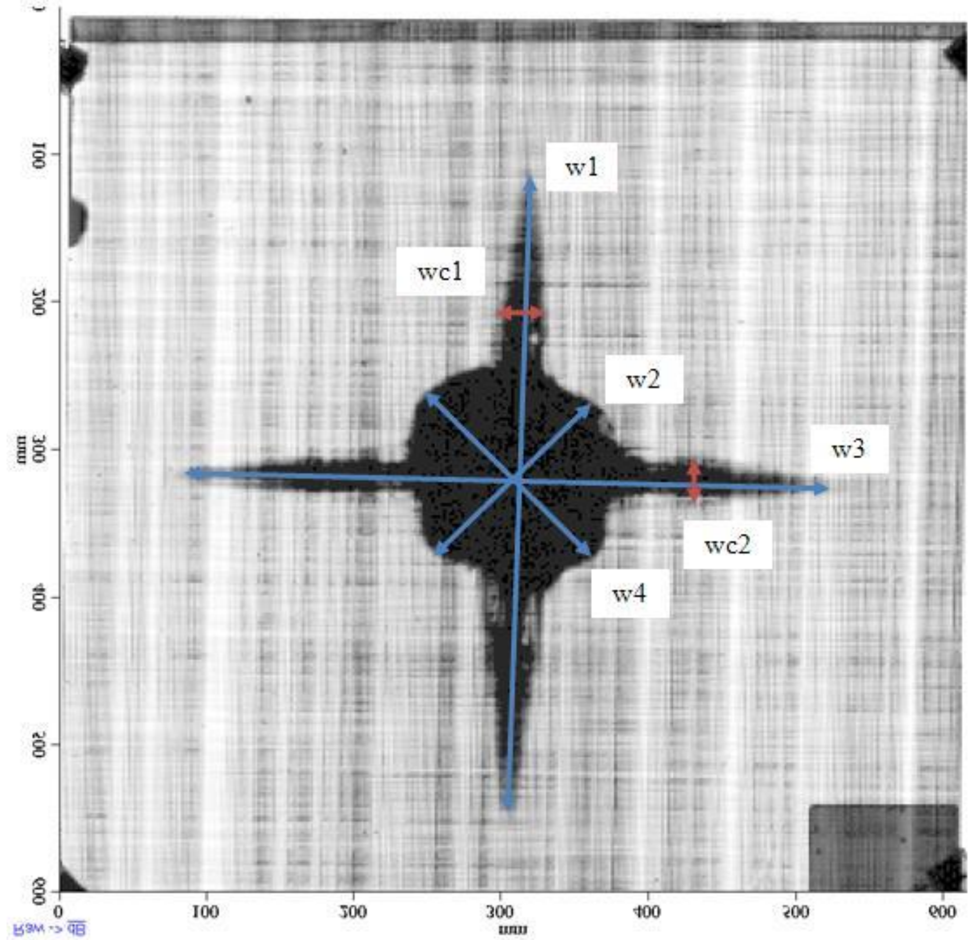

Figure 4-12 Diagram of measurements taken from the C-scan images

4.2.3 Cross Sectioning

After the NDE techniques were performed the samples could be sectioned and dyed to see the shape of the damage cone at desired cross sections of the sample. The samples were cut using a vertical ban saw. Once the samples were sectioned the damaged regions were dyed with a mixture of blue dye and water. The dye would soak into the gaps thus showing where the delaminations were occurring.

4.2.3.1 Sample Selection

Not all of the test samples were sectioned for dyeing. Each sample group had 12 samples and 5 of these were sectioned to view the damage cone shape. The samples that were selected were the highest partial and the lowest complete as well as a few samples as the initial velocities increased. This sample size would give a variety of results when the initial velocity was close to the V_{50} and when the initial velocity was above the V_{50} by different amounts. The samples cross sectioned were done along the w3 direction which exposed primary fibers. A few other samples were sectioned along the w2 direction to expose the secondary fibers.

4.2.3.2 Cross Section Process

Because of the flexibility of the Dyneema fibers it was found that the simplest way to cut the panels was by using a band saw at high speed. This gave a clean cut and did not induce additional damage that would show up during the dyeing process. The samples were cut with a precision toothed blade at a speed of 1000 feet per minute. The samples were fed slowly and cooled with an air jet to prevent overheating which could cause melting of the fibers.

Originally, the samples were attempted to be cut with a diamond coated wet saw as is used for many composites. Instead of giving a clean, smooth edge the cutting surface became flared out due to the fibers being pushed instead of cut. This induced damage by separating the layers which would cause issues when dyed. For this reason the samples were only cut using a ban saw.

4.2.3.3 Dyeing Process

Once the samples were cut a dye was used to make the damage that was sustained during impact visible. The dye that was used was the color American Blue from the company Private Reserve Ink. This dye was mixed with water at a ratio of 99.5% water to 0.5% dye. This ratio made the damage obvious without completely overpowering the sample.

The process for dyeing the samples is as follows. The cut surface was first cleaned with acetone to make sure there was no dirt or debris left over from cutting. The sample was held by a two binder clips and placed on a table so that the cut edge was parallel to the table surface. The dye/water mixture was the added using a disposable transfer pipette and spread out with a cotton swab. This was done until the entire cut surface was coved with a layer of dye. The sample was then left to soak for about 10 minutes. After soaking the remaining dye was wiped up with a paper towel. The sample was then flipped upside down and left to hang for drying. Once dry the sample would be colored in areas where delamination occurred. This technique was used for all of the samples that were dyed.

4.2.3.4 Edge Pull-In

In the cases where the cross delamination reached the free edge of the panel, pull-in of the material would occur. To quantify this damage the same dyeing technique was used as described above and specific measurements were taken. Measurements of Edge pull-in include the depth that the pull-in occurred at, the amount of pull-in that occurred, and the width of the cross delamination at the free edge. The depth that the edge pull-in occurred at was recorded from the strikeface of the panel towards the backface. This was taken as a percentage of the entire thickness of the panel. It should be noted that the amount of pull-in recorded was the maximum and this occurred in the primary fibers. The pull-in decreased moving away from the primary fibers until there was no pull-in at all. Figure 4-13 shows the measured regions for edge pull-in.

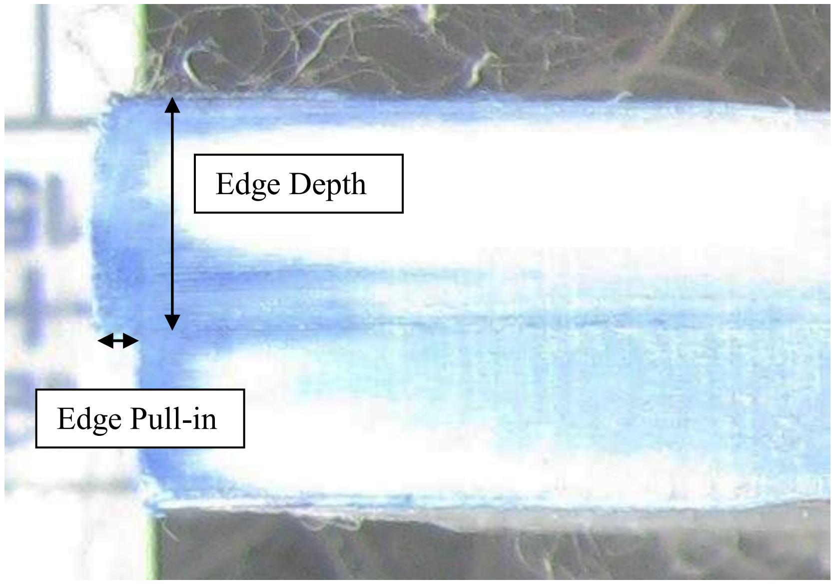

Figure 4-13 Measurements taken for edge pull-in

The most useful samples for looking at edge damage were the 1.5 psf 8x8" and the 2.5 psf 14x14" sets because in these cases only one substantial delamination would reach the free edge. In the 2.5 psf 8x8" cases there were usually multiple layers where delaminations reached the free edge so it was difficult to determine which ones were the major ones. For this reason most of the data collected were from these test sets.

4.2.4 Microscopy

The preparation of the material involved first isolating a piece of material in resin and then polishing the desired edge. A sample about 1x1in was placed in a plastic cup and filled with Beuhler Epoquick resin. This was a two part quick curing clear epoxy resin that is commonly used for microscopy. Once the resin cured, the sample was removed from the plastic cup and fitted onto a Beuhler polishing system. This system runs automatically applying pressure and rotating the sample along the polishing surface. First wet sanding was done with successively finer sandpaper then polishing was done with successively finer grit.

Table 3 Process used for sample polishing

time (min)	speed (rpm)	pressure (lbs)	grit size
until sample surface was reached	170	hand pressure	240
10	170	17	320
10	170	12	400
20	120	10	600
20	200	10	12.5μm
20	200	10	9.5μm
20	200	10	5.0μm

The samples were then observed under an optical light microscope. Images were captured from the microscope to be used for observations and measurements.

It should be noted that due to the flexibility of the fibers, many of the images were not as useful as originally hoped. During sanding and polishing usually the fibers and matrix are smoothed down and produce a clear viewing surface. Instead of grinding down the fibers, they were bent which made viewing the samples under a microscope difficult.

4.2.5 SEM Imaging

SEM imaging was used for observing the surfaces of laminas that were delaminated due to the impact. The process for obtaining a sample started with cutting a small piece of material with known delaminations validated from the C-scan imaging. Due to the delamination the samples would separate easily between the layers that were delaminated. The sample was then placed delamination side up on a specimen plate and attached with carbon tape. The sample was adjusted so the surface was at the correct focal length and was lastly placed in the SEM.

Numerous images were taken from different magnifications. Lower magnifications show distribution of residual matrix while higher magnification shows the individual fibers. Because the samples were separated by the delamination two viewing surfaces were obtained for each delamination. One was the surface closest to the strikeface and the other was the surface closest to the backface. For the figures in the SEM results section whenever a sample is separated and the two sides are viewed, each was signified with "strikeface" and "backface" to indicate which side of the sample was being viewed. Extensive SEM imaging was not done on all panels tested; instead just on some specific regions in panels to see how the damage differed between the cross delamination region and the dynamic cone region.

These are all of the procedures for the testing and damage analysis methods that were used during this research. The next section shows all of the results that were observed and measured from the testing.

Chapter 5

RESULTS

This chapter separates the results from testing into two parts. The first as the calculated V_{50}s that were generated from the methods outlined earlier using the velocity data gathered during the impact tests. The second is composed of images and measurements resulting from the damage analysis done to the panels after the impact tests were done. The results from both of these sections are compared and discussed given the different damage mechanisms that were affected due to changing the panel size of the Dyneema.

5.1 Impact Testing

Once the impact tests were completed, the raw velocity data was reduced using the different V_{50} calculation techniques outlined in section 2.2. The first and simplest method performed was the using the Military 662F Standard. Because the 662F method does not use all of the test points it is important to define the range between the highest and lowest 2 V_I data points. This is given in Table 4 as the range of inputs. The calculated V_{50}s for all 6 test conditions are in this table as well. Sometimes in ballistics there are "mixed results" which means that there were some partial penetrations that occurred at a velocity that are higher than the velocities of some complete penetrations. This usually shows inconsistency in materials or when a single test panel is impacted multiple times. In the data below it shows that there was some inconsistency with the results especially in the thick 8 x 8 sample.

Table 4 Results from Military 662F Standard

Test	AD (psf)	Size (in x in)	$V_{BL}(V_{50})$ (fps)	Range of Inputs (fps)	Range of Mixed Results (fps)
PE-1.5_01	1.5	24	1762	230	0
PE-1.5_02	1.5	14	1855	90	0
PE-1.5_03	1.5	8	1898	339	0
PE-2.5_04	2.5	24	2676	92	6
PE-2.5_05	2.5	14	2760	143	0
PE-2.5_06	2.5	8	2846	317	180

The data in Table 4 shows that the V_{50} for the thicker 2.5 psf samples was higher than the thinner 1.5 psf samples for all panel sizes which is expected. The interesting note was that there was an increase in V_{50} as the panel size was decreased. It is difficult to draw any real conclusions from this method because the range of input initial velocities is very large in some cases. This is why additional data analysis was done to get a clearer result.

The V_I and V_R data was plotted and fitted with the Lambert or Gama & Gillespie equation using the software Easy Plot. As mentioned in Chapter 2, the Gama & Gillespie equation was used in cases when the Lambert equation would not result in a converging curve in Easy Plot. The V_{50} (V_{BL}), p, β, and ς terms were determined by using an equation fitter in Easy Plot to generate a curve that fit into the test data. Every equation that the curve fitter produced had a maximum distance between the curve and an outlying data point which is designated as the max deviation. The tests that resulted in large max deviations were due to large ranges of mixed results. If the All the information involved in the curve fitting of the data can be found in Appendix C. The resulting curve fitting parameters are given below in Table 5.

Table 5 V_I/V_R curve fit parameters

Test	Curve Fit Method	β	V_{BL} or V_{50}(fps)	p	$V^{max}_{A,R}$	max deviation (fps)
PE-1.5_01	Gama/Gillespie	1.01	1762	--	10.2	253
PE-1.5_02	Lambert	0.986	1834	2.29	--	189
PE-1.5_03	Lambert	0.971	1871	2.26	--	200
PE-2.5_04	Lambert	1.05	2655	1.91	--	274
PE-2.5_05	Gama/Gillespie	1.07	2722	--	3.14	456
PE-2.5_06	Gama/Gillespie	1.15	2854	--	4.71	530

Once each of the 6 data sets was fit with a curve the curves themselves could be compared against each other. Figure 5-1 shows each of the test data sets along with the curve that was fit to the data.

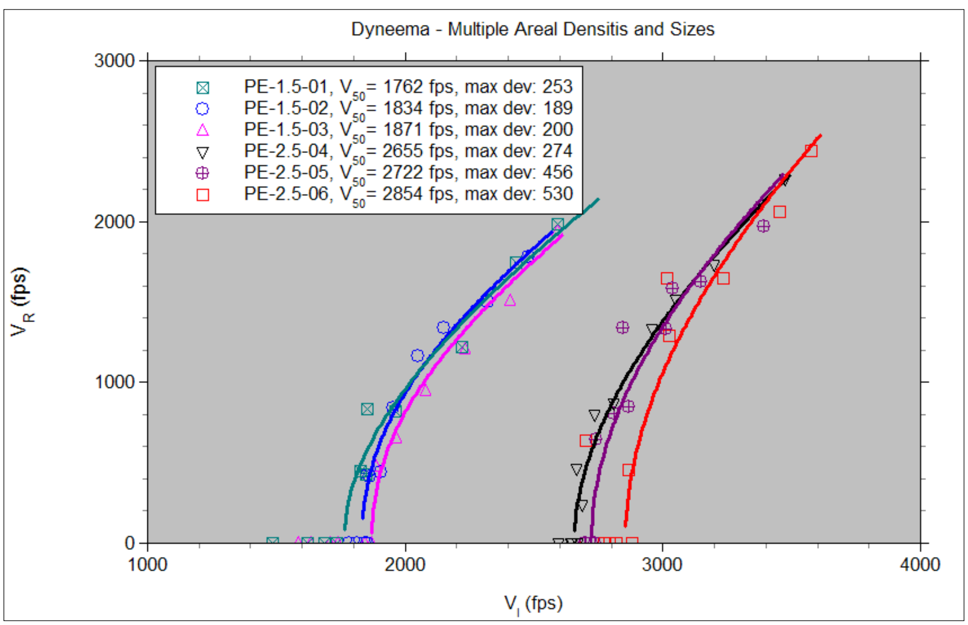

Figure 5-1 Areal Density and Panel Size Comparison of V_I/V_R curves

5.1.1 Comparison between Methods

Table 6 shows a comparison between the 662F military standard and the curve fitting technique. Also given is the difference between the two and the percent difference. For each test the results were nearly identical with none of the results being off by more than 1.4%. The final V_{50} that was taken as the official value for the rest of the research conducted was decided to be from the curve fitting results. It was felt that these most closely represent the actual results from testing because the tests were specifically done for this type of data analysis.

Table 6 Variation in V_{50}s between methods

Test	V_{50} 662F	V_{50} Curve Fit	Difference	% Difference
PE-1.5_01	1762	1762	0	0.00%
PE-1.5_02	1855	1834	21	1.13%
PE-1.5_03	1898	1871	27	1.42%
PE-2.5_04	2676	2655	21	0.78%
PE-2.5_05	2760	2722	38	1.38%
PE-2.5_06	2846	2854	8	0.28%

These calculated V_{50}s were compared using the Probability of Penetration method described earlier. All of the results fell within the expected range which was another confirmation that the curve fit results were reasonable. The full set of Probability of Penetration plots are attached in Appendix C.

5.1.2 V_{50} Analysis

Now that the V_{50}s were calculated some additional comparisons could be made. Figure 5-2 shows the resulting V50s depending on the areal density and size of the tested panels.

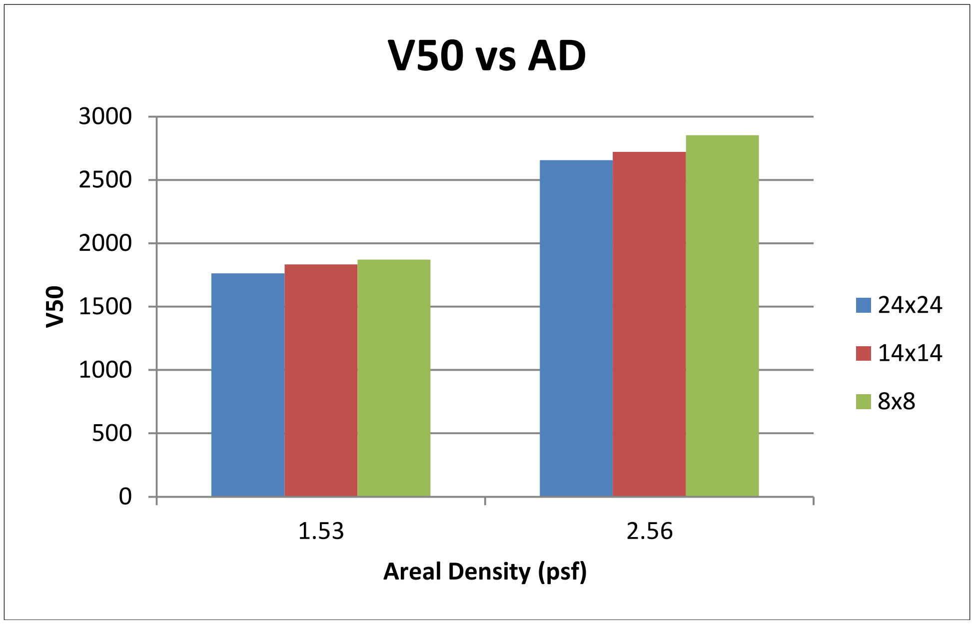

Figure 5-2 V_{50} vs. areal density of different samples

Given that the mass of the projectile (m_P) was recorded as 2.85 grams, the resulting energy dissipation for the different calculated V_{50}s for each test condition are given in Figure 5-3.

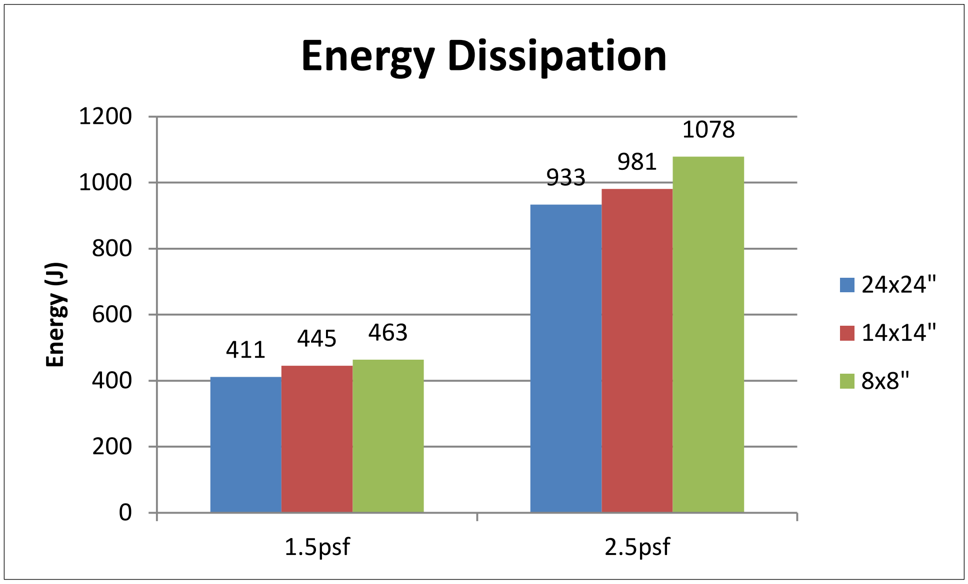

Figure 5-3 Energy Dissipation (J) at V_{50}

5.1.3 Final V_{50} Summary

As expected the thicker panels with the higher areal density had a higher V_{50}. V_{50} for 2.5 psf panels were approximately 1.5 times higher than the 1.5 psf panels for all panel sizes. Energy dissipation at V50 for the 2.5 psf panel was 2.3 times higher than the 1.5 psf panels. This was simply due to the higher mass and the associated increase in material thickness that the projectile had to travel through.

The real question was what would happen when the material stayed the same and the only change was in the size of the impacted panel. It was observed that the smaller panel size for both the thin and thick samples resulted in an increased V50 in the range of 6-8%. The additional gain of ballistic performance came with an uncertainty in predicting the residual velocity based on the fit curves. For the smaller samples the range between highest partial and lowest complete was much higher and there were many cases where a low velocity would fully exit the material with a high residual while a higher initial velocity would be stopped completely. This was most obvious in the 2.5 psf 8x8in sample case. A few of the impacts fit right along with the data from the larger panels but most of the data points showed an improvement in ballistic performance. More extensive studies are required with significant increase in the number of test panels to construct the overall probabilistic velocity response (PVR) curve for each panel size. Comparisons between the entire PVR curves or values based on lower probability of penetration (e.g. V_{01} or V_{05}) may be more sensitive to panel size effects than V_{50}.

5.2 Damage Analysis

The observation that smaller panels would increase the ballistic performance in Dyneema is interesting but the data from testing alone does not show why this phenomenon occurs. The material needed to be analyzed post impact to observe the damage modes that occurred.

5.2.1 Witness Plate Deformations

The witness plates were used to measure the maximum deflection from the damage cone formed by the Dyneema during the impact. After the witness plates were measured the data was analyzed to determine if there was a significant difference between dynamic cones of the different panel sizes.

5.2.1.1 Max Displacement

Once the maximum displacement for each witness plate was recorded the maximum values for each test were compared against each other. These were almost always the highest partial recorded or very close to the highest. Figure 5-4 shows the 6 separate tests and the corresponding maximum deflection for each.

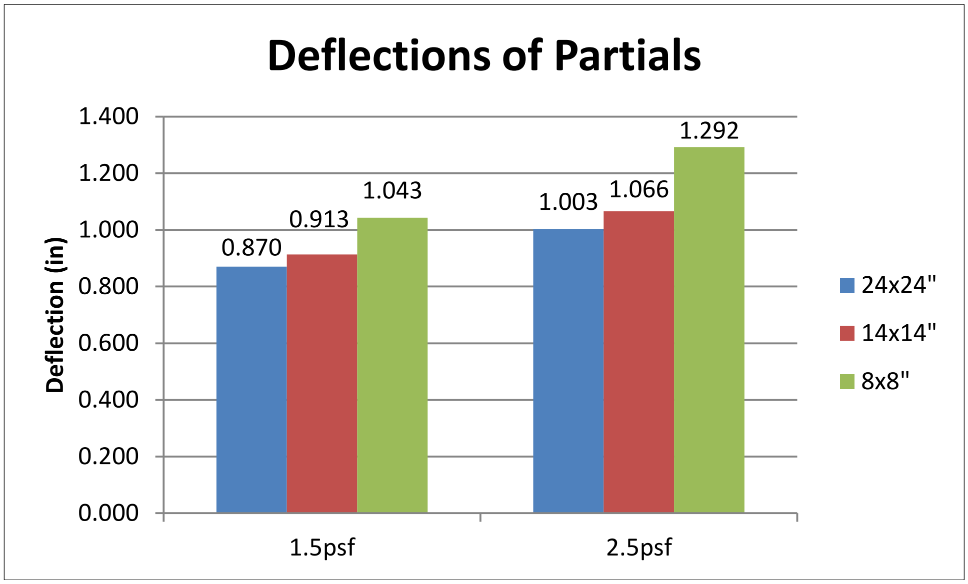

Figure 5-4 Maximum deflection of partial impacted witness plates for each test case

It was observed that when the in-plane dimensions of the panel are decreased the maximum deflection of the material increases. This means that the size of the dynamic cone that is formed during impact deepens as the panel size is decreased.

It can also be observed that larger deflection occurs in the thicker 2.5 psf samples than the thinner 1.5 psf ones. This may seem counter intuitive at first but it should be noted that it is caused because the velocity of the projectile is much higher near the V_{50} of the thicker samples; therefore much more energy is imparted into these samples during the impact event. This difference in energy is between 411 and 463 Joules for the 1.5 psf samples and 933 and 1073 Joules for the 2.5 psf samples as shown in Figure 5-3.

5.2.1.2 Dynamic Cone Width

The widths of the maximum deflected witness plates were measured and the data is displayed below in Figure 5-5. This along with the maximum deflection shows the shape of the dynamic cone. In none of the cases were the dynamic cones wider than the panel size so that case did not have to be addressed.

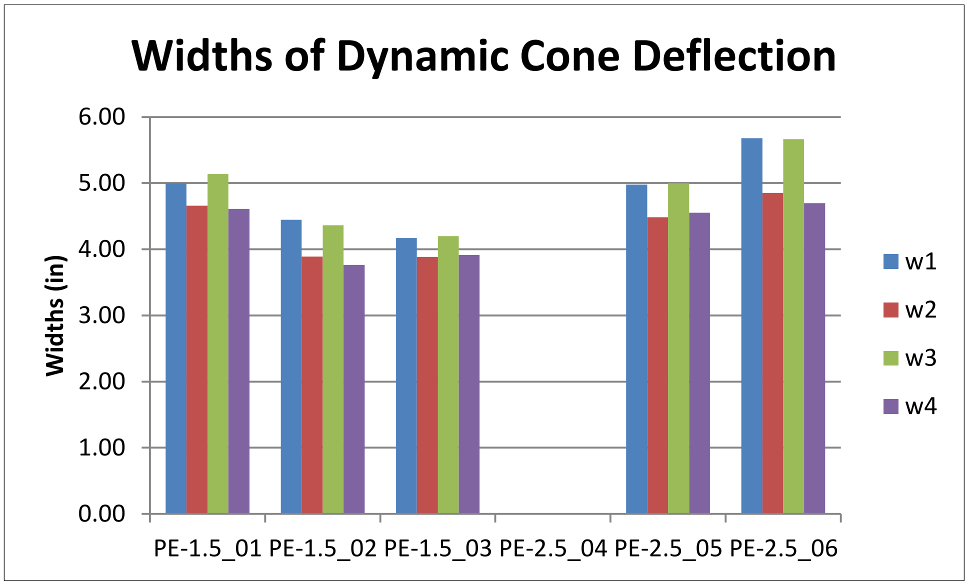

Figure 5-5 Averaged measured widths/diameter from the witness plates (from left to right: 1.5 psf 24x24in, 1.5 psf 14x14in, 1.5 psf 8x8in, 2.5 psf 24x24in, 2.5 psf 14x14in, 2.5 psf 8x8in)

The main observation that was made from the witness widths was that the widths in the w1 and w3 directions were longer than those in the w2 and w4 directions. This seems logical because the w1 and w3 directions are in the primary fiber direction so it would be expected that these regions would be more affected. As with the deflections measured in the witness plate, the larger widths in the measured dynamic cone are caused by the greater amount of energy from the increased velocity to reach the V50 or the thicker samples.

5.2.1.3 Profile Shape

Once the profiles of the dynamic cones were measured a few observations were made. Generally the slope of the cone is linear until the bottom of the cone where it flattens out until the cone ends. Also, at the maximum point of the dynamic cone directly under the projectile there is an extended bulge about a ½ inch wide. The size of the bulge is roughly the same size for each test because it mostly depends on the projectile size (see Figure 4-9 in Chapter 4.2.1). The measured angle of the dynamic cone is displayed below for the maximum deflection for each test set. The complete list of images taken can be found in Appendix B.

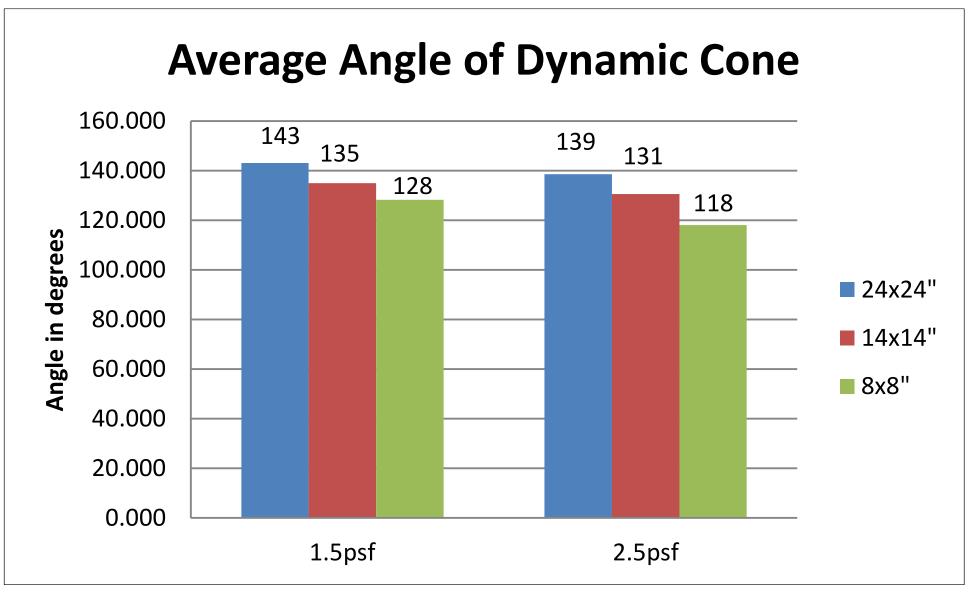

Figure 5-6 Measured angles from witness plate profiles

From these results it can be seen that there is a trend for the angle (recall that the angle is defined at the cone apex) to get smaller as the panel size decreased (i.e. the side slope of the cone is getting steeper). This makes sense because the recorded widths of the witness plates did not show any noticeable trends between each other yet the maximum deflections became larger as the panel size decreased. With a larger deflection and the width remaining the same the included angle at the apex of the dynamic cone would have to decrease. This results in a deeper damage cone that has the same nominal base diameter. Additional work was needed to explain how this was happening.

In the following sections, detailed information on the damage is given first for the 1.5 psf followed by the same data for the 2.5 psf panels.

5.2.2 C-Scanning

The C-scanning gave a way to compare internal damage without having to damage the panel. This shows damage that was only sustained during the impact event. In the following section all of the data collected from the C-scanning is compared and analyzed for the 1.5 psf and then 2.5 psf samples.

5.2.2.1 1.5 psf Samples

The results for the scanning images for the 1.5 psf samples are found below. These were all taken using the Pitch Catch so it shows all of the damage that occurred in the through thickness of the panel. Figure 5-7 shows the general image results for the three different panel size conditions. Complete list of images can be found in Appendix B.

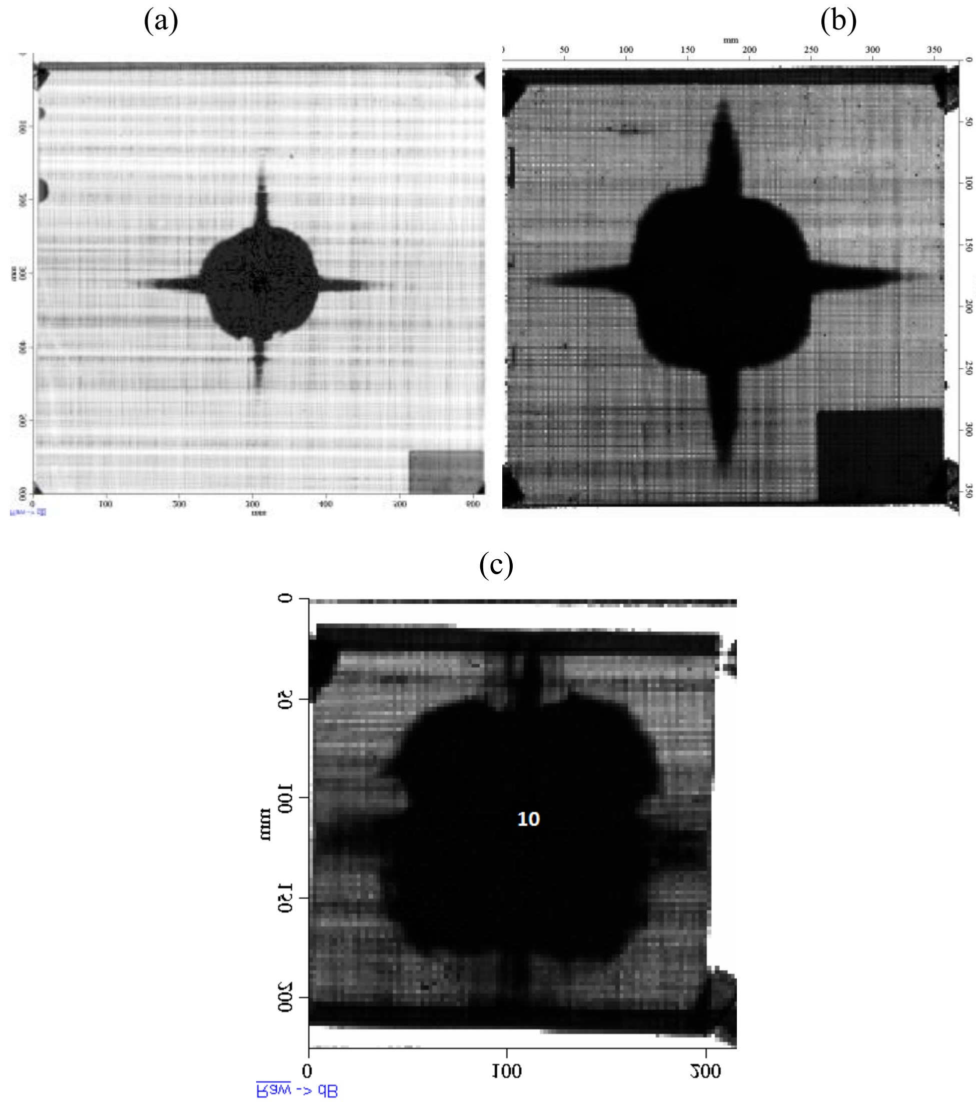

Figure 5-7 Example C-scan of 1.5 psf partial penetration samples at V50 (a) 24x24” PE-1.5_01_10 (b) 14x14” PE-1.5_02_10 and (c) 8x8” PE-1.5_03_10 samples

Once all of the images were taken the different dimensions described in section 4.2.2 were compared against the V_I/V_{50}. The different regions of damage are separated into the circular area and the area of the cross. Comparing how the size of these regions change as the initial velocity is altered will help draw conclusions about what happens during the impact event. This information can be seen in Figure 5-8. The main velocity of interest is when the initial velocity is close to the V_{50}. Figure 5-9 shows the average damage that occurs per region given test samples that were impacted with a velocity within ±5% of the calculated V_{50}. Table 7 below compares the area of the original panel to the total area of damage that is visible in the C-scan.

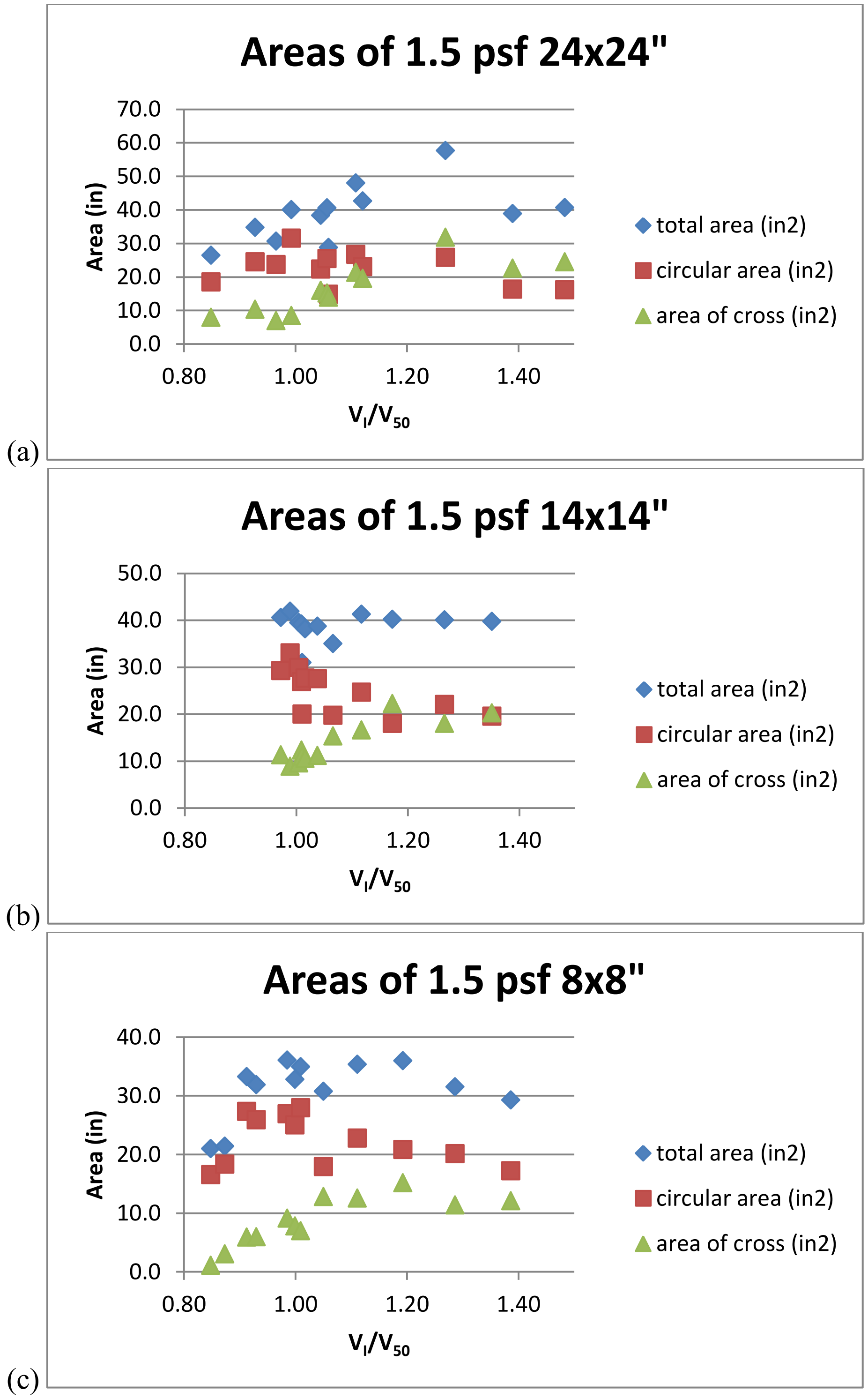

Figure 5-8 Areas of delamination in 1.5 psf (a) 24x24" (b) 14x14" and (c) 8x8" samples

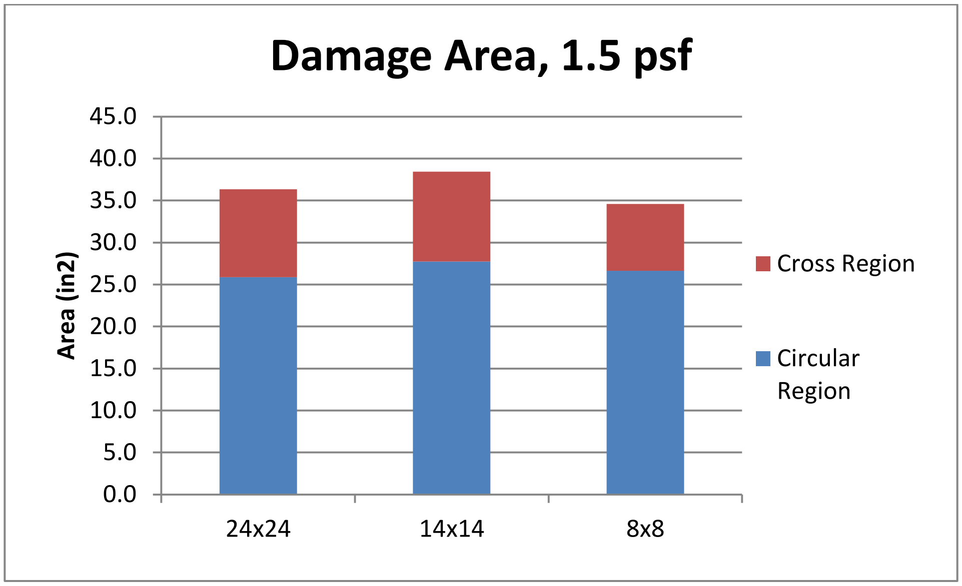

Figure 5-9 Damage Areas of 1.5 psf at V_{50} by region

Table 7 Comparison of damage area to total panel area in 1.5 psf samples

Test	Panel Area (in2)	Damage Area (in2)	% Area Damaged
PE-1.5_01	576	36.3	6.31%
PE-1.5_02	196	38.4	19.60%
PE-1.5_03	64	34.6	54.05%

The information that can be gathered from the C-scan area data for the 1.5 psf case, above in Figures 5-8 and 5-9 is that the area delaminated regions generally stays the same in all three samples when near the V_{50} of the material. The 8x8" case is a little smaller mainly because the delamination reached a free edge and is limited by panel size. The other note of interest is that as the V_I/V_{50} ratio increases the delamination from dynamic cone formation decreases and the delamination from the cross region increases. This trend can be seen in all three panel size cases. The delamination size for both regions increases up until the V_I/V_{50} ratio reaches 1.0. This is generally understood because there is less energy in the projectile for all of these partial penetrations. The maximum damage that is sustained during a partial impact is when the initial velocity is at the V_{50}. Another observation, shown in in Table 7, is that although the area of damage is staying about the same, the relative damage compared to the area of the panel is changing. For the large 24x24in panel less that 10% of the panel's area is affected, but in the small 8x8in panel more than 50% is disturbed.

In Figure 5.10, the damage widths for the central circular damage region (w2 and w4) and the cross region in the primary yarns (w1 and w3) are measured for the 1.5 psf panels of the three panel sizes according to Figure 4-12.

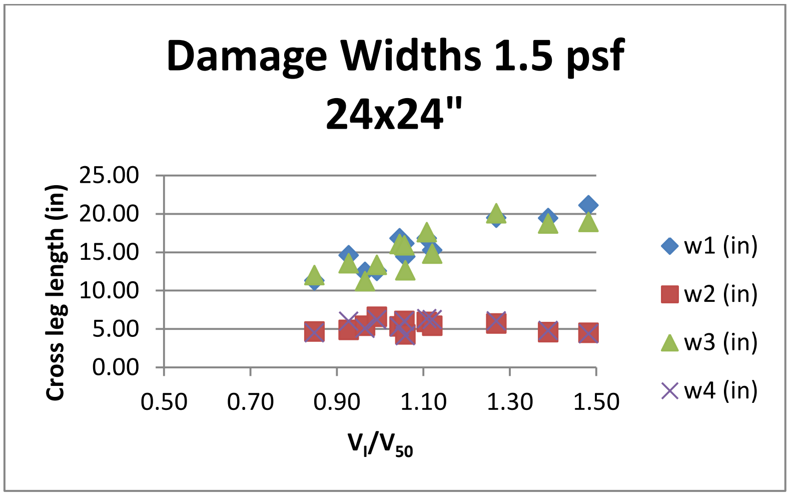

(a)

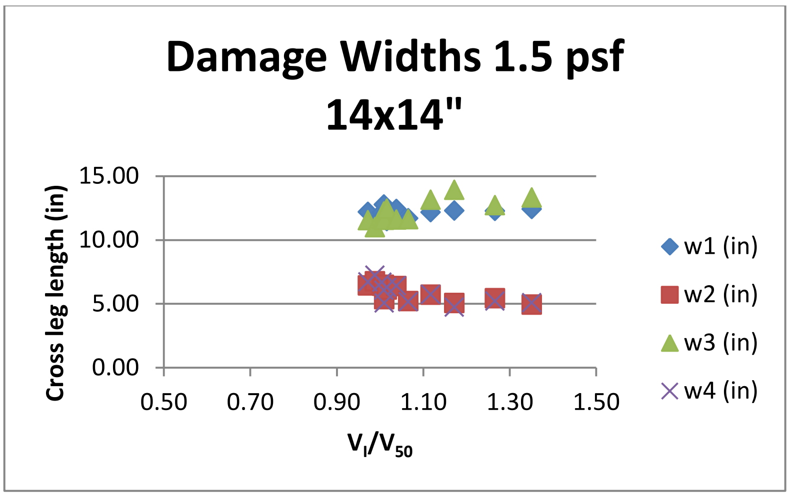

(b)

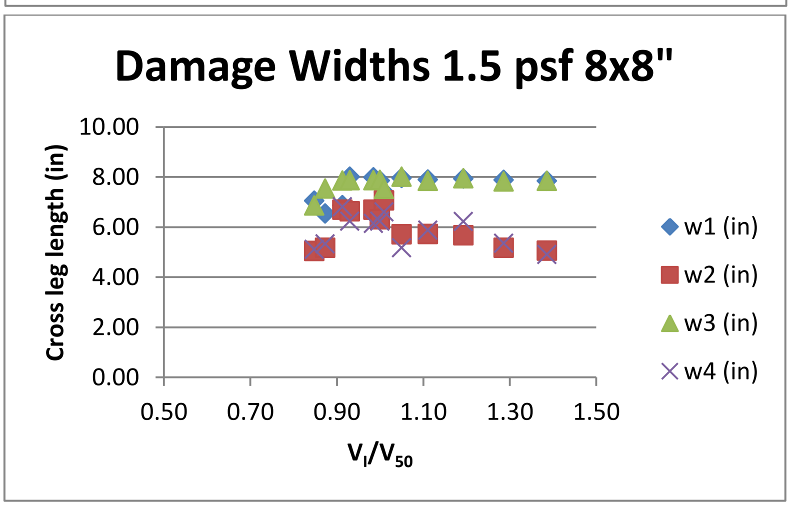

(c)

Figure 5-10 Damage widths of 1.5 psf (a) 24x24” (b) 14x14" and (c) 8x8" samples

The damage sizes in orthogonal directions are most comparable between the widths taken in the circular damage region and the cross damage region. Obviously the cross damage length is larger hence why the w1 and w3 measurements are larger than those in the w2 and w4 directions. Results presented in Figure 5-10 show that the length of the cross damage increases with impact velocity until a plateau is achieved. In the case of the 24x24inch panel the cross delamination arrests within the panel at a length of approximately 20 inches. For both smaller panels the cross lengths propagate to the panel boundary.

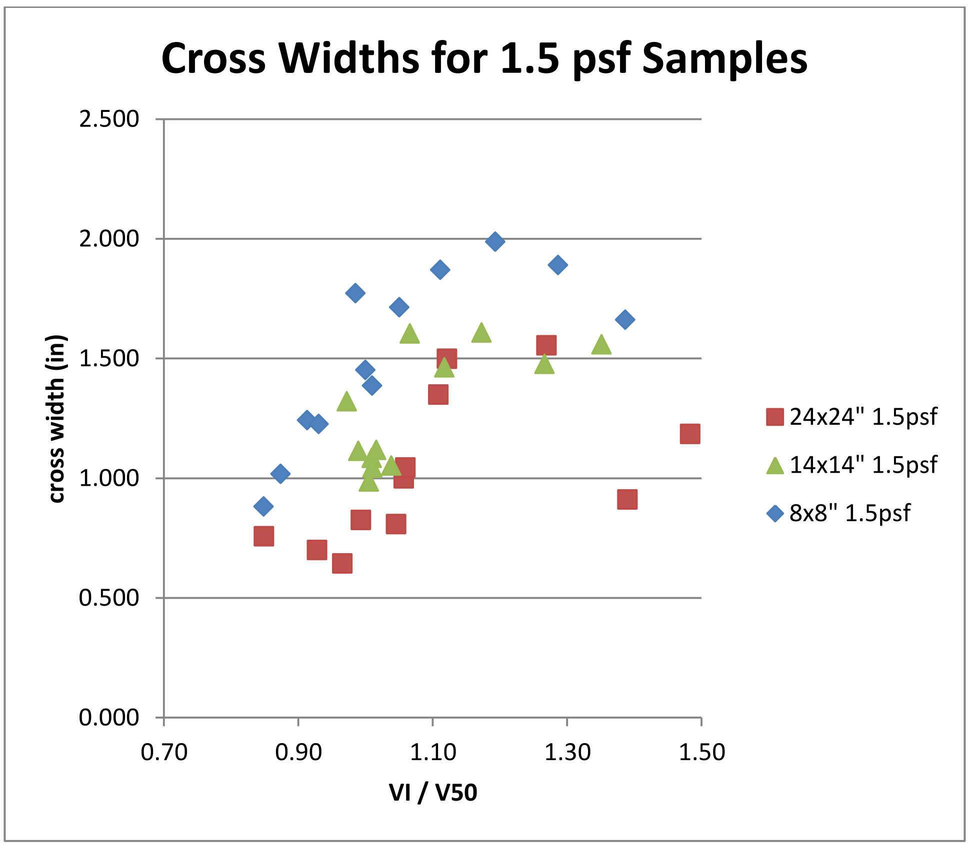

Figure 5-11 Measured cross leg widths from C-scans of 1.5 psf samples (wc1-4)

Additionally the widths of the cross damage legs were measured from each C-scan image. Each sample has four cross legs that were measured (see Figure 4-12). These leg widths were averaged and plotted against the V_I/V_{50} as can be seen in Figure 5-11. This data showed that as the initial velocity was increased the cross width also tended to increase, like the cross area as mentioned previously. This phenomenon also seemed to increase as the panel size decreased. It is also interesting to compare the width of the primary yarns in the cross delamination to the size of the 30 caliper FSP. At the lower range of velocities, the widths are approximately twice the diameter of the FSP and grow to 5-6 times the diameter at a velocity of 1.2 V50 before decreasing at higher velocity. The width growth of the cross delamination is an indication of complex load transfer mechanisms spreading load into the secondary yarn regions.

5.2.2.2 2.5 psf Samples

The same results for the scanning images were done for the 2.5 samples as were done for the 1.5 psf samples. Figure 5-12 shows the general image results for the three different panel size conditions. Complete list of images can be found in Appendix B.

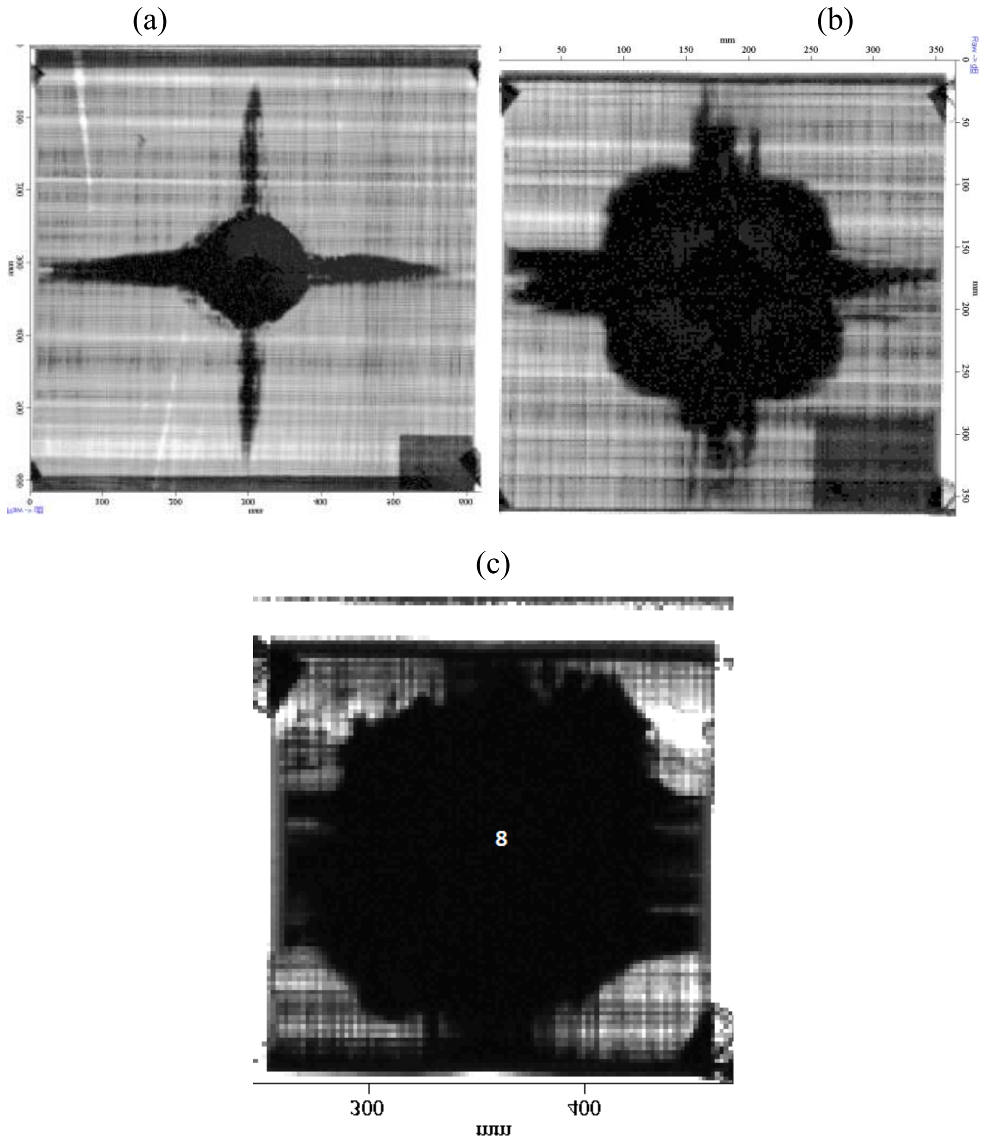

Figure 5-12 Example C-scan of 2.5 psf sample at V50 (a) 24x24" PE-2.5_04_08 (b) 14x14" PE-2.5_05_02 (c) 8x8" PE-2.5_06_08

The same measurements were taken for the 2.5 psf as were done for the 1.5 psf samples and are shown in Figure 5-13 and Table 8.

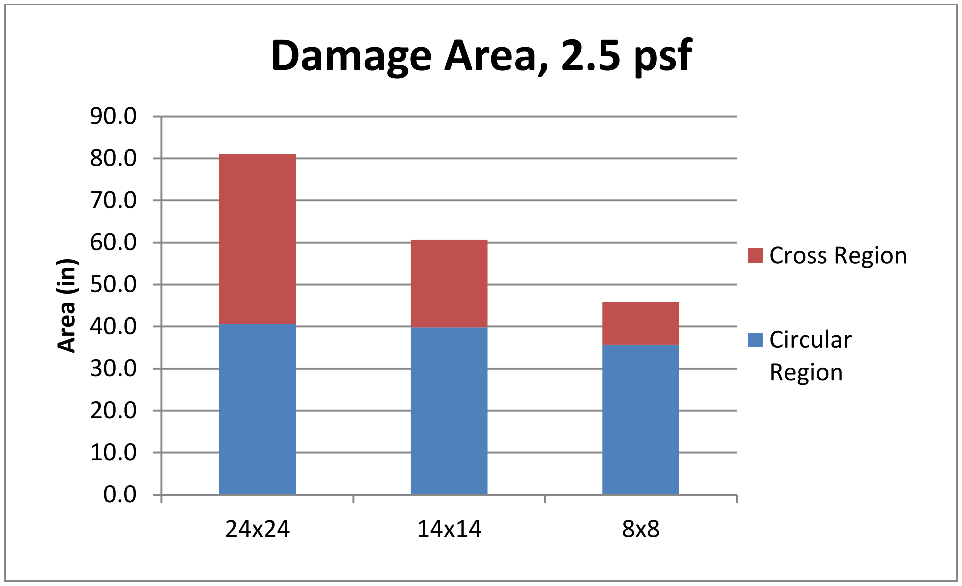

Figure 5-13 Damage Areas of 2.5 psf at V_{50} by region

Table 8 Comparison of damage area to total panel area in 2.5 psf samples

Test	Panel Area (in2)	Damage Area (in2)	% Area Damaged
PE-2.5_04	576	81.0	14.07%
PE-2.5_05	196	60.7	30.95%
PE-2.5_06	64	45.9	71.74%

Similar trends were found in the plots comparing the area of damage against the V_I/V_{50} ratio. For this reason these plots are not here but can be found in Appendix C. The damaged regions in the 2.5 psf samples were larger than that of the 1.5 psf samples. This is because there is more energy imposed on the thicker panels than the thin ones to reach the V_{50} of the material. There are also more layers that can be delaminated during Phase IV of the impact which can dissipate the additional energy. Because the damage propagated farther, the central circular delaminations reached the free edge which decreased the cross damage region for the smaller panels as shown in Figure 5-13. The circular damage region generally stayed the same size with an approximate diameter of 8 inches (equal to the smallest panel size). The decrease in damage in the cross region clearly showed that there is a change in the amount of damage that occurs within a 2.5 psf panel when the panel size is changed.

The width/diameter of the central delamination region and the length of the cross delaminations were significantly different for the thicker 2.5 psf panels compared to the 1.5 psf results. The width/diameter of the central region was approximately equal to the size of the 8x8 in panel. In this panel, cross delamination could not form. In the case of the 14x14in panel, the central region was approximately the same diameter and the cross delaminations were present and extended to the panel boundaries (i.e. w1 and w3 was equal to the panel size of 14 inches). In the large 24x24in panel, the central circular region was same size and the cross delaminations arrested within the panel boundaries with lengths in the range of 19 and 23 inches. Because the damage in the cross region was so high a noticeable trend was not observed relative to an increase of the V_I/V_{50} ratio.

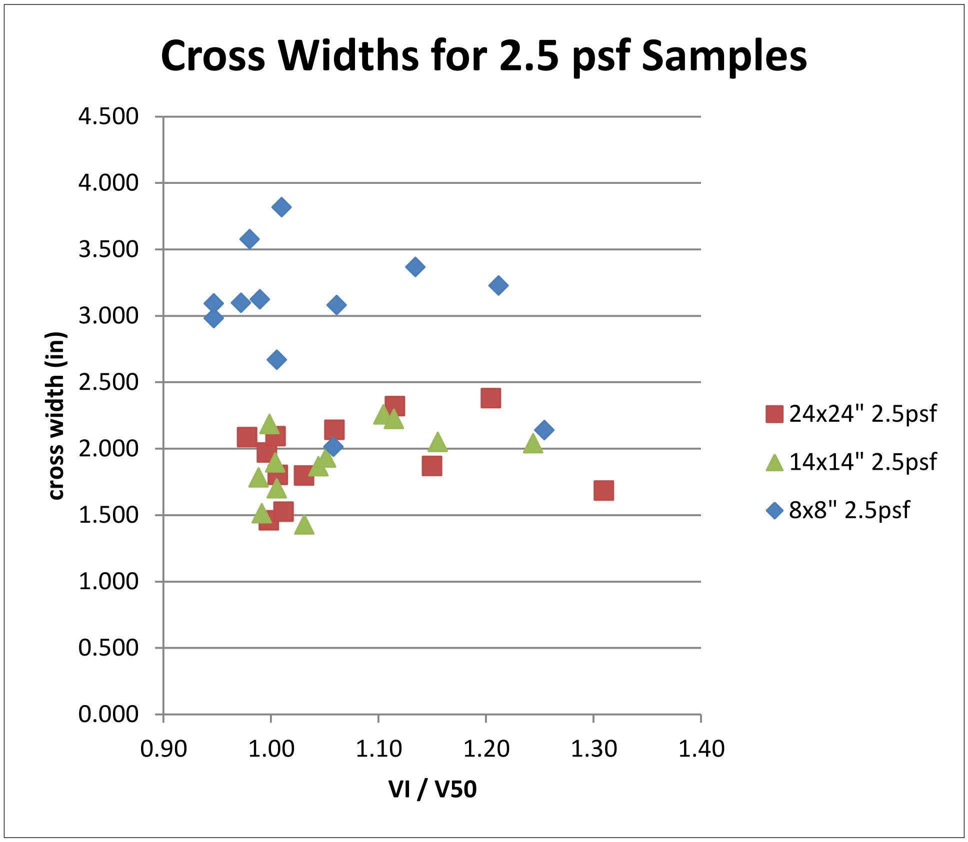

Figure 5-14 Measured cross leg widths from C-scans of 2.5 psf samples

Figure 5-14 shows that the cross widths increased as the panel size decreased for the 2.5 psf samples, similar to the results for 1.5 samples. There also is a noticeable increase as the panel size becomes smaller. Unlike the 1.5 psf samples a trend showing a relationship between cross width relative to V_I/V_{50} cannot be seen.

The image results from the C-scans begin to give more information on how the panel size can causes changes on the ballistic limit of materials. One minor observation was that as the V_I/V_{50} ratio increased the cross delamination length increases as well for the 1.5 psf samples but not noticeable for the 2.5 psf samples as mentioned earlier. The major note of interest is that when the panel size is reduced the cross damage that propagates in the w1 and w3 direction becomes much smaller because it reaches a free edge instead of being able to damage material farther away from the impact site. Because the delamination cannot continue in the w1 and w3 direction instead the width of the cross damage begins to increase. Evidence of this process is shown in Figure 5-14. Regardless of the increased cross widths there is still a significant drop in the areal size of the damage as shown in Figure 5-13 and Table 8. This observation based on projected area of damage through thickness would imply that less material is damaged therefore less energy is being dissipated in the smaller panels resulting in a drop in V_{50}. The results from testing showed instead an increase in V_{50}s for smaller panels so additional damage analysis was conducted to study through-thickness damage mechanisms to gain further insight.

5.2.2.3 Pulse-Echo

The Pitch-Catch method was useful to determine what areas where affected by the impact but it was not useful in knowing how damage propagated in the depth of the panel. Pulse-Echo C-scanning was done to get an idea of where within the panel the cross and circular damage regions were occurring.

(a) (b)

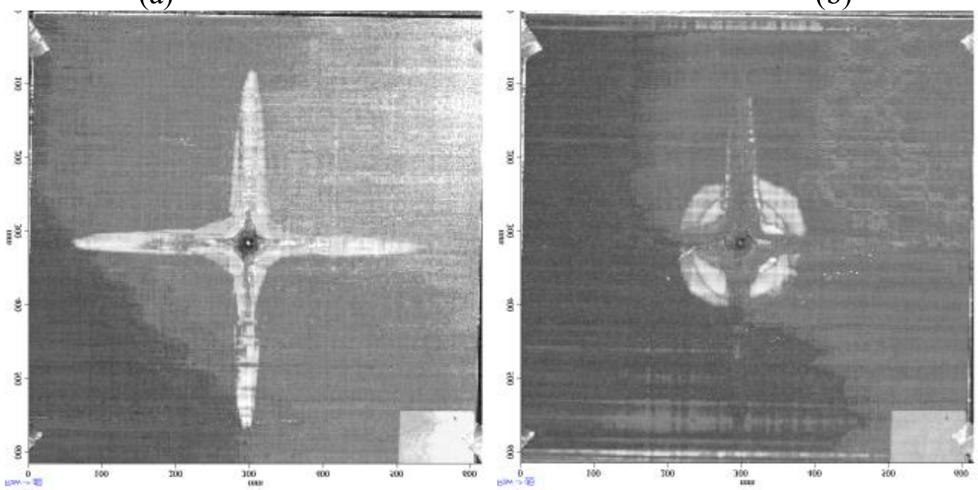

Figure 5-15 Pulse Echo scan of 2.5 psf Dyneema showing both the (a) cross damage region near midsection and the (b) dynamic cone damage region near the backface

In Figure 5-15 the damage in the two different zones can clearly be seen. Scanning was focused on a region that occurred in the mid-plane of the panel and a region near the backface of the material. The resulting images show that the cross damage is entirely localized near the mid-plane of the material while the cross damage caused from the dynamic cone effects on the backface. In Figure 5-15 (b) the image of the cross can be seen blocking out parts of the circular damage region. These regions are damaged but they are blocked by due to a shadowing effect because the signal is delayed when going through the cross damaged region before it reaches the lower damage.

These resulting images gave reason to do in depth analysis on the through thickness damage that occurred within the Dyneema panels. Due to the limited capabilities of the Pulse-Echo C-scanning it was decided that specific samples would needed to be sectioned and analyzed. The next section goes over the results from this analysis.

5.2.3 Cross Sectioning and Dyeing

The cross sectioning and dyeing of the Dyneema was done to analyze the damage cone within the material. The C-scanning was able to show how the damage propagated from above, this method was then used to see it in the cross-section.

5.2.3.1 0/90° Sections

All of the samples that were sectioned were done along the 0/90° direction corresponding to the w3 direction from the C-scanning. This is the direction where the cross delaminations were observed in the C-scans. Also the C-scanning found that these delaminations were found close to the middle of the panel so that is where they were expected to be found. Table 9 and 10 provide details on the panels that were sectioned and dyed.

Table 9 1.5 psf samples selected for 0/90° cross sectioning

PE-1.5_01_##		PE-1.5_02_##		PE-1.5_03_##	
Sample	VI/V50	Sample	VI/V50	Sample	VI/V50
10	0.99	08	1.01	10	1.00
12	1.05	09	1.01	07	1.01
02	1.12	03	1.07	02	1.05
05	1.27	01	1.17	04	1.19
06	1.39	07	1.35	06	1.39

Table 10 2.5 psf samples selected for 0/90° cross sectioning

PE-2.5_04_##		PE-2.5_05_##		PE-2.5_06_##	
Sample	VI/V50	Sample	VI/V50	Sample	VI/V50
06	1.00	10	1.00	01	0.95
11	1.01	08	1.01	04	0.98
01	1.06	01	1.04	12	1.01
04	1.15	03	1.11	02	1.06
10	1.31	05	1.24	03	1.21

Once the sectioned had been dried the damage cone could be plainly seen. The images taken showed a similar hourglass damage shape that occurs in high velocity impacts of most composite laminates. This hourglass comprises of a region close to the strikeface where shear and compression occur in Phase II and III, then tension-shear from Phase IV closer to the backface of the material. There is a general inflection point where this transition will occur and by looking at the images it seemed to shift farther down in the panel as the V_I/V_{50} ratio was increased. This was noticed in the 1.5 psf and 2.5 psf cases and can be seen in Figures 5-16 and 5-17. The 1.5 psf samples do not have as much of the hourglass shape because more of the material failed in tension-shear than in-plane shear because the stress wave hits the backside of the material earlier so Phase III is much shorter.

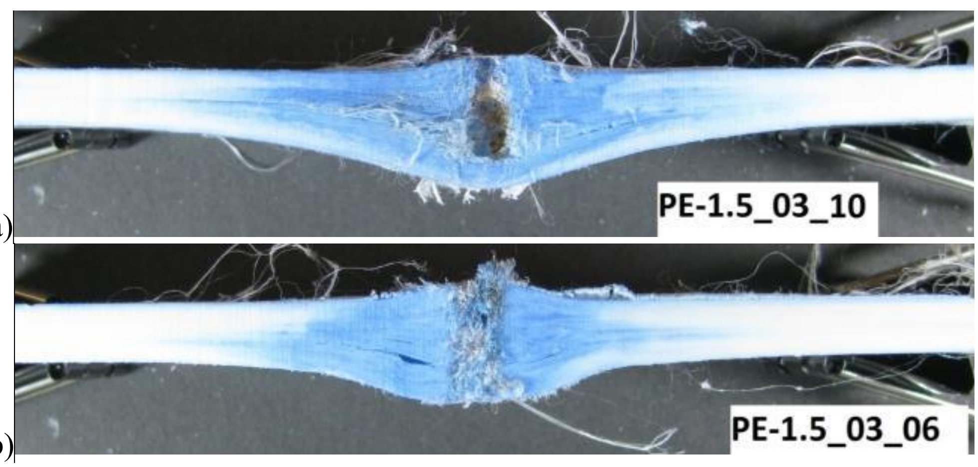

(a)

(b)

Figure 5-16 Cross section of 8x8” 1.5 psf Dyneema showing damage shape between VI/V50 ratios of (a) 1.00 and (b) 1.39

(a)

(b)

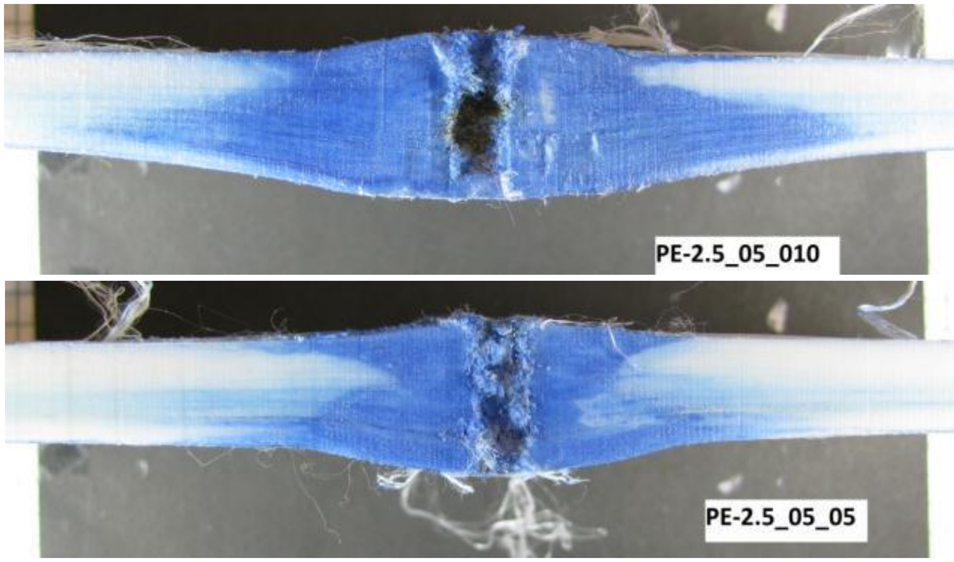

Figure 5-17 Cross section of 14x14” 2.5 psf Dyneema showing damage shape between V_I/V_{50} ratios of (a) 1.00 and (b) 1.24

Another noticeable feature was that the delamination that made up the cross shape in the C-scan imaging was seen also. Sometimes it was faint but the delamination was there and for many cases it reached all the way to a free edge, like in Figure 5-18. The depth in the panel where this delamination occurred also shifted downward as the V_I/V_{50} ratio was increased. For a full list of images see Appendix B. The damage cones for the 24x24” samples appeared no different than the 14x14in samples in either the 1.5 psf or 2.5 psf case, so for this reason their pictures are omitted. The only difference was the distance in the cross delamination which can already be plainly seen in the C-scan images.

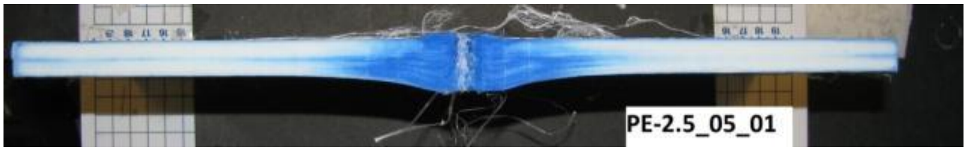

Figure 5-18 Cross delamination propagating all the way to the free edge in a 2.5 psf 14x14" panel.

The smaller 8x8" samples had large gaps between many of the lamina sheets as seen in Figure 5-19. This helps confirm what the witness plates showed which was for smaller test samples, larger dynamic cone formation occurred. This is consistent with the larger deflections for smaller panels that were observed in the witness plates. The smaller panel size allows edge pull-in to occur. It requires less force to pull in the edges than to stretch the primary fibers so more deflection results. More deflection slows the projectile over a longer distance and time, allowing delamination instead of breaking backface fibers in tension-shear. This change in energy dissipation can take the same energy input but change the result from a complete penetration to a partial, thus increasing the ballistic performance of the material.

Figure 5-19 Cross section of 8x8" 2.5 psf Dyneema panel showing gaps between laminas

5.2.3.2 +/- 45° Sections

In addition to the 0/90° direction, cross sections were made in the +/- 45° directions, specifically along the w2 direction. This was a region that was completely composed of secondary fibers. Due to the large cross delaminations it was expected that the damage in the +/- 45° direction would appear differently than in the 0/90° direction. For this reason some additional samples were sectioned and dyed to observe the damage that occurred in this region. The materials that were selected for sectioning in this direction were the samples already sectioned in the 0/90° direction that were 8x8". This was chosen because no damage ever propagated to a free edge in the +/- 45° direction therefore there would be little difference from the other panel sizes.

The resulting images, like the one in Figure 5-20, showed similar damage regions as seen in the 0/90° images. The only major difference is that the damage does not propagate as far and there is no large delamination layer that created the cross damage in the primary fiber direction. This was to be expected because the images from the c-scan did not show damage propagating as far away from the impact site as in the primary fiber direction. It was found that there was only one case where any delamination reached a free edge of the material in either the w2 or w4 direction. The one case where it occurred was where the two cross delaminations grew wide enough that one corner delaminated completely.

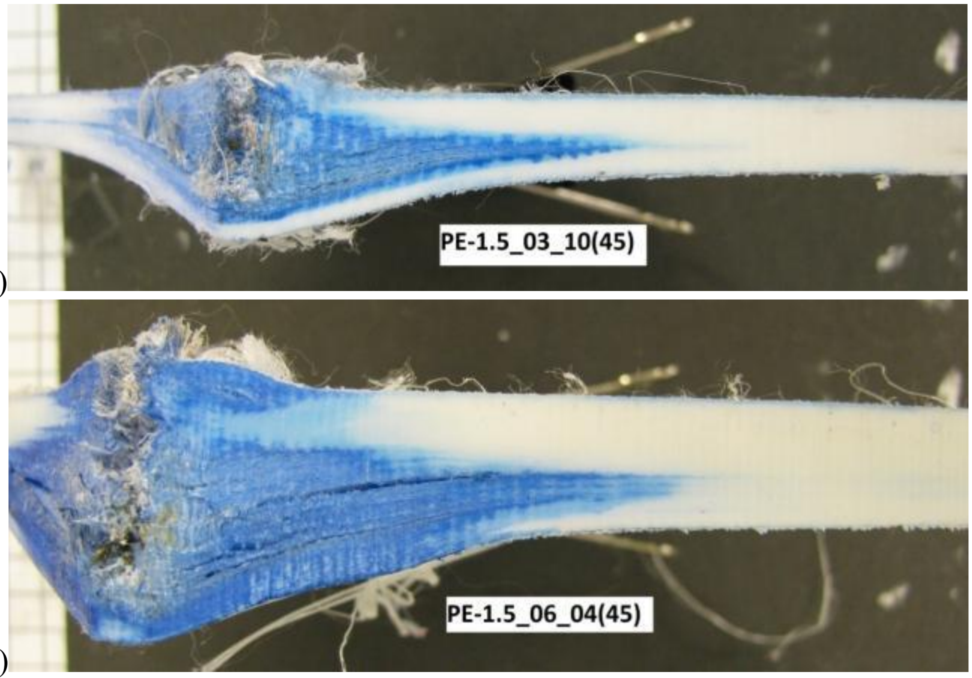

(a)
(b)

Figure 5-20 Cross section of 8x8” (a) 1.5 psf and (b) 2.5 psf Dyneema samples in the +/- 45° direction

The major observations made from the cross sectioning are as follows. There were similar damage cones that occurred in both of the 1.5 psf and 2.5 psf samples. The major difference being that the size of the damage cone is larger in the thicker samples because the applied energy from the projectile is much higher thus creating more damage. The other note of interest is that the thinner 1.5 psf samples were mostly failed in tension-shear as opposed to the 2.5 psf samples which had a noticeable region where only shear occurred. As the initial velocity increased the inflection point in the material was shifted lower in the thickness of the panel. This shows that the initial velocity of the projectile also contributes to the location of the inflection point within the panel.

A major find with this analysis was finding the cross delamination that occurred. The delamination which made up the large cross shapes in the C-scans turned out to be caused from only one or a few interlaminar delaminations that stretched far from the impact site. In the smaller panels where the delaminations reached a free edge it appeared to pull in some of the material. Additional measuring was done to see how this pull-in compared between panel sizes. The nature of how the delamination between and within the laminas was also of interest so it was investigated and will be discussed further.

5.2.4 Edge Pull-in

In all of the 14x14" and 8x8" test cases cross delamination reached a free edge of the material for some or all of the samples. This created a region where material below the damaged lamina would pull-in due to the movement of the primary fibers in the dynamic cone. The three measurements that were used to categorize this damage were the distance that the material pulled in from the edge, the depth that the delamination occurred in the panel as a percentage of the overall thickness, and the width of the delamination that was seen on the edge of the panel. These can be seen below in Figure 5-21.

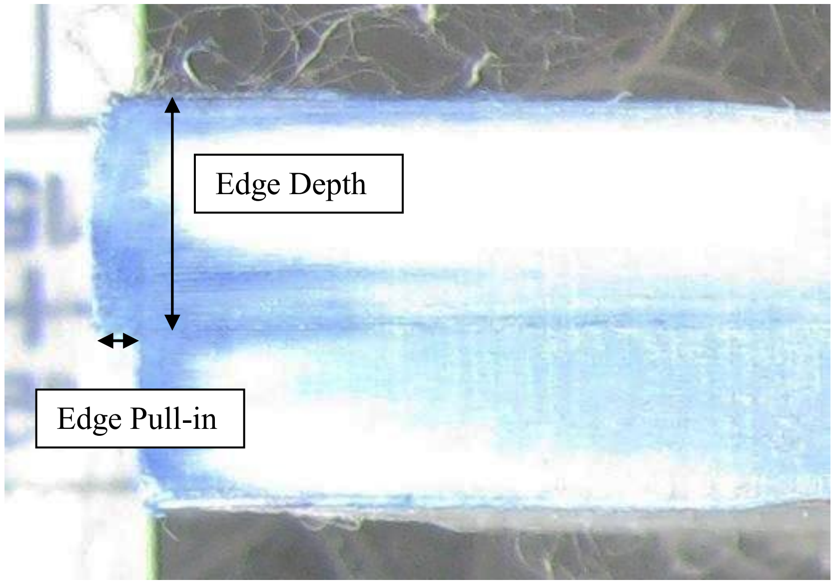

Figure 5-21 Measurements taken for edge pull-in as seen on a sectioned panel (width of delamination measurements are not seen here but was measured from edge of un-cut panel)

When the cross delamination reached the edge sooner the damage would spread causing the width of the cross damage to become wider and allow the edge to pull in even more. How this damage compared between areal densities and panel sizes was a subject of interest.

Measurements of the edge pull-in were taken and averaged, as seen in Figure 5-22. There was no measurable edge pull-in for either of the 24x24" cases so those do not appear in the Figure 5-22. The data shows that edge pull-in did occur in the other four test sets and that as the panel size decreased more edge pull-in was present. Additionally, more edge pull-in occurred in the thicker samples than in the thinner ones.

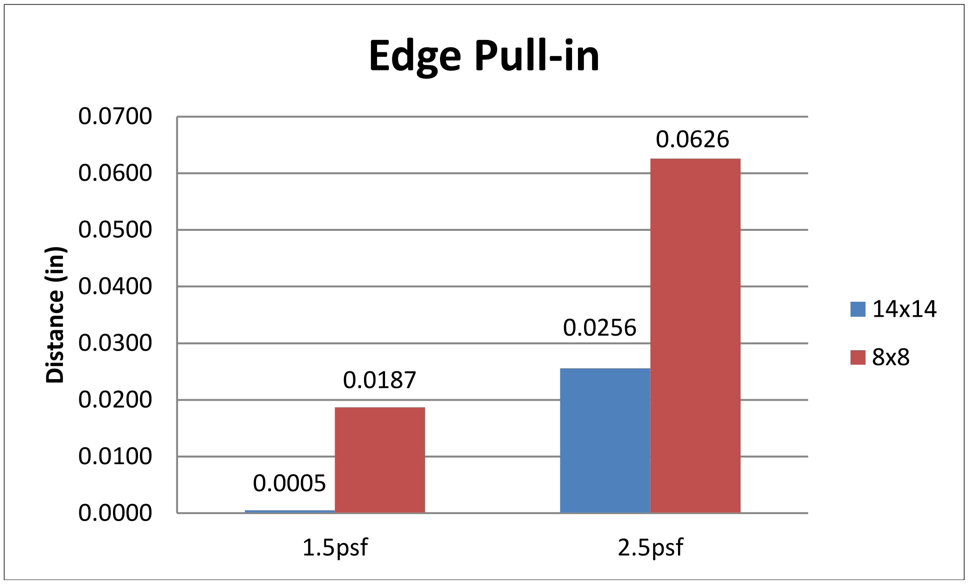

Figure 5-22 Average measured pull-in distance of Dyneema panels

Figure 5-23 shows the depth as a percentage of the panel thickness from the strike face that the pull-in occurs vs. the V_I/V_{50} ratio. The 1.5 psf samples showed fairly inconsistent results with edge pull-in occurring in the range of 30-60% of the thickness for both panel sizes. However, in the 2.5 psf samples it was seen the depth of edge pull-in increased linearly with increasing impact velocity. At the highest velocities (1.2 V50) edge pull-in occurred at 70% of the thickness strike face for both panel sizes. At V50, the depth of the edge pull-in was notably higher for the 8x8in panel (60%) than the 14x14in panel (50%). It was mentioned earlier that the inflection point of the damage cone shifted downward as well so these deformation modes appear related. As the V_I/V_{50} ratio increases above 1.0 more laminas are broken in compression-shear and fewer in tension-shear.

(a)
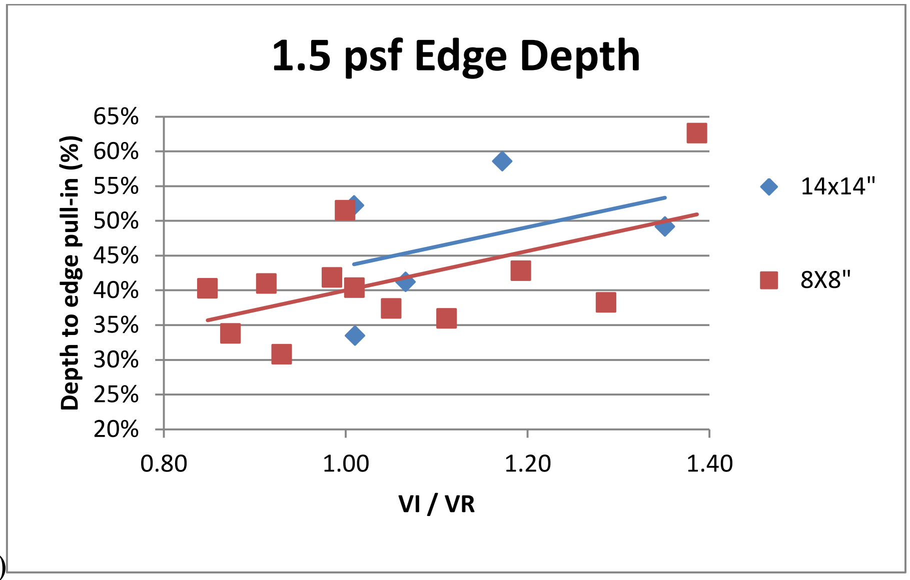

(b)
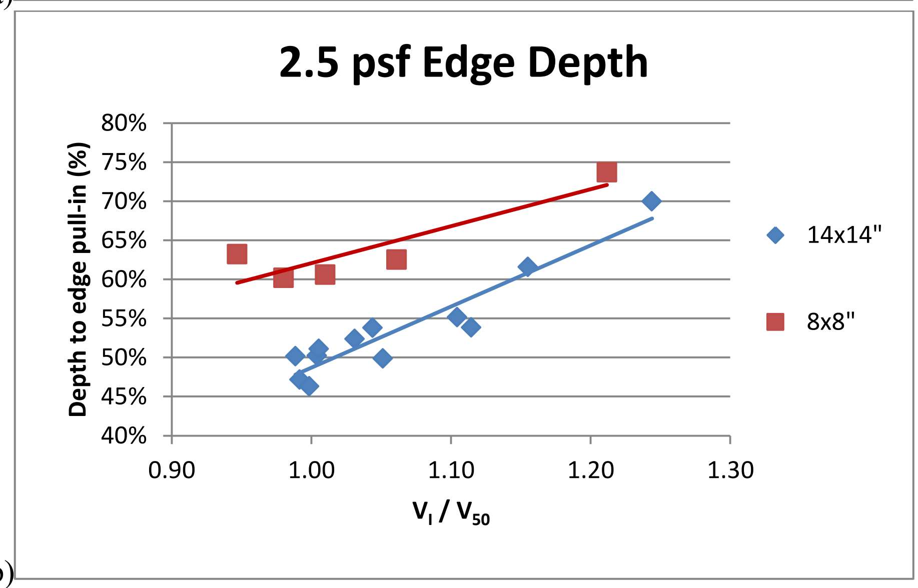

Figure 5-23 Depth that edge pull-in occurred as a percentage of total thickness in (a) 1.5 psf and (b) 2.5 psf samples

The width of the delamination visible on the edge, as seen below in Figure 5-24, showed a trend for increasing as the V_I/V_{50} ratio increased. This corresponds similarly with the cross delamination widths from the C-scan images that were discussed earlier. This makes sense because this damage is the same except one is only visible from C-scanning while the other is visible once the delamination reaches a free edge.

(a)

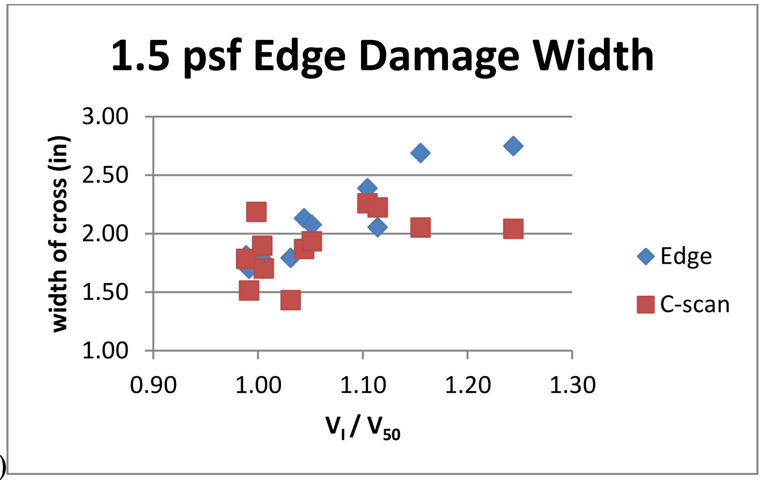

(b)

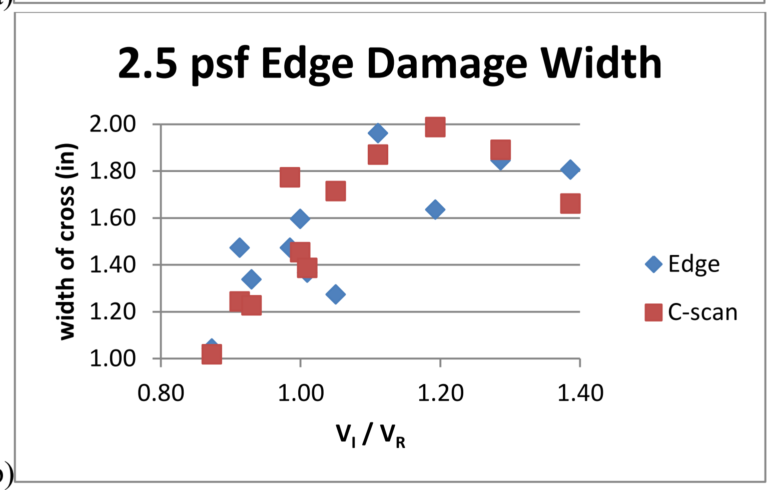

Figure 5-24 Width of the delamination at the free edge in (a) 1.5 psf and (b) 2.5 psf samples

The main observation made from measuring the edge pull-in was that the thicker and smaller the panel became the more edge pull-in would occur. This can explain where the additional material came from in order to create larger deflections in the dynamic cone for the smaller panels. Another question that still has not been answered is where and how were the microstructures of the lamina failing. Additional microscopy and SEM work was done to determine where the delaminations went in the laminas.

5.2.5 Microscopy

Microscopy was performed to look at the cross section of the material up close to see the crack propagation paths caused by interlaminar delamination. If done properly with Dyneema the resulting images should show the 0/90° fiber orientation and the cracks that make up the interlaminar delamination. All of the samples were taken in the w3 direction corresponding with the C-scanning.

5.2.5.1 Undamaged Sample

First imaging was done on an undamaged sample so that comparisons could be made to the impacted samples. The images taken of a region of undamaged samples, like in Figure 5-25, clearly shows the different 0 and 90° laminas that were stacked and consolidated using compression molding. Due to the difficulty to cut Dyneema the resulting images were not as clear as they would be with other stiffer fiber/matrix systems. This is why the fibers in the 0° are especially difficult to see. During polishing many of the fibers are deformed or pulled out which result in poor image quality. It was also noticed that the laminas had some waviness associated with them and did not have uniform thickness.

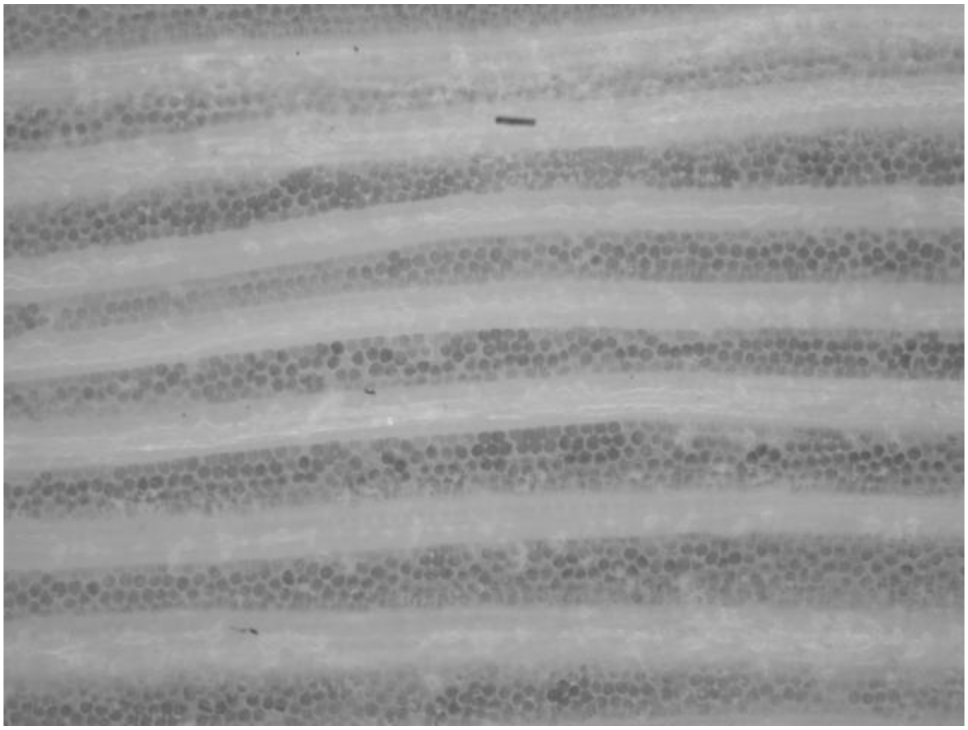

Figure 5-25 Cross section of undamaged Dyneema at 100x magnification

5.2.5.2 Damaged Samples

In the following sections where imaging was done on damaged panels, samples were taken from a number of different locations. These locations will be described in this section. When close to the impact site many layers had delaminations so a single sample of material could be separated along multiple delamination planes. There were three major zones in the through thickness that were of interest; close to the strikeface of the material, along the major delamination that caused the cross damage, and near the backface of the material. These areas can be seen in Figure 5-26(a). The main sample was pulled apart near these zones and the natural separation occurred at the weakest bonded layer. Samples were also taken far from the impact site as can be seen in Figure 5-26(b).

(a)

(b)

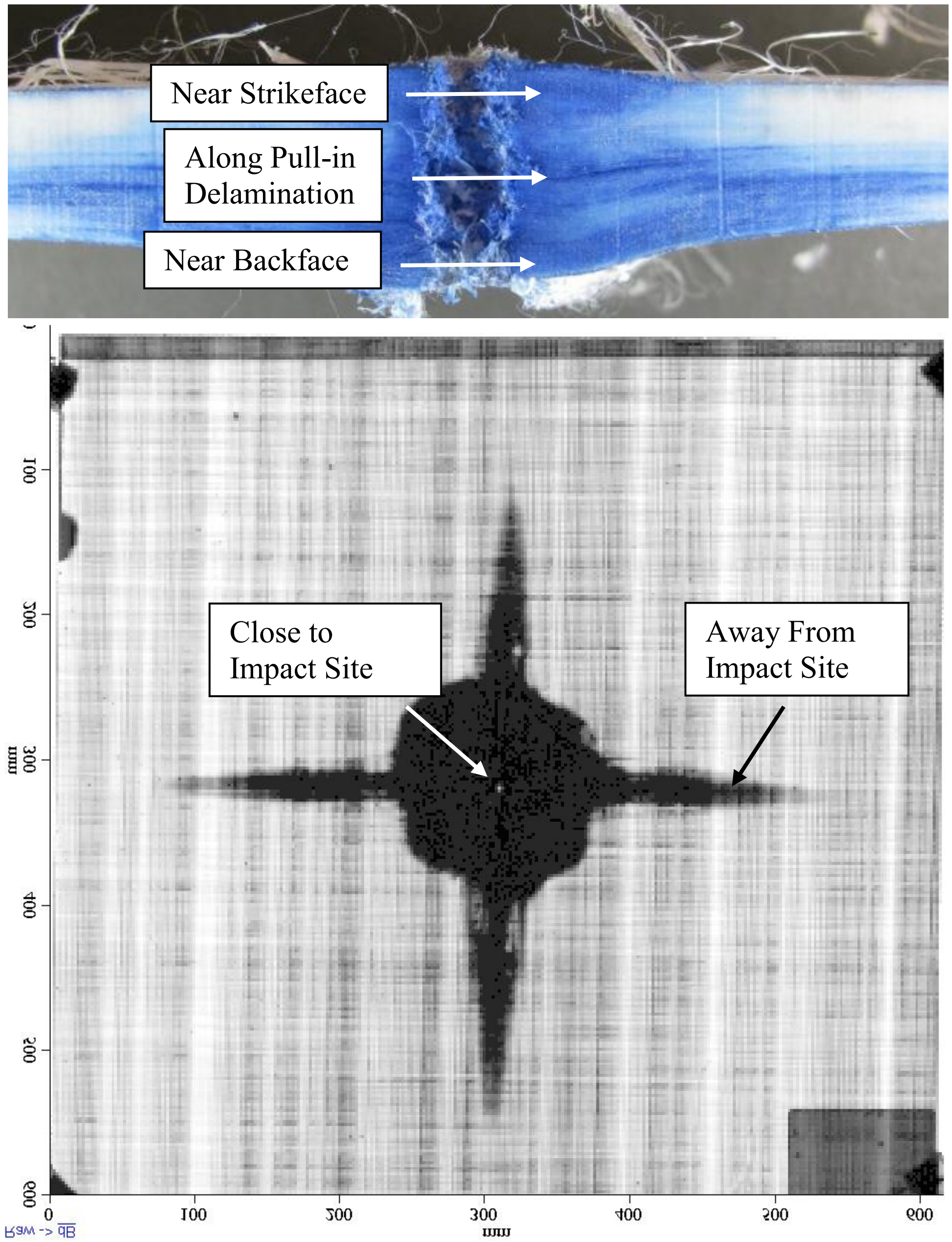

Figure 5-26 Locations of Microscopy and SEM samples in the (a) through thickness and (b) the surface of the panel

Figure 5-27 is a damaged sample taken near the strikeface of the panel directly under the impact site. The microscopy samples that were prepared on damaged samples had similar issues to the undamaged samples only amplified. Due to the voids created during the delamination, the fibers were more prone to deforming instead of being cut during polishing. This resulted in images like that of Figure 5-27 which on the right side becomes very difficult to distinguish between the 0° and 90° laminas. Looking at the change in image quality and the fibers moving up and away on the right side in Figure 5-25 it shows that the delamination is growing in that region because the sample was unable to polish and instead the fibers smeared.

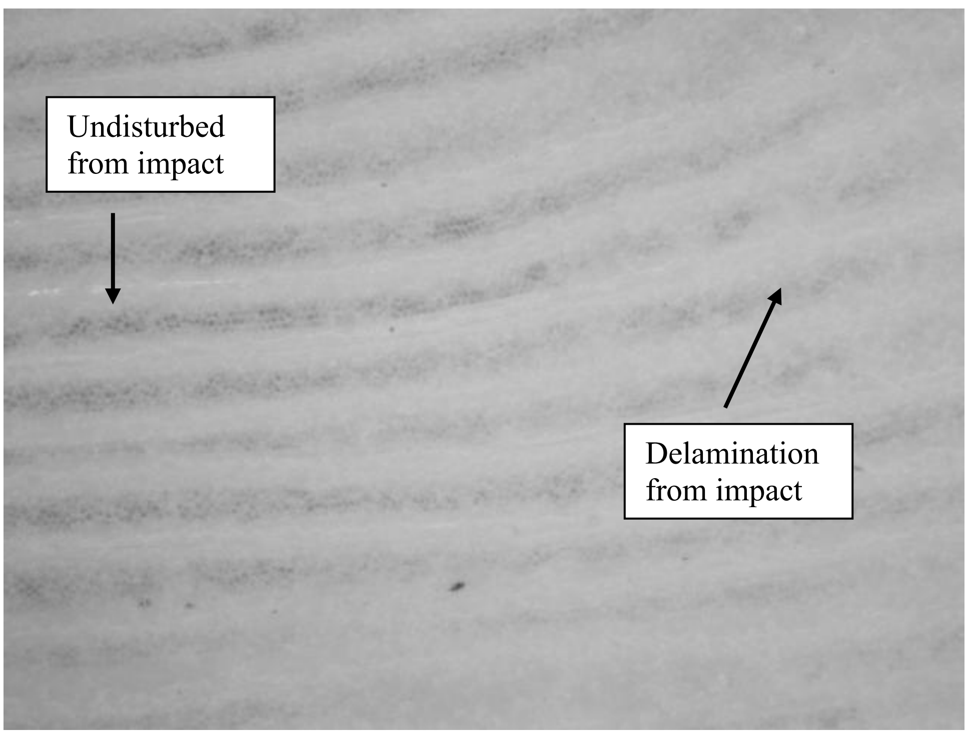

Figure 5-27 Cross section of damaged Dyneema near the strikeface at 50x magnification

Larger cracks, like the one in Figure 5-28, make up the start of the cross delaminations that propagate far away from the impact site. The delaminations were easily noticeable but it was impossible to determine if the delamination occurred within a lamina, between laminas, or both. Initially microscopy was going to be used as the primary method for micro-scale damage analysis but after working with the material it was realized that other methods may be better suited for damage analysis.

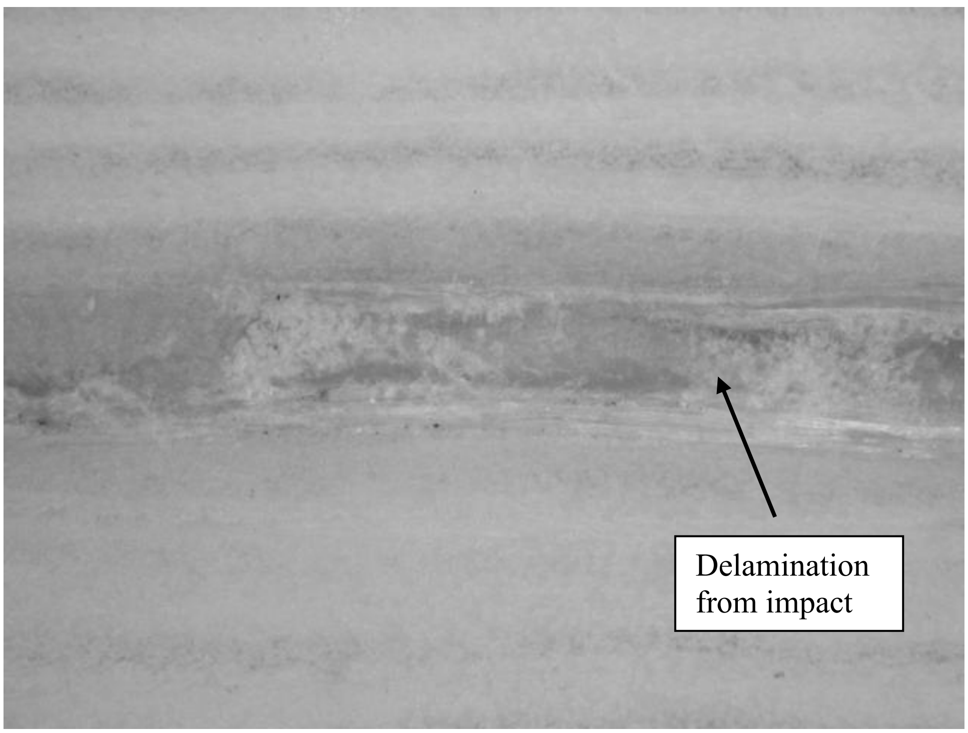

Figure 5-28 Cross section of damaged Dyneema along major delamination plane at 50x magnification

5.2.6 SEM

After microscopy did not make for a viable method for analyzing all of damage to the microstructure of the material SEM imaging was used in addition. This method looked at the surface of laminas instead of the cross section of the laminate like in the microscopy images.

5.2.6.1 Undamaged SEM Imaging

To know how the material reacted to an actual impact, one sample was manually delaminated for comparison purposes. This was done by taking an intact piece of material, cutting a small notch with a band saw, and separating the sample with a thin wedge under primarily Mode I peel loading. This was done generally in the mid-thickness of the material. The laminas would separate at the weakest point which was suspected to be between laminas. Given that the sample separated easily and carefully it was assumed that limited damage was done to the viewing surfaces (compared to impact loading).

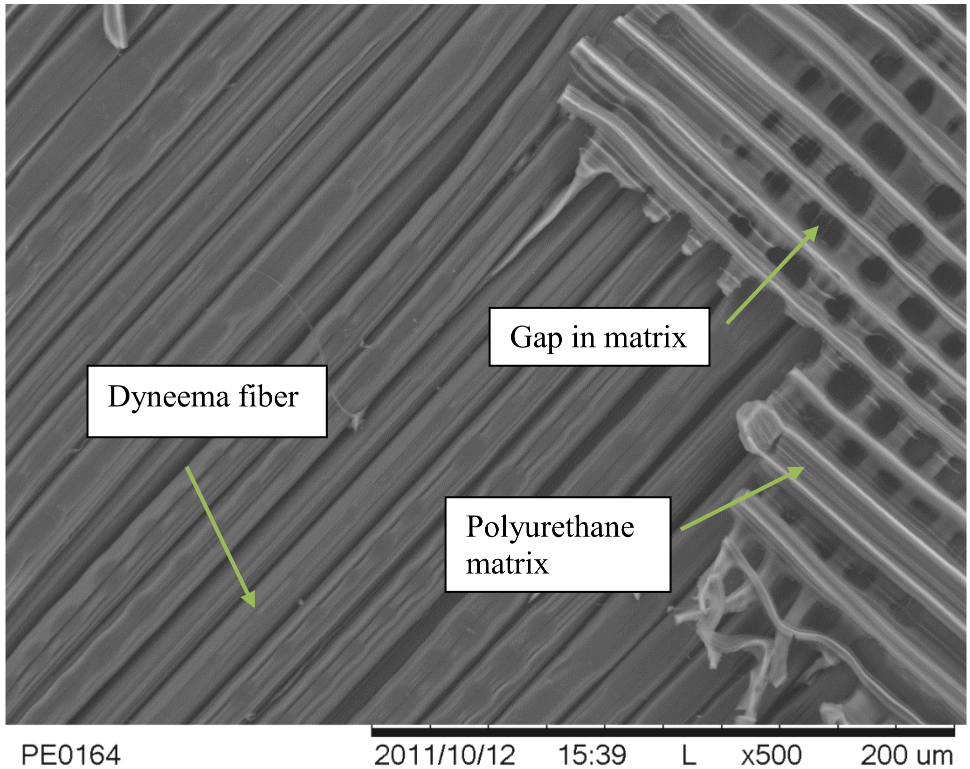

Figure 5-29 Non-impacted manually delaminated Dyneema sample

A number of different observations should be made from Figure 5-29 for future reference when comparing other SEM images. Figure 5-29 is a top down image of a separated sample between two laminas. The majority of the image on the left is made of undamaged tightly packed unidirectional fibers in the 0° direction that have no matrix on them. On the right the matrix can be seen because on that side more matrix remained on this lamina while on the left the matrix remained on the other lamina surface that was removed. It is easy to tell that the separation occurred between laminas because on the remaining matrix valleys can be seen running perpendicular to the fibers on the left. The valleys are where the 90° fibers from the other lamina were before being separated. The question of which lamina the matrix remains will become a major focus in future sections so it should be well understood that the matrix will remain on the fibers on one lamina or the other. In the undamaged case the matrix did not stay on one lamina or the other. This observation will be used later to determine Mode I cracking.

It can be observed that the fibers and matrix separate cleanly. This shows that the adhesion between the fibers and matrix in the laminate are very weak and would. It was observed through all of the imaging done that there was a tendency for separation between the matrix and fiber and not within the fiber or within the matrix.

As discussed earlier the Dyneema HB-26 laminates are made up of sheets that are 4 plies of Dyneema laminas. Throughout the damage analysis process no evidence was found that the laminas delaminated any easier between these sheets or between the laminas within the sheets. The processing of the Dyneema HB-26 laminate made the lamina interfaces basically uniform.

Another observation made in Figure 5-29 is that there are gaps in the matrix where the fibers were directly contacting each other with no matrix in between. This contact between the fibers also created deformation in the form of fiber denting which was covered earlier in section 3.2.1. It should be noted that when fibers are in direct contact with each other there is less matrix to provide load transfer. This is why delamination occurs generally at the interfaces between laminas instead of within laminas.

5.2.6.2 SEM Imaging of Damaged Material

The samples from delaminated regions were taken from multiple sections. Some samples were from the cross delamination while others were in regions where dynamic cone formation occurred. Most of the samples and images were taken from primary fiber regions. Any samples that were taken that contained secondary fibers will be noted. Use Figure 5-26 as a reference of where a specific sample was taken in the panel. All of the samples have the primary loading direction in the w3 direction. This means that all of the images with fibers running horizontally were primary fibers and any fibers running vertically were secondary fibers.

The imaging that is discussed in this chapter was to determine what crack paths the delamination took. Cracking could have spread through the panel along the fiber / matrix interface or cohesively within the matrix. Another interest was if the cracking was only between laminas or within them as well. The last interest was if the cracks tended to travel along the primary fibers in the 0º direction.

The sample taken near the strikeface underwent more compression due to the projectile pushing material out of the way and creating a shear plug. It was noticed that the fibers and matrix were not very affected at all. The matrix tended to stay on one lamina, in this case the side closer to the backface. This is shown in Figure 5-30.

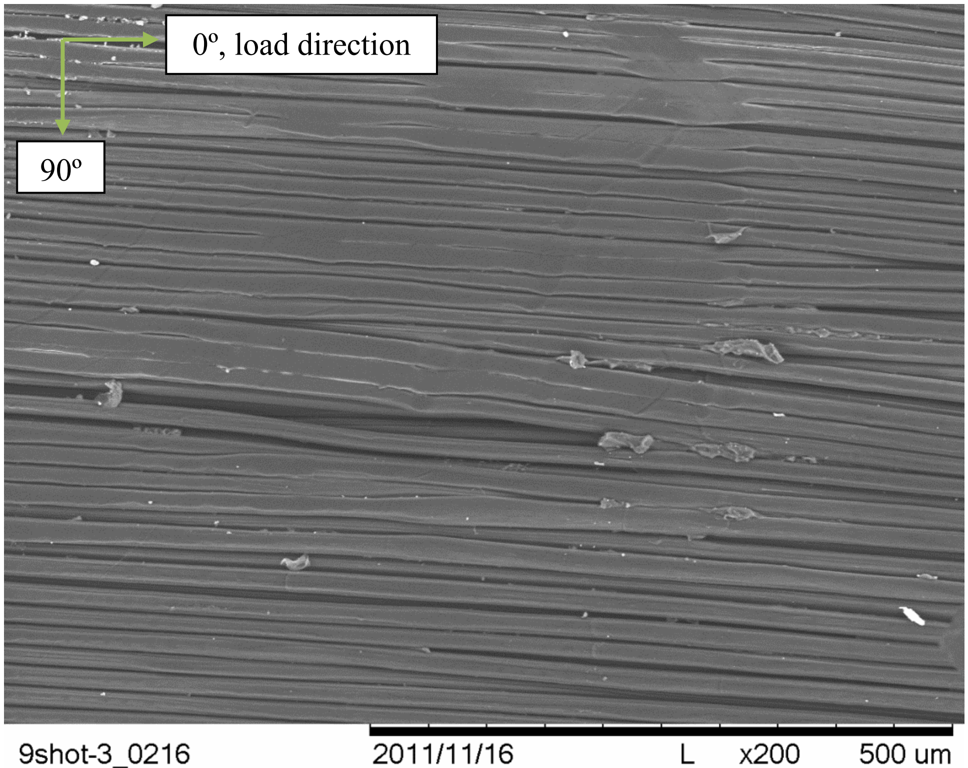
0º, load direction
90º
9shot-3_0216
2011/11/16
L
x200
500 um

(a)

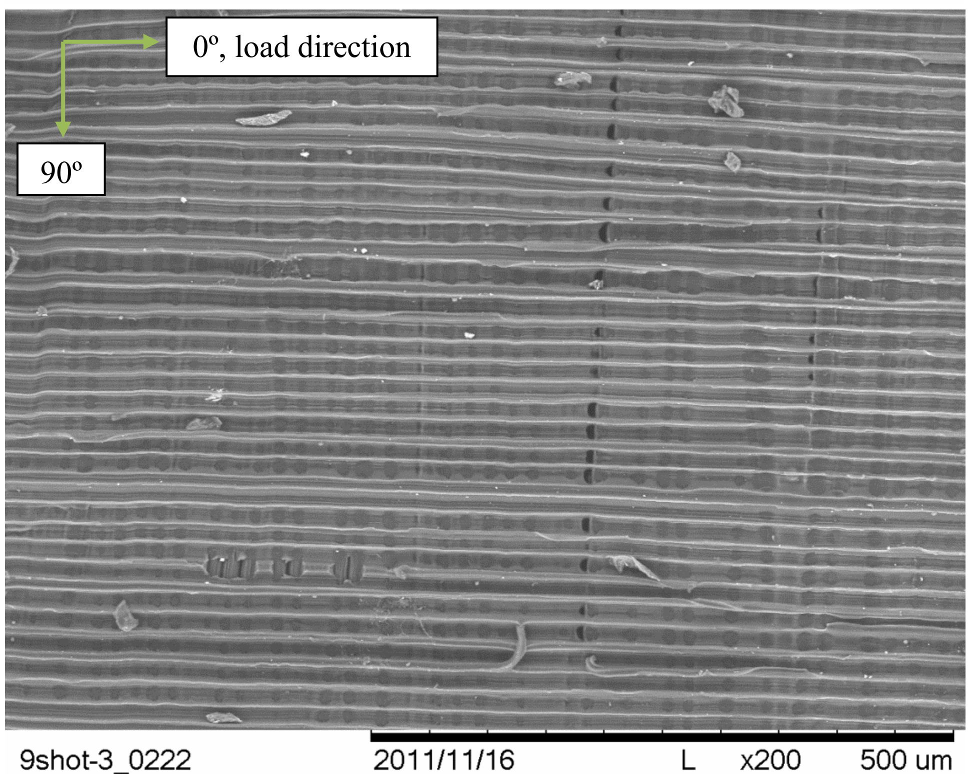
0º, load direction
90º
9shot-3_0222
2011/11/16
L
x200
500 um

(b)

Figure 5-30 SEM of Dyneema close to impact site, close to strikeface. (a) strikeface (b) backface

The next delamination that was observed was one that occurred along the pull-in delamination, see Figure 5-26. Because this is less than 1.0 inch from the impact site there is excessive amount of deflection from the dynamic cone formation. This should mean that the failure occurs in mode I. As the delamination moves farther away from the impact site it should transition into mode II, which is covered later.

Images that were taken from this region, like seen in Figure 5-31 show that the matrix was not left cleanly on one lamina. Instead the distribution of matrix is random and appears on both the 0º and 90º laminas, which signifies that this region underwent mode I cracking. Another observation is that there are more cases where cracks transfer between laminas as can also be seen in Figure 5-31. Additionally, there are some regions where entire laminas begin to separate due to the matrix cracking. This can be seen in Figure 5-31 (a).

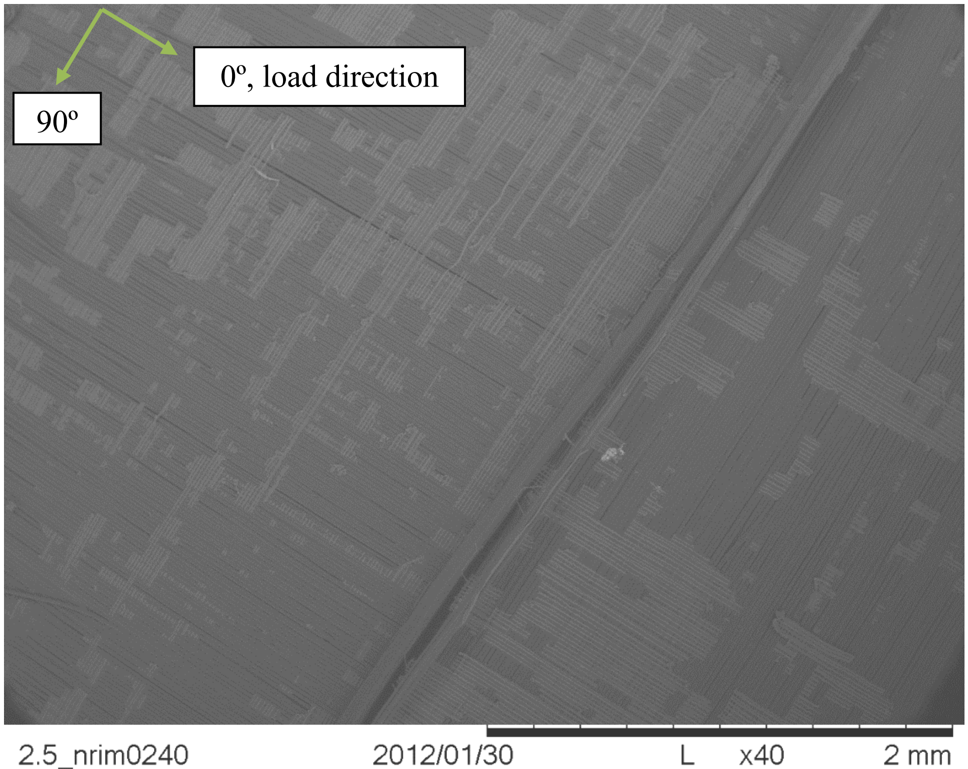
0º, load direction
90º
2.5_nrim0240
2012/01/30
L
x40
2 mm
(a)

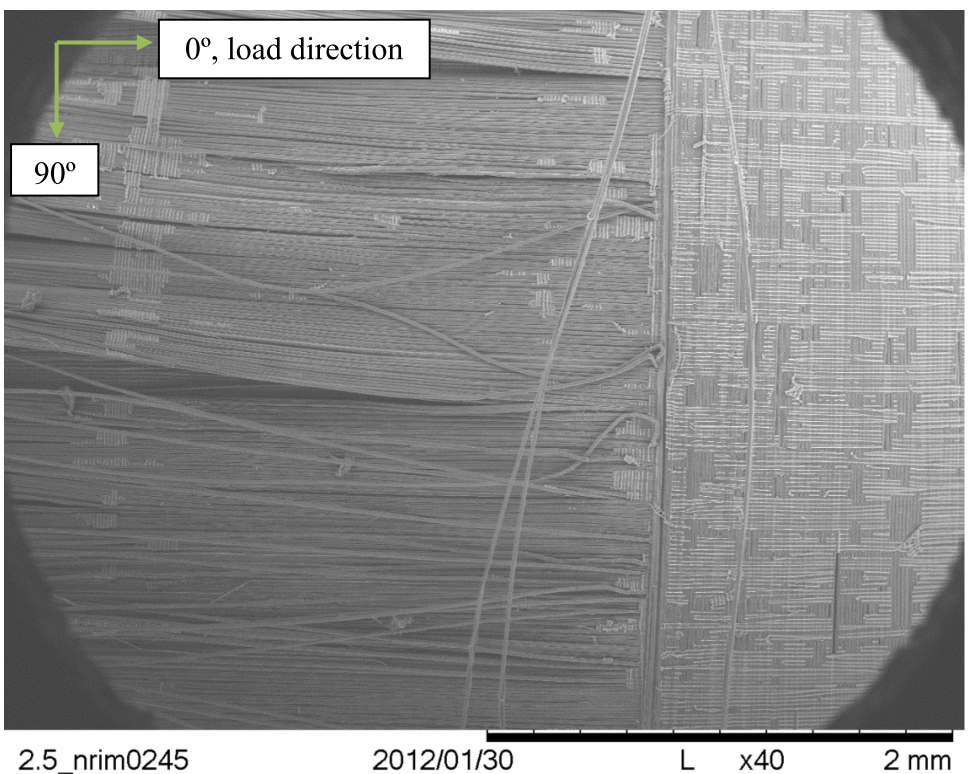
0º, load direction
90º
2.5_nrim0245
2012/01/30
L
x40
2 mm
(b)

Figure 5-31 SEM of Dyneema close to impact site, along pull-in delamination (a) strikeface (b) backface

Images that were also taken close to the impact site but near the backface showed similar results as the ones close to the strikeface. The matrix tended to stay to one side which in this case was closer to the strikeface. The matrix is very shifted, as seen in Figure 5-32 (a), probably due to the large amount of displacement that occurred from the material moving due to the dynamic cone formation. The dynamic cone bends the fibers more than any other region of damage during the impact so it would make sense that the matrix is disturbed more here than in any other part of the panel. The fibers remained unbroken but in a few cases there were some instances of fiber buckling.

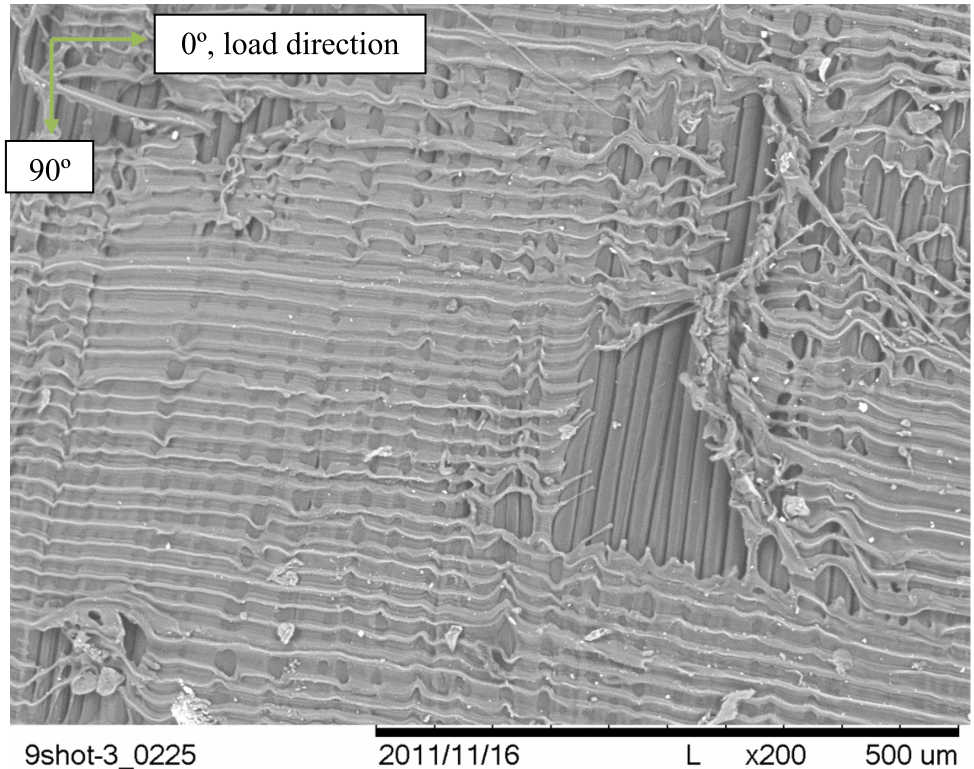
0º, load direction
90º
9shot-3_0225
2011/11/16
L
x200
500 um

(a)

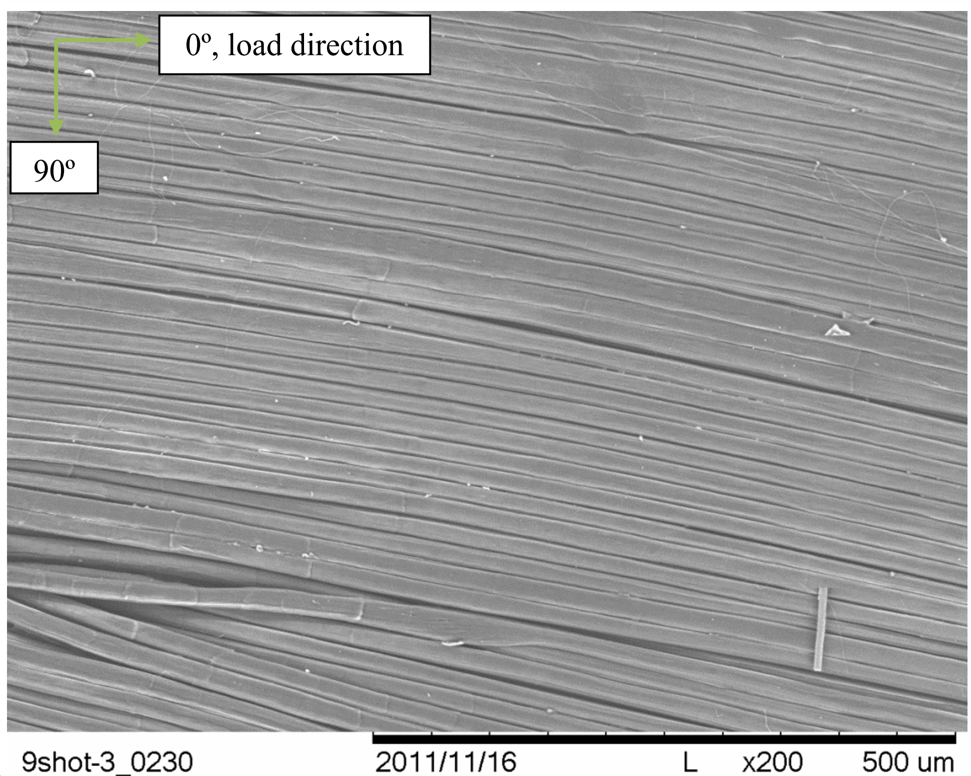
0º, load direction
90º
9shot-3_0230
2011/11/16
L
x200
500 um

(b)

Figure 5-32 SEM of Dyneema close to impact site, close to backface. (a) strikeface (b) backface

The SEM images taken close to the impact site show that regions where major delamination occurred, especially along the pull-in delamination, show that delamination occurred between multiple laminas and even within laminas. This is expected because of the 0/90 construction. In all of the imaging that was done there was no evidence of tensile fiber breakage away from the impact site. The fibers broken by tensile or shear fracture were directly under the projectile and could not be measured using SEM imaging.

Close to the cross delamination region the matrix did not tend to stay on one side or the other. When closer to the outsides of the panel the matrix did have a tendency to stay on one side of the lamina. The matrix would stay on the backface side of the sample when close to the strikeface and it stayed on the strikeface side of the sample when close to the backface. This is most likely caused because the primary fibers in the direction of the loading were under more stress which caused them to move more than the less active fiber lamina that was perpendicular to the load direction. This would cause the delamination to occur between the matrix and the primary fibers.

5.2.6.2.1 Far From Impact

Samples that were taken far away from the impact site should have had little damage but still were delaminated because the samples separated easily for image preparation. The samples used for imaging were taken as far as 8 inches away from the impact site. The images in Figure 5-33 show the sides of the delaminated sample.

All of the fibers are intact and there is very little disturbance in the matrix, which has stayed almost completely on the side closer to the strikeface.

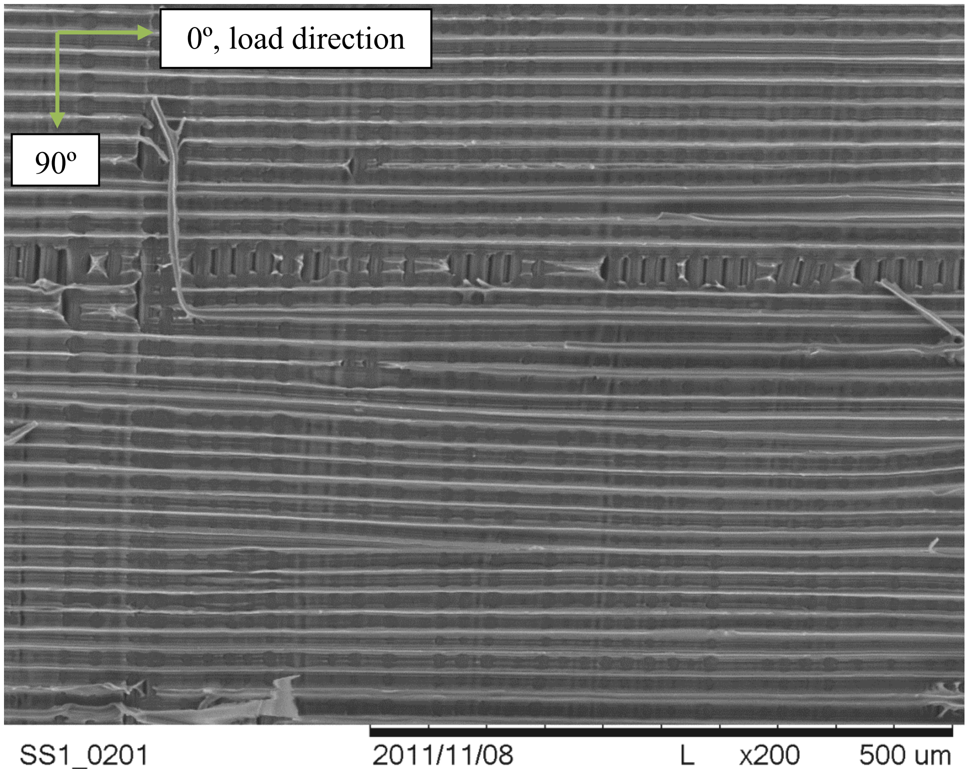

(a)

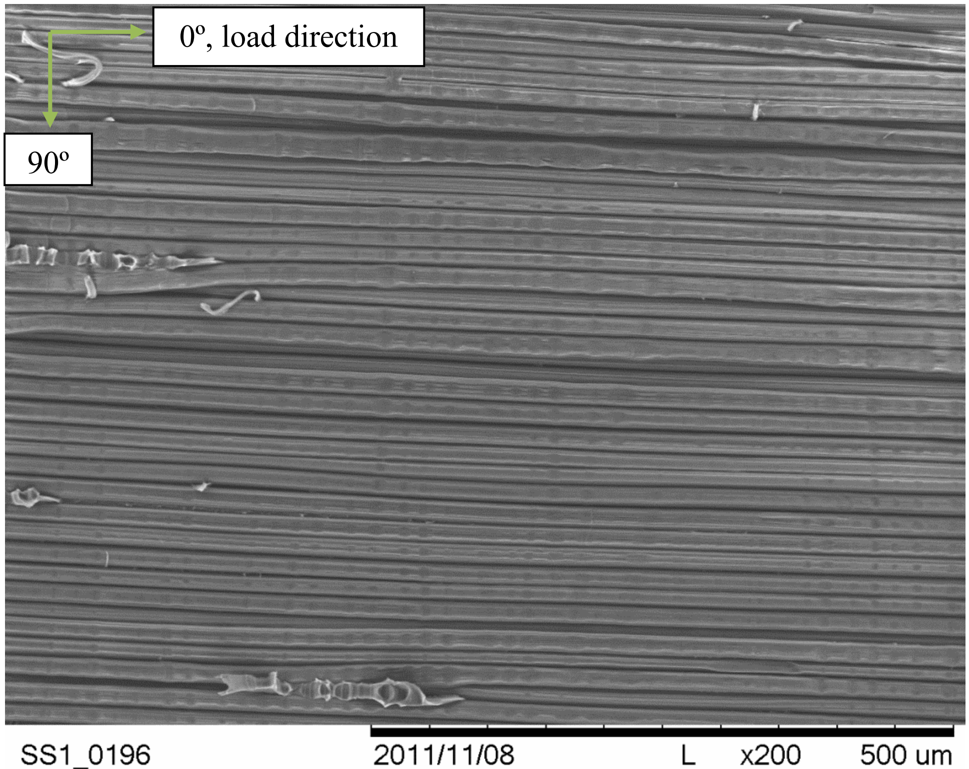

(b)

Figure 5-33 SEM of Dyneema damage far from impact site (a) strikeface (b) backface

The failure that occurred far from the impact site, as seen in Figure 5-33, was predominately mode II. Mode II failure left the fibers and matrix nearly intact with the matrix remaining on one specific lamina. The only damage sustained was just the separation between the matrix and fibers. It was known that this bond was weak so it was not surprising that it would occur. The other note of interest is that in all of the cases the matrix tended to remain on the side of the laminate closer to the strikeface. This goes along with the idea mentioned previously that the matrix delaminate away from the primary 0º fibers that are under tension during the impact.

5.2.6.2.2 In +/-45° Region

The last sample was taken close to the impact site and along the cross delamination similar to the same region in one of the previous samples. The difference was that in this case all of the fibers were secondary fibers instead of primary fibers like all of the other cases. This sample was taken from the w2 direction instead of the w3 direction like all of the others.

Figure 5-33 shows the two surfaces from the delaminated sample. Some debris got onto the sample which is why there are some large particles on the surfaces. The main observations were that the matrix tended to stay on one lamina which implies mode II cracking but there were some cases where matrix cracks allowed delamination paths to transfer between laminas. This time the matrix stayed on the backside part of the sample which could occur because both of these laminas consist of secondary fibers and not directly loaded by the projectile but instead by adjacent fibers.

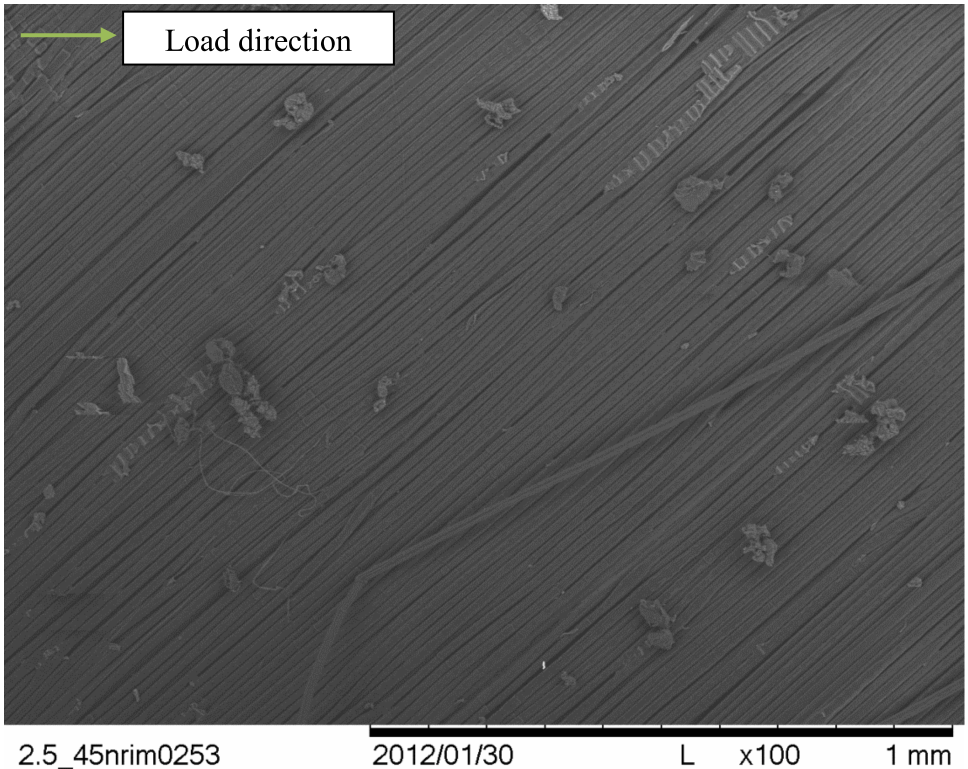
Load direction
2.5_45nrim0253
2012/01/30
L
x100
1 mm

(a)

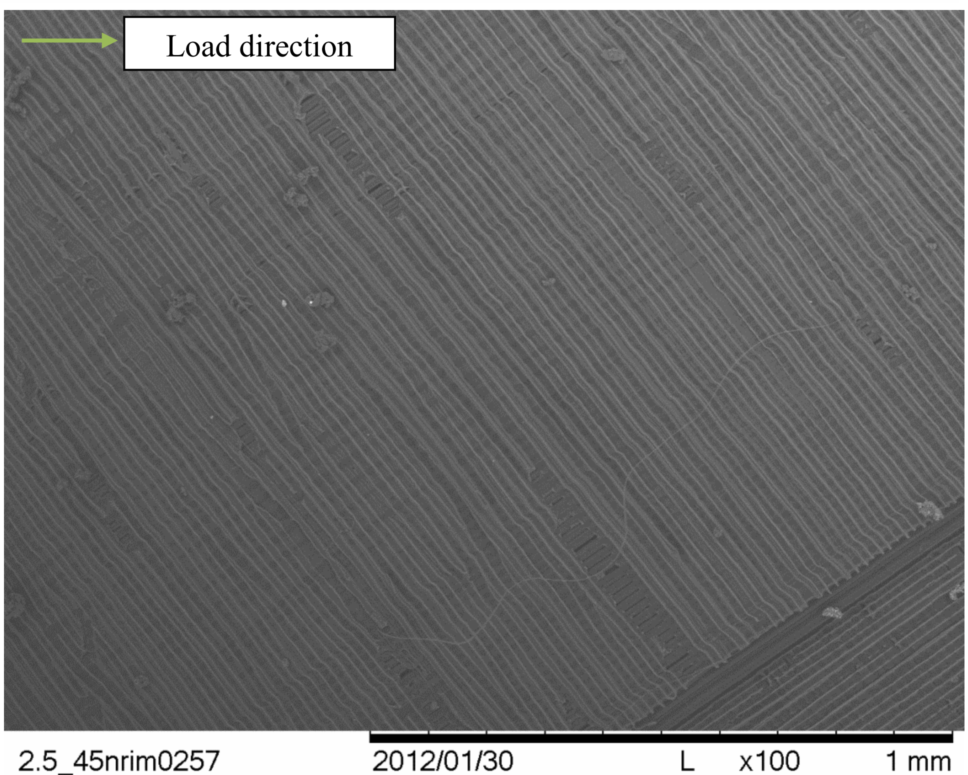
Load direction
2.5_45nrim0257
2012/01/30
L
x100
1 mm

(b)

Figure 5-34 SEM of Dyneema close to impact site, secondary fibers. (a) strikeface (b) backface

After all of the SEM imaging had been done some conclusions could be made about the damage propagation caused from impact. No fiber breakage was observed away from the impact site. The only breakage observed was in fibers being sheared directly by the projectile. In regions of large deformation like underneath the dynamic cone region there was a large amount of crack propagation that would travel through the laminas. This mode I failure caused major gaps in the smaller panel sizes which were not as abundant in the larger panels. This occurred both in the 1.5 psf and 2.5 psf samples but was more exaggerated in the 2.5 psf samples. Farther from the impact site mode II failure was predominant.

Near the impact site the cracks would move throughout the laminas regularly because of the Mode I failure. Moving away from the impact site the crack moving between laminas became less and less frequent as the major failure mode became Mode II. If there were jumps between laminas the crack would directly go from a primary fiber in the 0º direction, through a 90º lamina and begin again in the next 0º lamina. The matrix in the mode I regions did not tend to one side of the material or another, but in the mode II regions it did. All of the cases where primary 0º fibers were directly in contact with 90º fibers in the next lamina, it was found that the 90º fiber lamina would keep the matrix. An example of a crack path is given below in Figure 5-35.

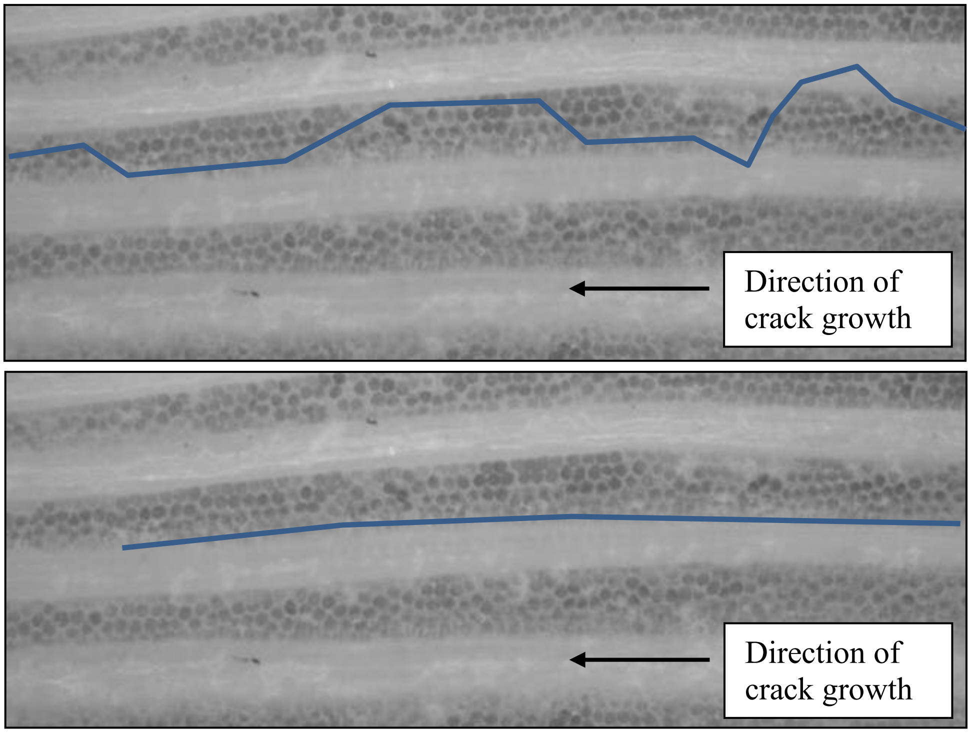

(a)
(b)

Figure 5-35 Schematic showing crack paths based on SEM observations (a) close to impact site and (b) along the pull-in delamination

Once the SEM imaging was complete the entire scale of damage analysis had been observed. This analysis started originally looking at the large scale deformations that occurred during the impact and then eventually down to the failure of the microstructure within the laminate. All of this information gathered can now be used to explain the original findings from the high velocity impact testing.

Chapter 6

CONCLUSIONS FROM DATA

During a high velocity impact the projectile is slowed down by different damage mechanisms that occur within the material. The initial Phase I, II, and III all involve local damage to the fibers like compression-shear and frictional sliding. These damage mechanisms are not affected by the size of the panel because the stress wave does not reach the edges of the panel at this point in time. The Phases beyond this point can be affected if the stress wave has reached a free edge of the material before the projectile has broken all the backface fibers in tension. If this occurs then a new set of damage mechanisms start occurring that are not thought of when comparing against an infinitely large panel.

The failure of unidirectional Dyneema HB-26 creates large delaminations in the primary fibers that form a cross shape. If a panel is small enough these delaminations can reach the free edge of the panel while the projectile is still moving through the material. At this point the primary fibers can no longer carry additional stress so the stress from the projectile is transferred along the sides of the cross delamination. Because the weak bond between the fibers and matrix, little energy is needed for the delamination to continue allowing the primary fibers to pull-in instead of breaking. The large deformation slows the projectile over a longer time and distance so there is less chance that the projectile will break the primary fibers in tension and exit the panel. The panel will continue to deform until it is restricted by its supports or the backface and strikeface completely separate. This resulting edge pull-in allows for large deflections which ultimately can increase the V_{50} of the smaller Dyneema panel.

The calculated V_{50} of the material may increase but this may not have actually increased the ballistic resistance of the material in the field. There may be impacts done on small panels with initial velocities at the V_{50} of an infinite panel that resulted in complete penetrations. The increased V_{50} came with a higher variability of results which would still make the V_0 of the material the same for any panel size.

This research showed that issues may arise when testing Dyneema HB-26 panels where delaminations reach the free edge of the panel. If not enough panels are tested the resulting calculated V_{50} may be inaccurate and the true value may in fact be lower. The main note from this research is that if Dyneema HB-26 panels are being tested for a high velocity impact application and delamination is reaching the free edge of the material, the calculated V_{50} can be higher than an infinitely large panel.

Future work related to this research could be done looking at different types of material like glass and aramid laminates. Other materials with similar mechanical properties to Dyneema laminates would be more susceptible to these effects. Additional testing and analysis could be done on even smaller Dyneema HB-26 panels, at some point the panels should be small enough where the extra energy gained from delamination does not make up the energy dissipated through breakage of the backface fibers in tension. Additionally, creating probabilistic velocity response (PVR) curves for each panel size would give a better understanding at how panel size affects probabilities other than the V_{50}. Continued testing may show that lower probabilities such as the V_{01} or V_{05} could be more sensitive to the effects of panel size.

REFERENCES

B. A. Gama, J. W. (2008). Punch shear based penetration model of ballistic impact of thick-section composities. *Composite Structures*, 356-369.

Dingenen, J. L. (1989). High Performance Dyneema Fibres in Composites. *Materials & Design*, 101-104.

DOD-USA. (1987, January 22). V50 Ballistic Test for Armor. *Department of Defense Test Method Standard*.

DSM. (2011, May 31). Safety Data Sheet, Unidirectional Sheet Material: HB26.

Dyneema, D. (2004, July). Customer Information Sheet: Recommended Pressure Cycle.

Dyneema, D. (2006, June 12). DSM Dyneema Press Release.

Kevin M. Ayotte, B. A. (2011). Ballistic Penetration Behavior of UHMWPE Soft Composite Laminates. *SAMPE*, 13.

Marissen, R. (2011). Design with Ultra Strong Polyethylene Fibers. *Materials Sciences and Applications*, 319-330.

McMaster-Carr. (n.d.). *Aluminum*. Retrieved June 19, 2012, from McMaster-Carr: http://www.mcmaster.com/#catalog/118/3648/=i1rfec

Misey, J. (1978). *Analysis of Ballistic Limit.* Aberdeen Proving Ground, Maryland: USA Ballistic Research Laboratory.

N.K. Naik, A. V. (2005). Ballistic Impact Behavior of Thick Composites: Analytical Formulation. *AIAA Journal*, 1525-1536.

NIJ 0108.01. (1985). *Ballistic Resistant Protective Materials.* U.S. Department of Justice, National Institute of Justice.

Roman, J. d. (2005). *Experiments on Epoxy, Polyurethane, and ADP Adhesives.* Composite Construction Laboratory.

Russell, B. P. (2013). The high strain rate response of Ultra High Molecular-weight Polyethylene: From fibre to laminate. *Internal Journal of Impact Engineering*, 1-9.

Shen, Q. (2012). Ultrasonic NDE Techniques for Impact Damage Inspection on CFRP Laminates. *Journal of Materials Science Research*, 2-16.

Tao Xu, R. J. (2007). Comparative Studies of Ultra High Molecular Weight Polyethylene Fiber Reinforced Composites. *Polymer Engineering and Science*, 1544-1553.

UL 752. (2006). *Bullet-Resisting Equipment.* Underwriters Laboratories Inc.

V. B. C. Tan, K. J. (2005). Perforation of flexible laminates by projectiles of different geometry. *International Journal of Impact Engineering*, 793-810.

Appendix A

FULL VELOCITY DATA FROM TESTING

1.5 psf sample data

Sample Name	Initial V (fps)	Residual V (fps)
PE-1.5_01_01	1938	no data
PE-1.5_01_02	1960	821
PE-1.5_01_03	1852	831
PE-1.5_01_04	1484	0
PE-1.5_01_05	2219	1220
PE-1.5_01_06	2430	1743
PE-1.5_01_07	2593	1982
PE-1.5_01_08	1622	0
PE-1.5_01_09	1688	0
PE-1.5_01_10	1736	0
PE-1.5_01_11	1848	430
PE-1.5_01_12	1828	447

Sample Name	Initial V (fps)	Residual V (fps)
PE-1.5_02_01	2150	1338
PE-1.5_02_02	2049	1165
PE-1.5_02_03	1955	844
PE-1.5_02_04	1783	0
PE-1.5_02_05	1814	0
PE-1.5_02_06	1863	411
PE-1.5_02_07	2478	1782
PE-1.5_02_08	1851	0
PE-1.5_02_09	1853	420
PE-1.5_02_10	1843	0
PE-1.5_02_11	2322	1502
PE-1.5_02_12	1904	444

Sample Name	Initial V (fps)	Residual V (fps)
PE-1.5_03_01	1740	0
PE-1.5_03_02	1965	651
PE-1.5_03_03	1587	0
PE-1.5_03_04	2232	1207
PE-1.5_03_05	2407	1506
PE-1.5_03_06	2594	1945
PE-1.5_03_07	1889	478
PE-1.5_03_08	1708	0
PE-1.5_03_09	1634	0
PE-1.5_03_10	1870	0
PE-1.5_03_11	2079	947
PE-1.5_03_12	1843	0

2.5 psf sample data

Sample Name	Initial V (fps)	Residual V (fps)
PE-2.5_04_01	2812	872
PE-2.5_04_02	2596	0
PE-2.5_04_03	2961	1332
PE-2.5_04_04	3053	1511
PE-2.5_04_05	3198	1731
PE-2.5_04_06	2666	463
PE-2.5_04_07	2645	0
PE-2.5_04_08	2650	0
PE-2.5_04_09	2737	797
PE-2.5_04_10	3477	2262
PE-2.5_04_11	2672	0
PE-2.5_04_12	2686	239

Sample Name	Initial V (fps)	Residual V (fps)
PE-2.5_05_01	2846	1342
PE-2.5_05_02	2722	0
PE-2.5_05_03	3038	1582
PE-2.5_05_04	3149	1625
PE-2.5_05_05	3391	1970
PE-2.5_05_06	2811	807
PE-2.5_05_07	2695	0
PE-2.5_05_08	2741	648
PE-2.5_05_09	2703	0
PE-2.5_05_10	2737	0
PE-2.5_05_11	2866	847
PE-2.5_05_12	3011	1334

Sample Name	Initial V (fps)	Residual V (fps)
PE-2.5_06_01	2699	640
PE-2.5_06_02	3025	1293
PE-2.5_06_03	3454	2059
PE-2.5_06_04	2794	0
PE-2.5_06_05	2699	0
PE-2.5_06_06	2821	0
PE-2.5_06_07	3233	1644
PE-2.5_06_08	2866	454
PE-2.5_06_09	2771	0
PE-2.5_06_10	3016	1647
PE-2.5_06_11	3575	2439
PE-2.5_06_12	2879	0

Appendix B

ADDITIONAL IMAGES

Full list of C-scan images:

1.5 psf samples:

PE-1.5_01_01

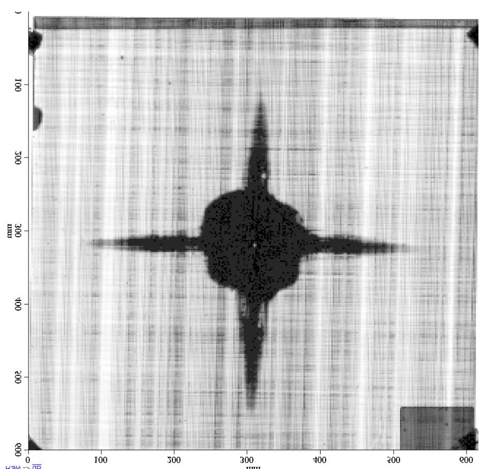

PE-1.5_01_02

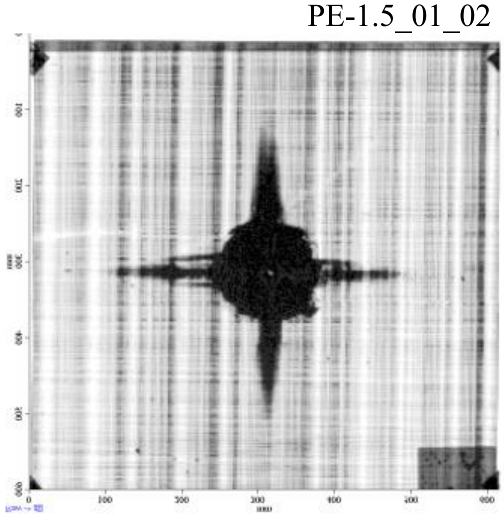

PE-1.5_01_03

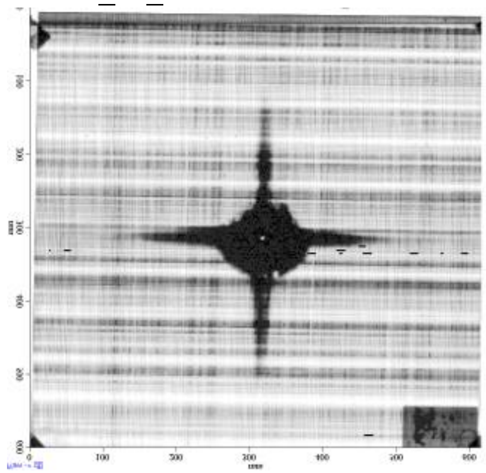

PE-1.5_01_04

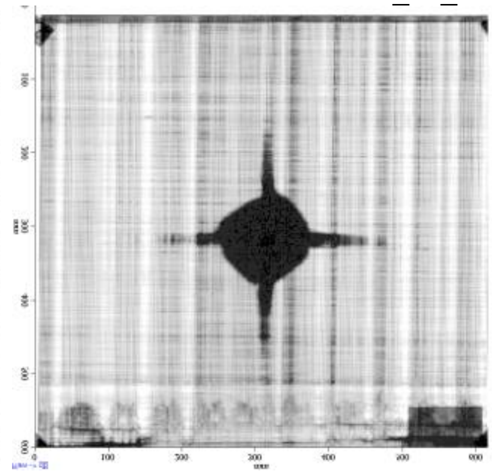

PE-1.5_01_05

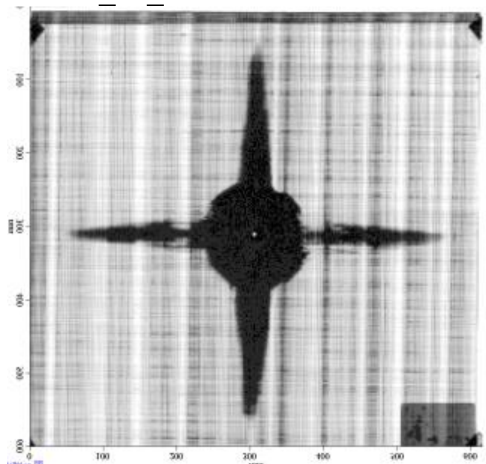

PE-1.5_01_06

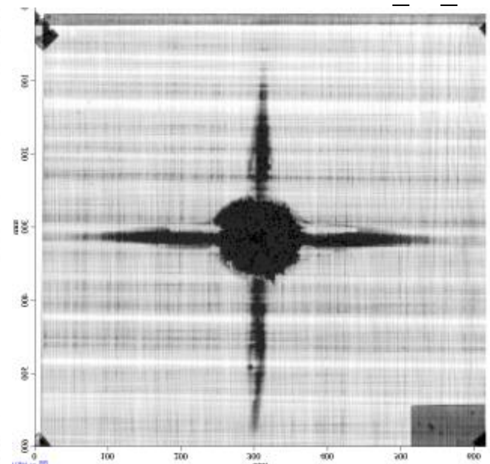

PE-1.5_01_07

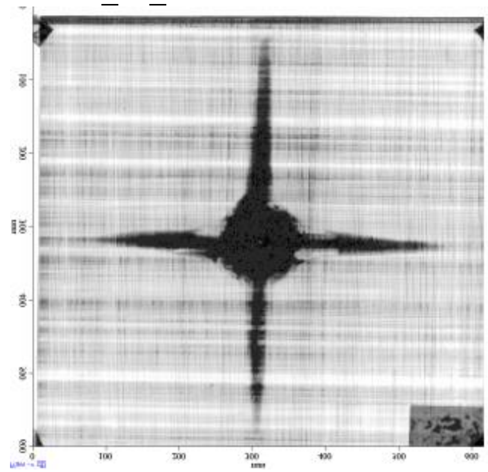

PE-1.5_01_08

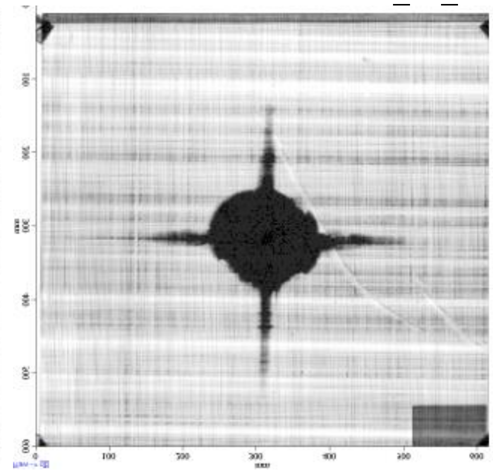

PE-1.5_01_09

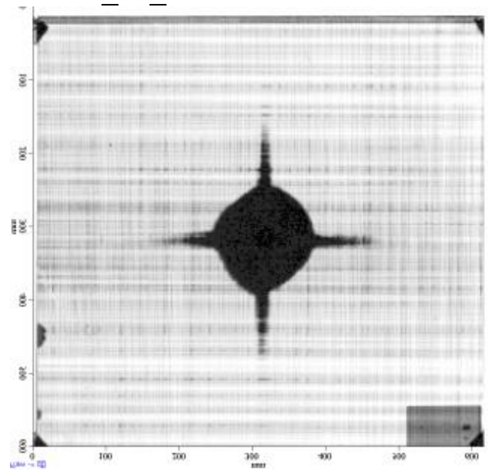

PE-1.5_01_10

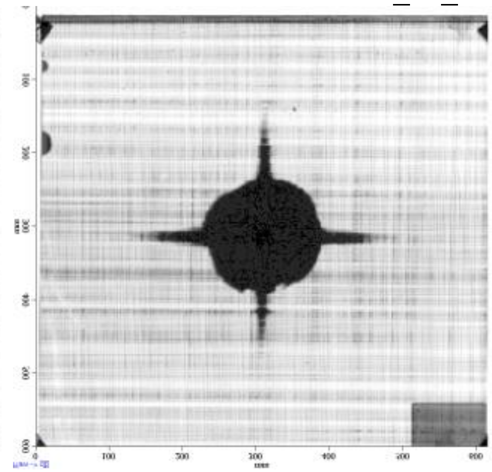

PE-1.5_01_11

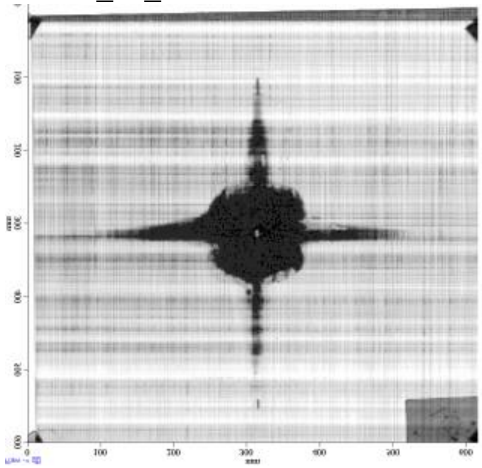

PE-1.5_01_12

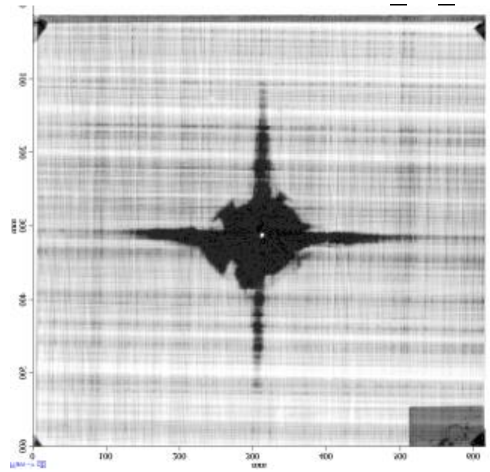

PE-1.5_02_01

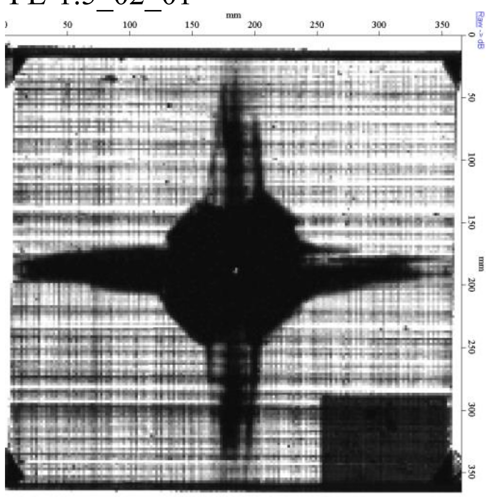

PE-1.5_02_02

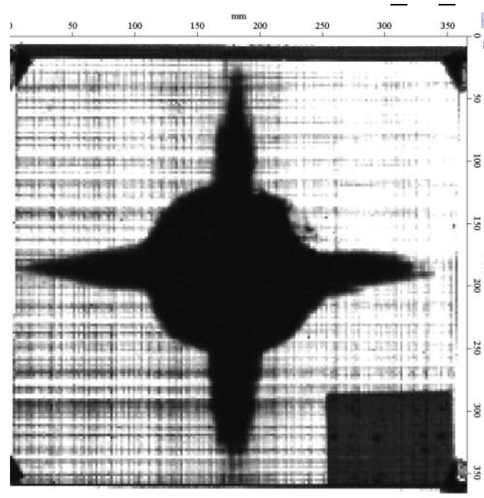

PE-1.5_02_03

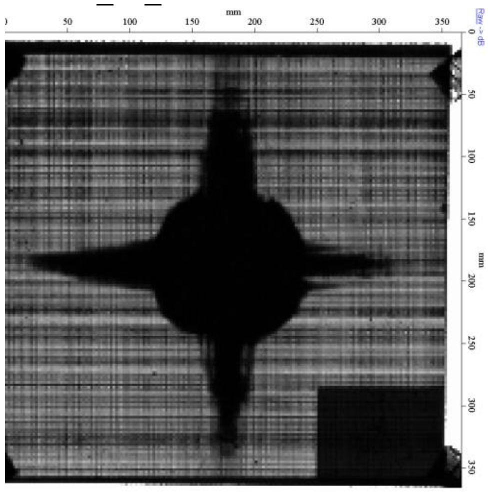

PE-1.5_02_04

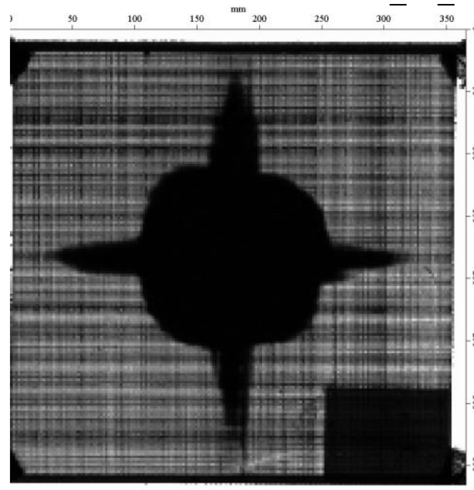

PE-1.5_02_05

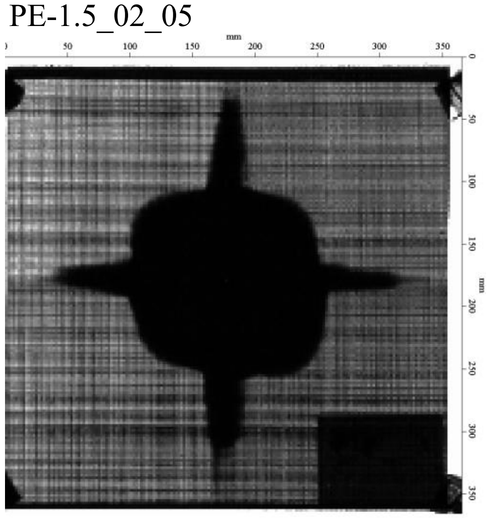

PE-1.5_02_06

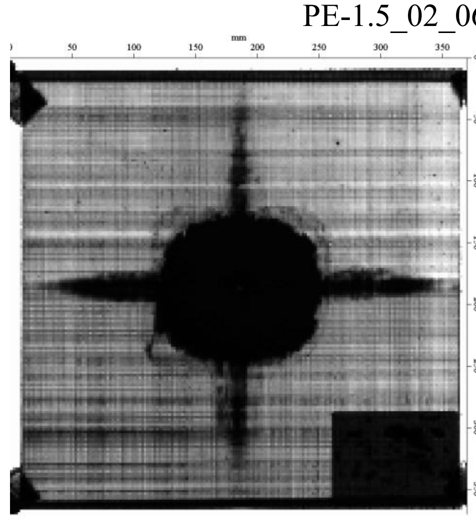

PE-1.5_02_07

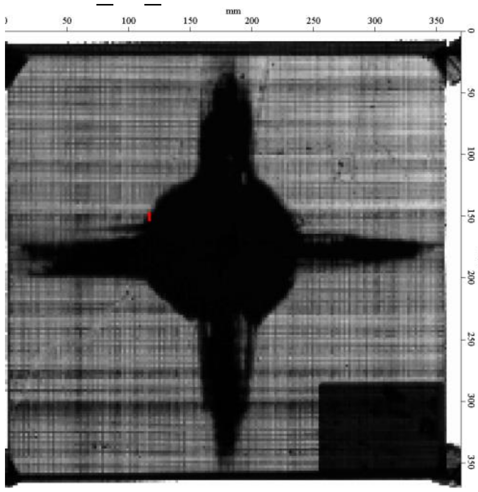

PE-1.5_02_08

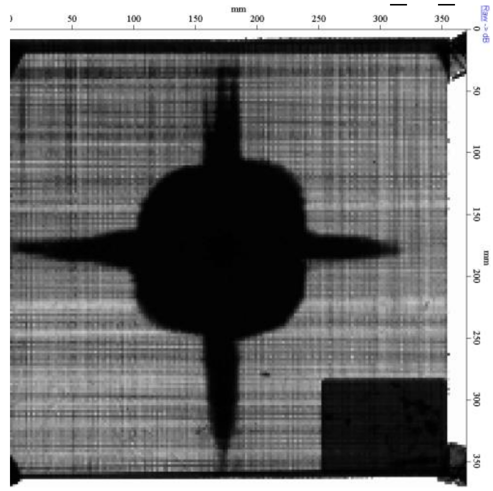

PE-1.5_02_09

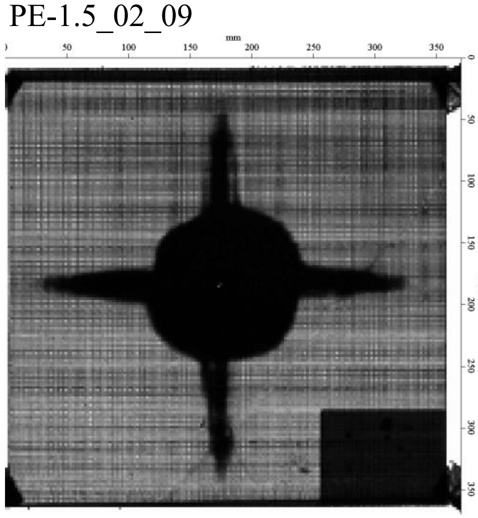

PE-1.5_02_10

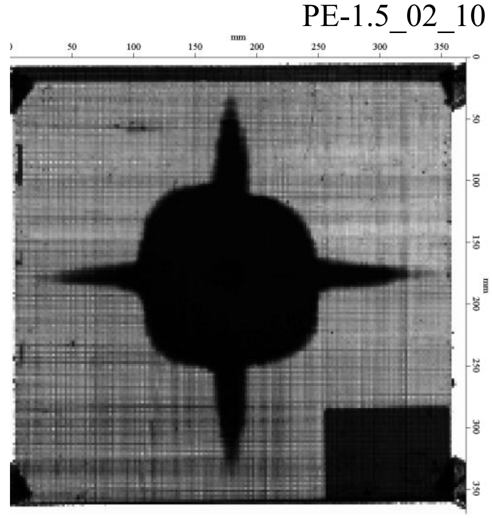

PE-1.5_02_11 PE-1.5_02_12

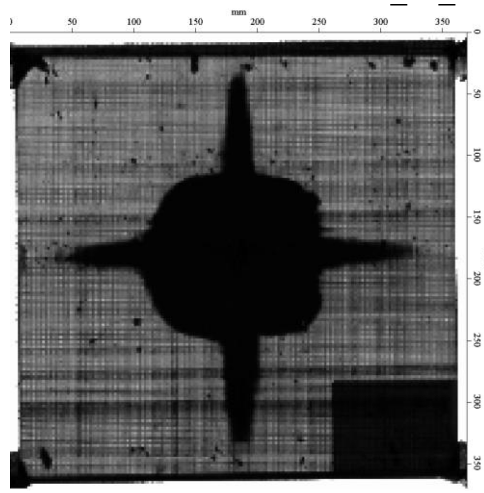

PE-1.5_03_01 PE-1.5_03_02 PE-1.5_03_03

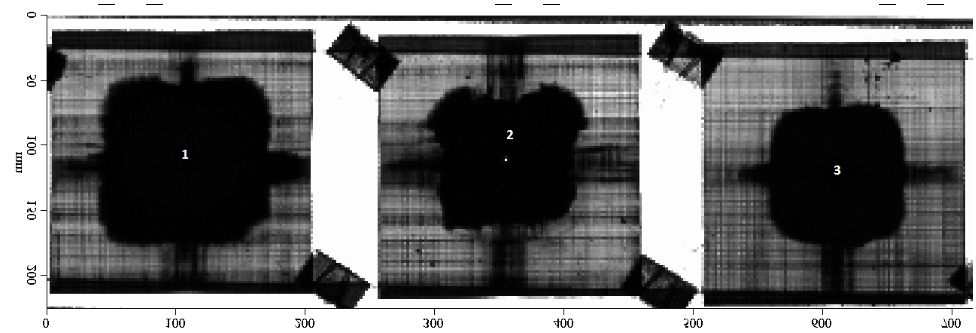

PE-1.5_03_04 PE-1.5_03_05 PE-1.5_03_06

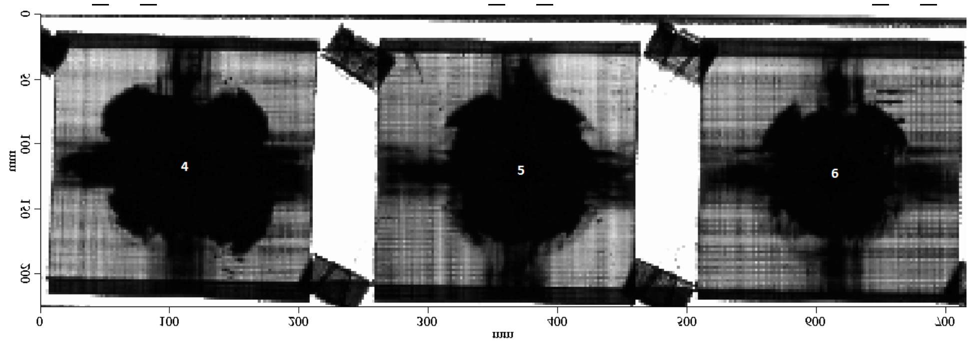

PE-1.5_03_07 PE-1.5_03_08 PE-1.5_03_09

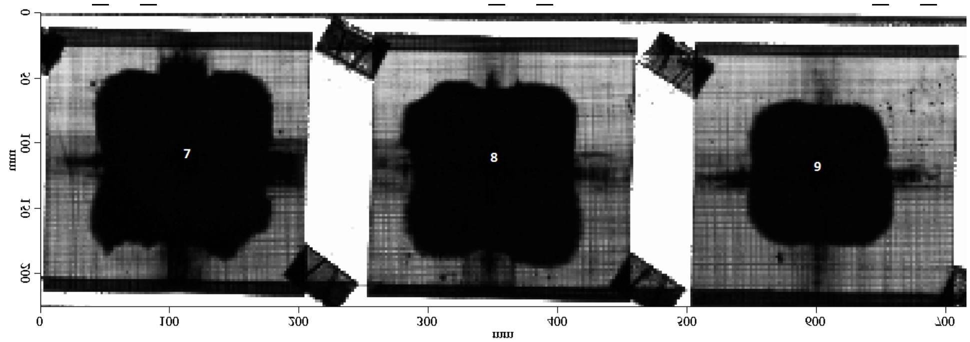

PE-1.5_03_10 PE-1.5_03_11 PE-1.5_03_12

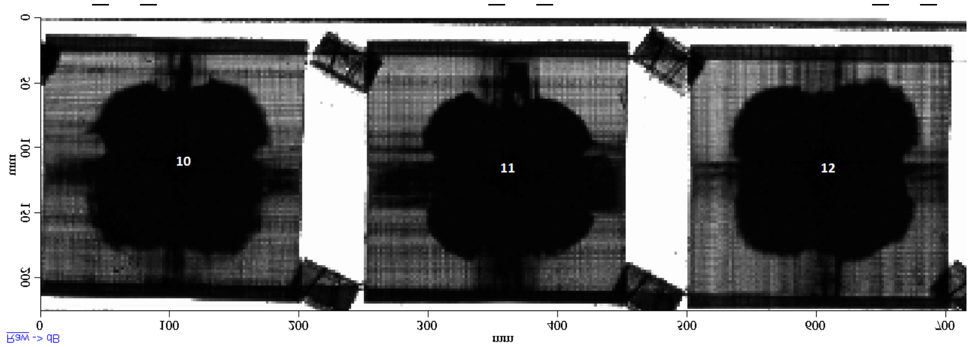

2.5 psf samples:

PE-2.5_04_01

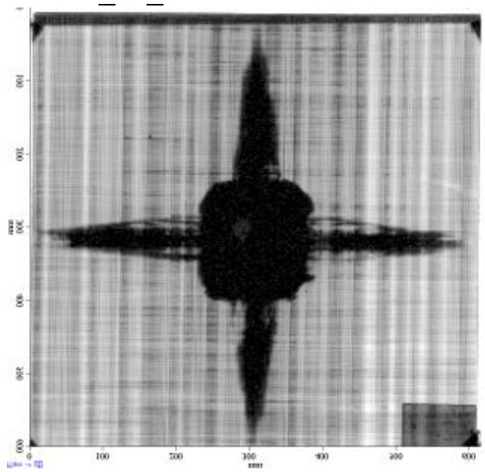

PE-2.5_04_02

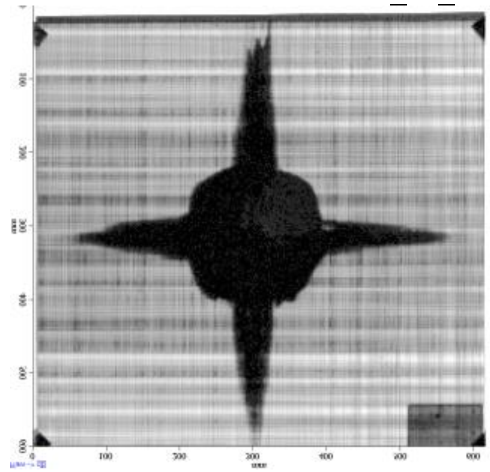

PE-2.5_04_03

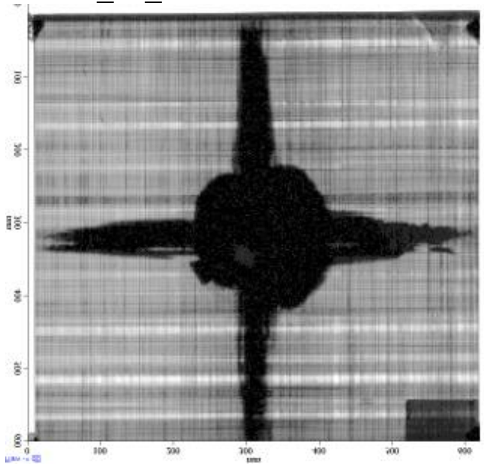

PE-2.5_04_04

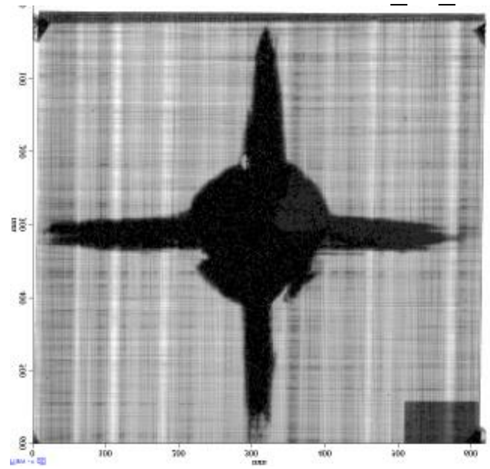

PE-2.5_04_05

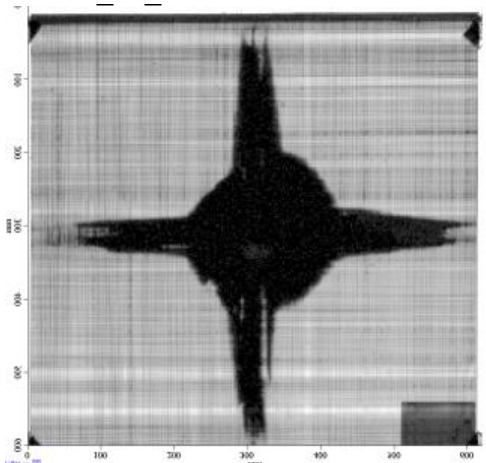

PE-2.5_04_06

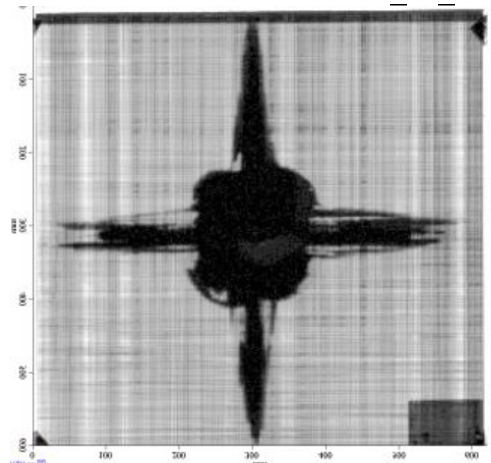

PE-2.5_04_07

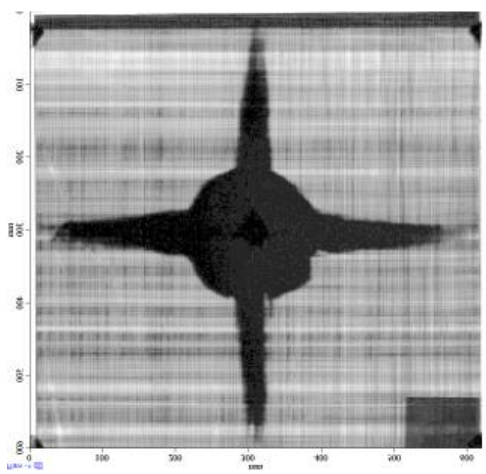

PE-2.5_04_08

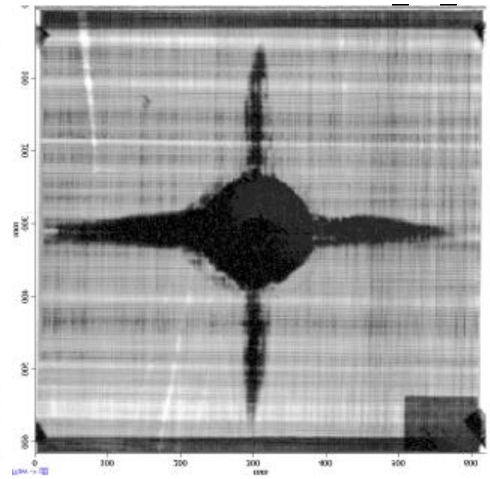

PE-2.5_04_09

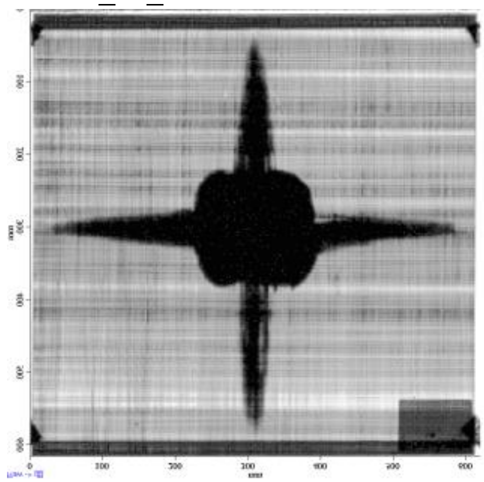

PE-2.5_04_10

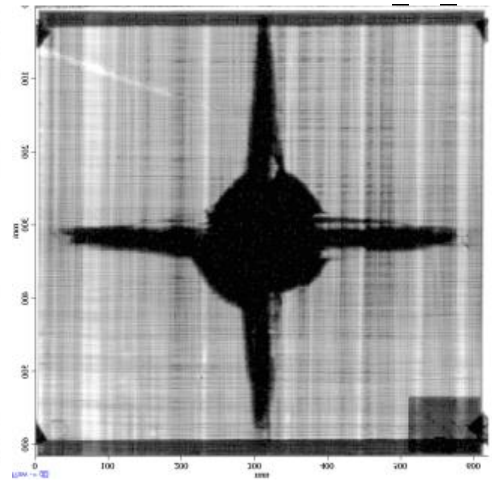

PE-2.5_04_11

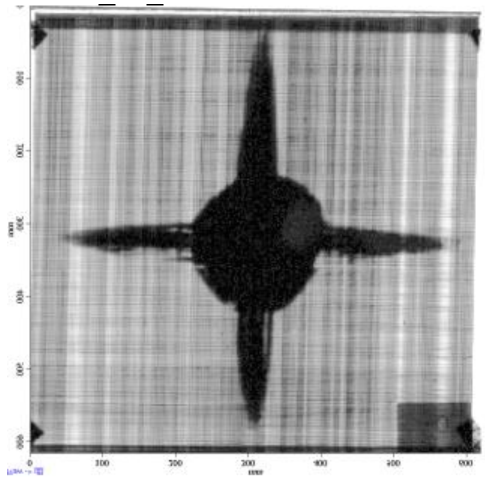

PE-2.5_04_12

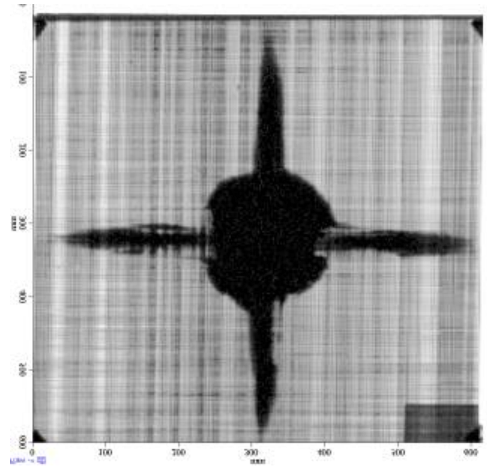

PE-2.5_05_01

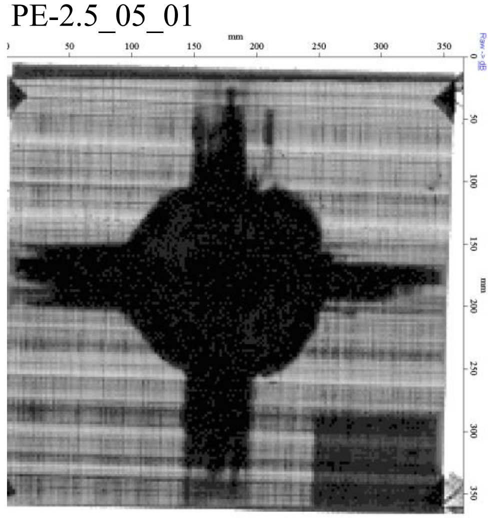

PE-2.5_05_02

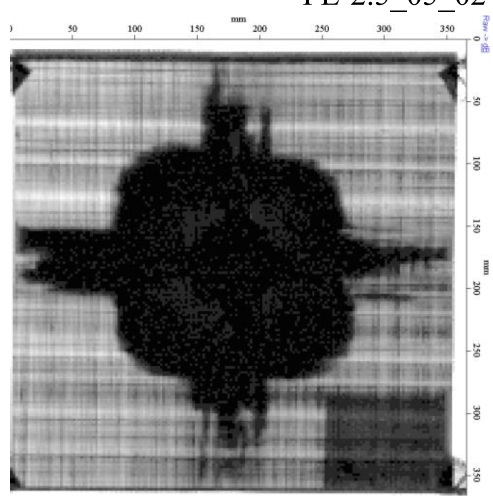

PE-2.5_05_03

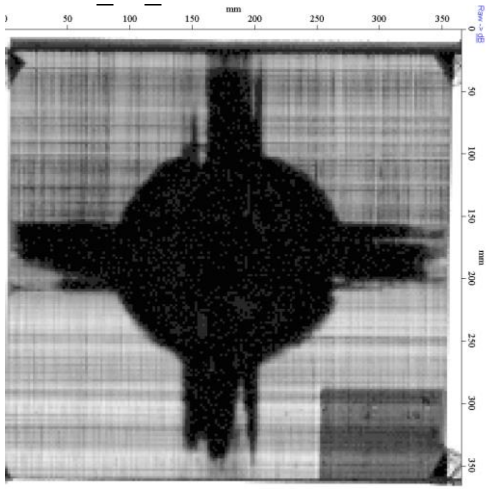

PE-2.5_05_04

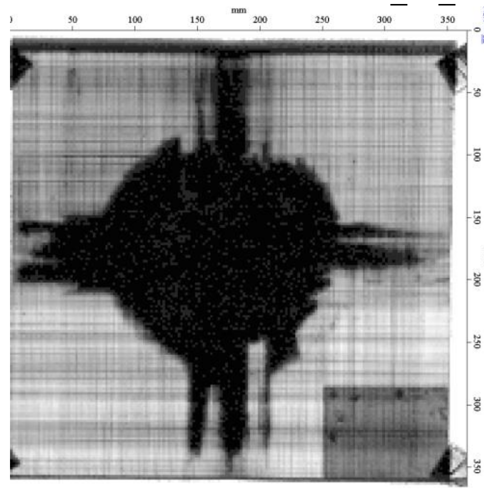

PE-2.5_05_05

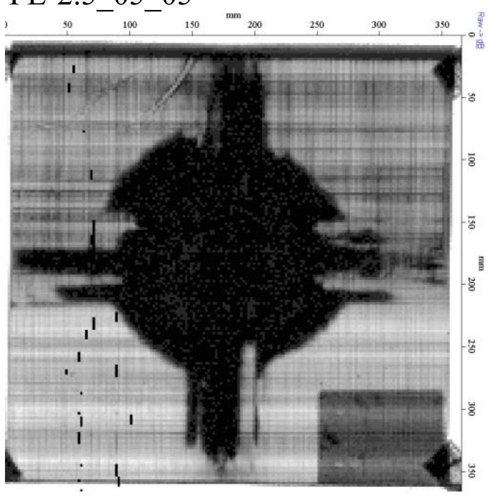

PE-2.5_05_06

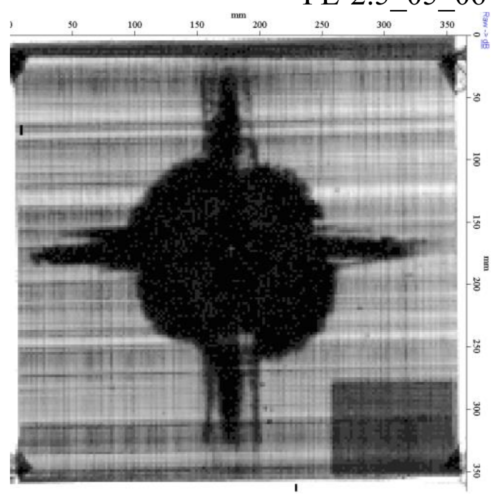

PE-2.5_05_07

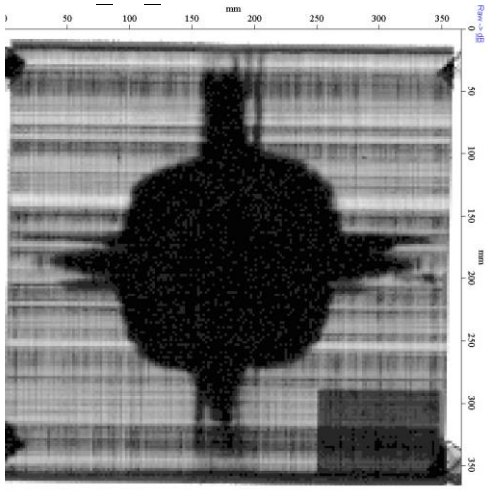

PE-2.5_05_08

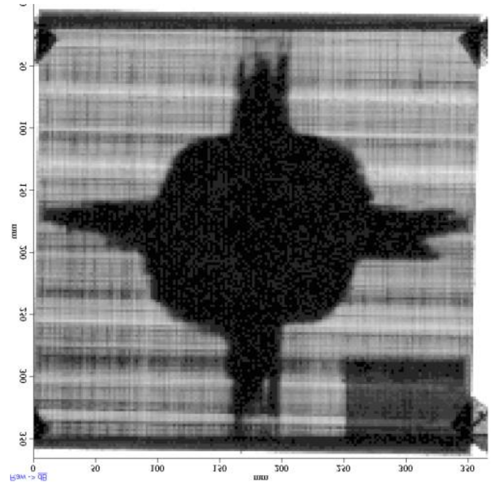

PE-2.5_05_09

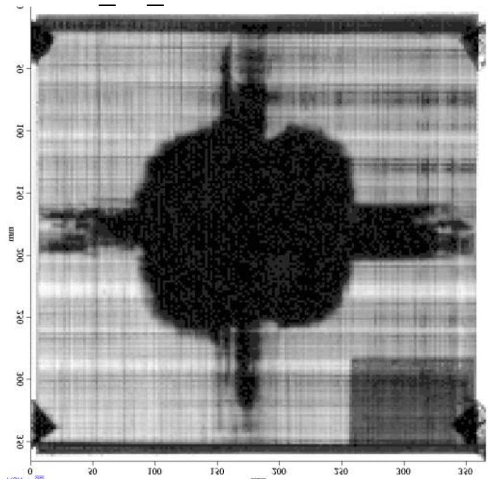

PE-2.5_05_10

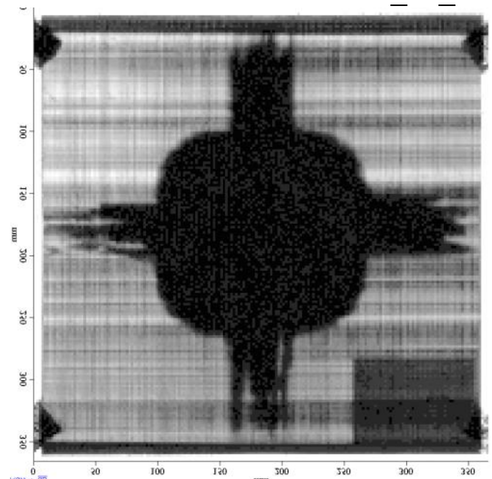

PE-2.5_05_11 PE-2.5_05_12

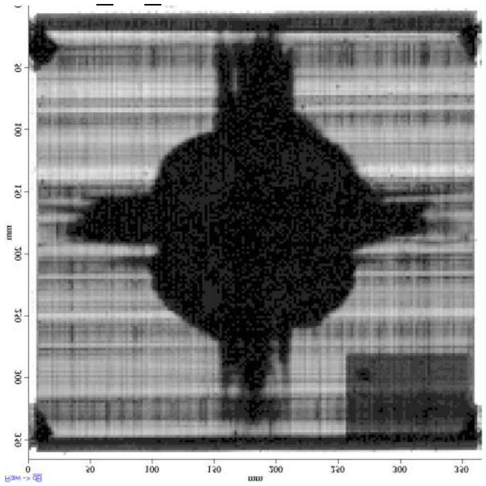

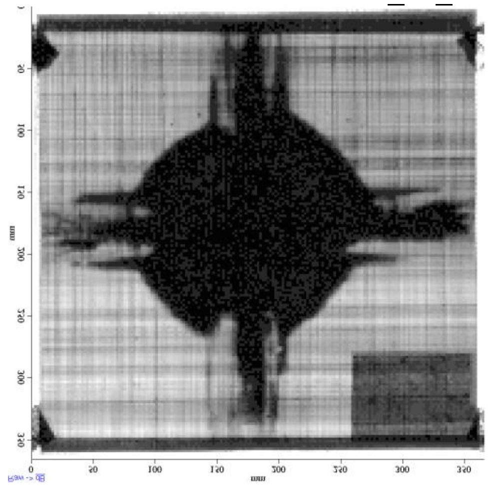

PE-1.5_06_01 PE-1.5_06_02 PE-1.5_06_03

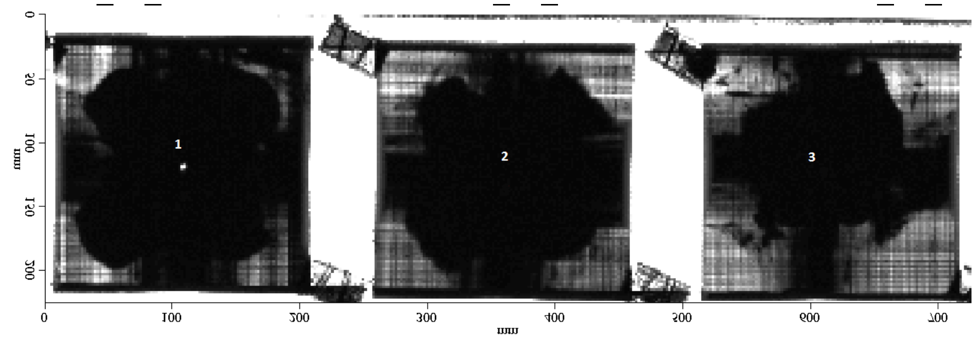

PE-1.5_06_04 PE-1.5_06_05 PE-1.5_06_06

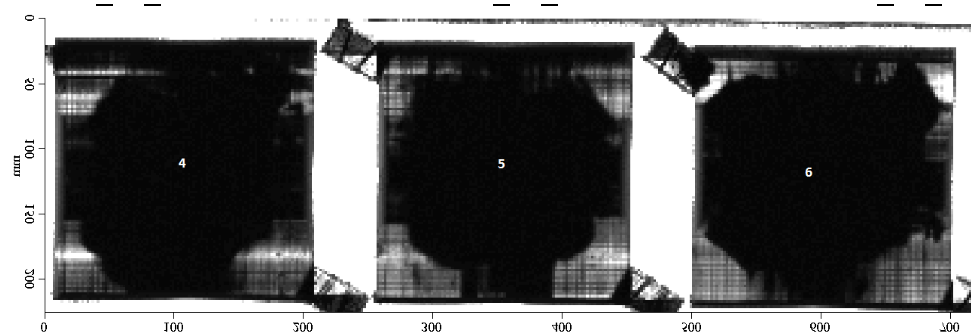

PE-1.5_06_07 PE-1.5_06_08 PE-1.5_06_09

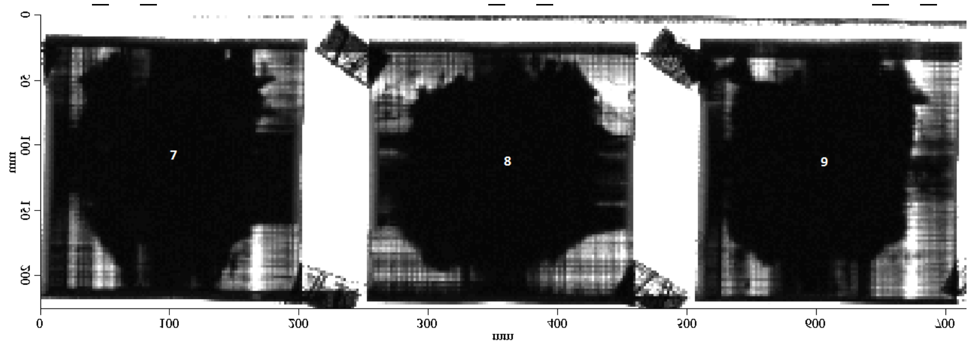

PE-1.5_06_10 PE-1.5_06_11 PE-1.5_06_12

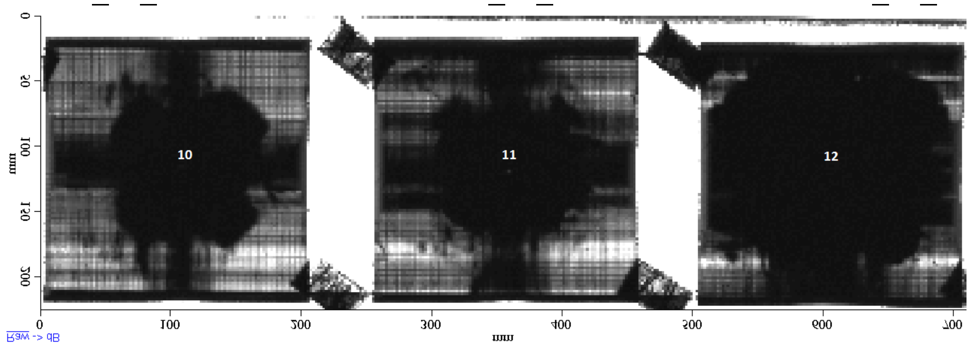

Cross section images of 1.5 psf samples:

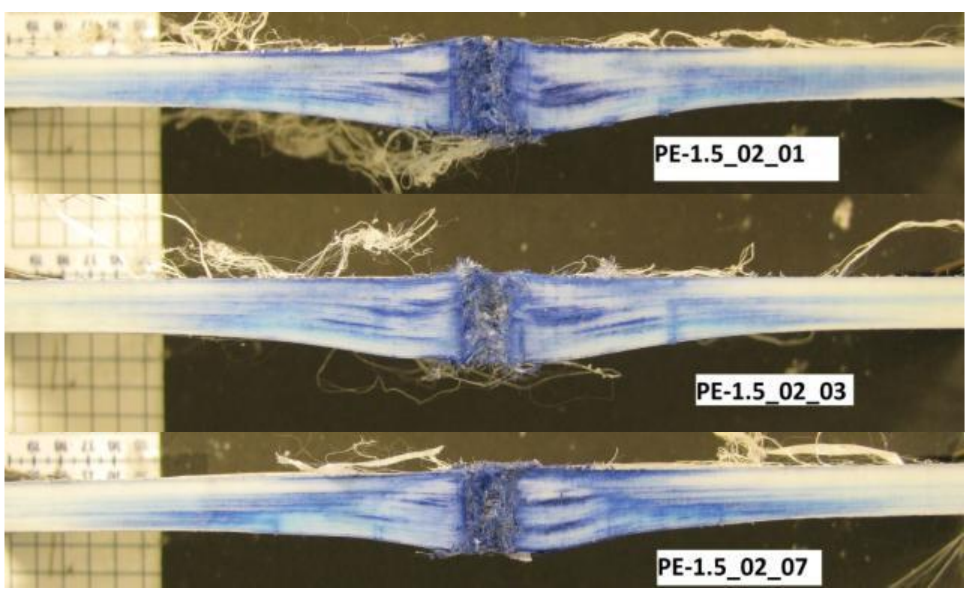

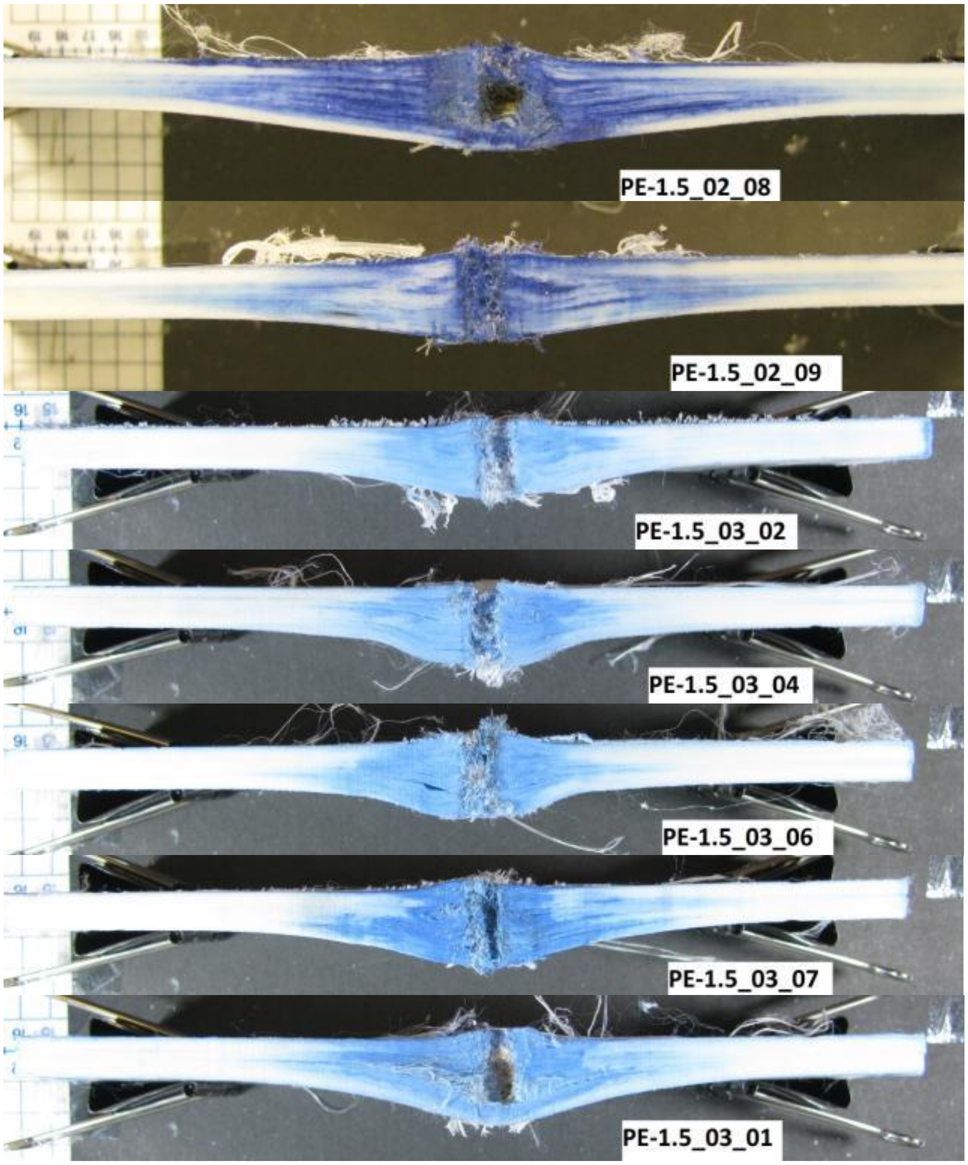
PE-1.5_02_08
PE-1.5_02_09
PE-1.5_03_02
PE-1.5_03_04
PE-1.5_03_06
PE-1.5_03_07
PE-1.5_03_01

Cross section images of 2.5 psf samples:

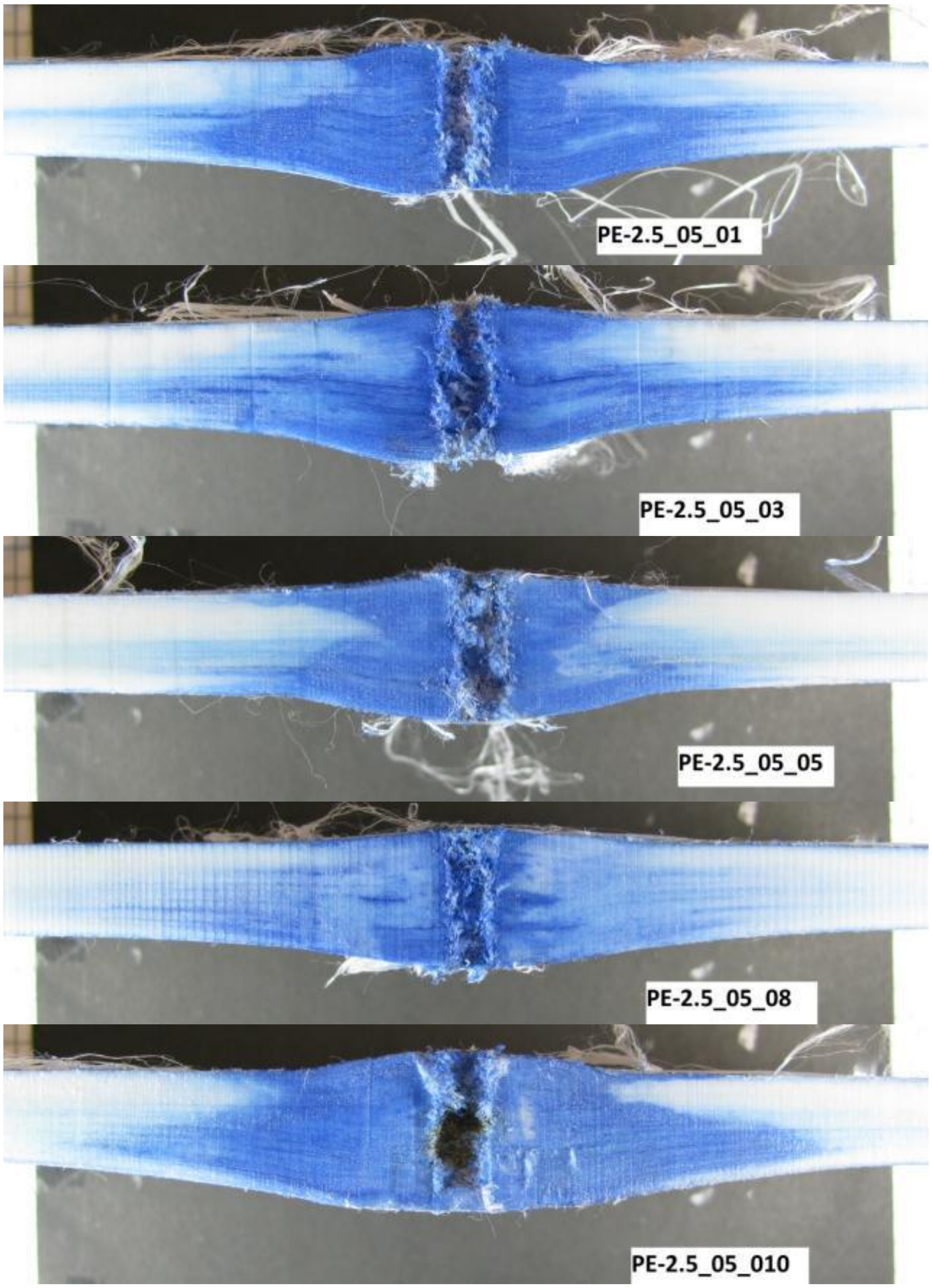

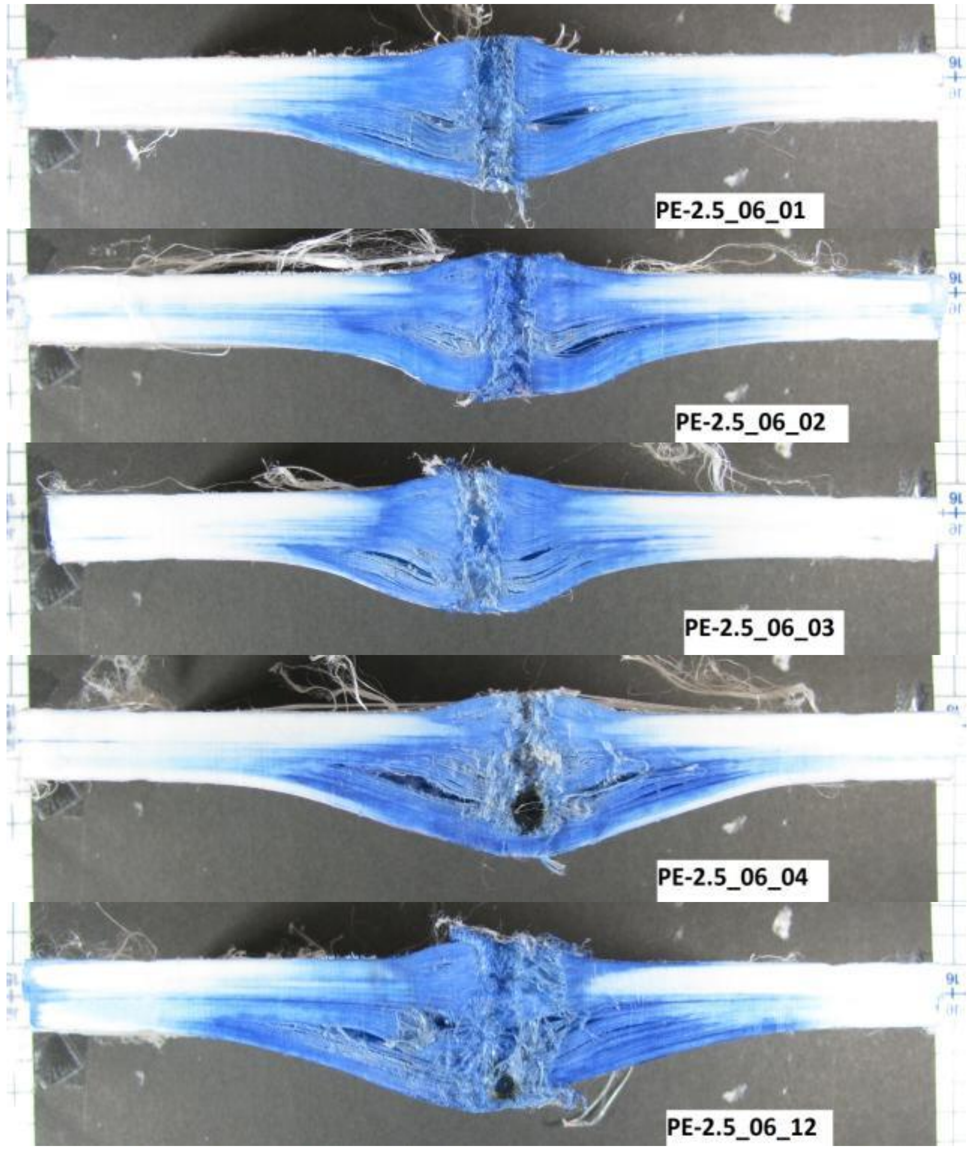
PE-2.5_06_01
PE-2.5_06_02
PE-2.5_06_03
PE-2.5_06_04
PE-2.5_06_12

1.5 psf and 2.5 psf samples cut at 45° angle:

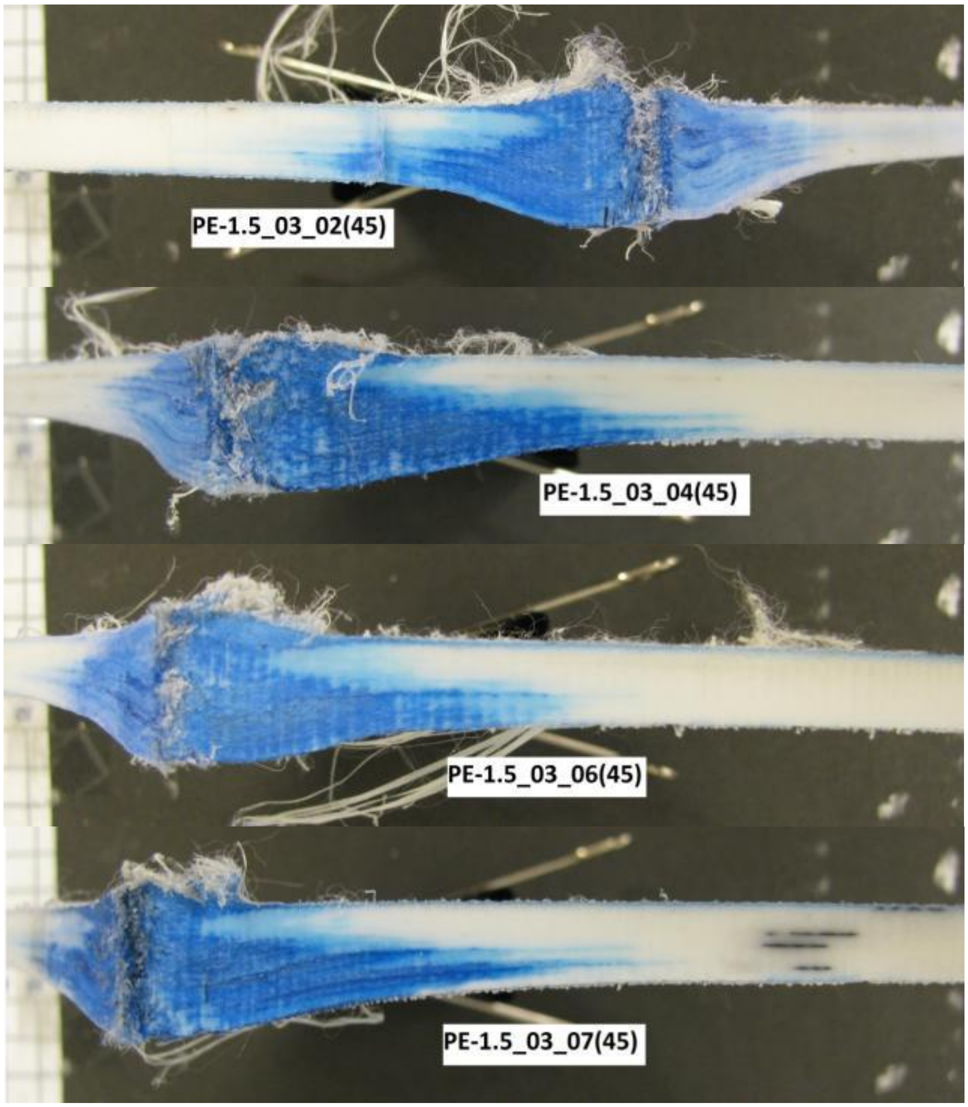

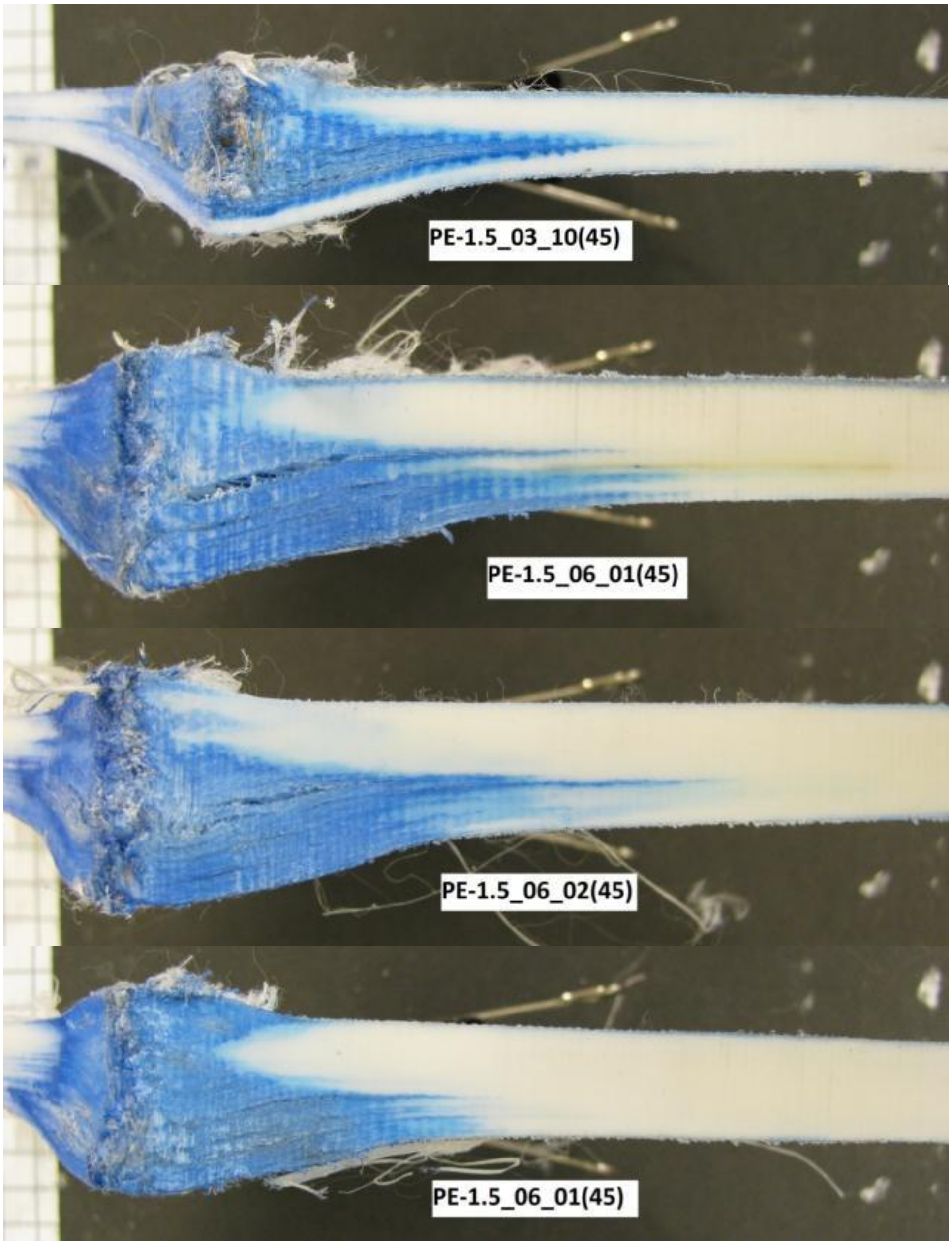
PE-1.5_03_10(45)
PE-1.5_06_01(45)
PE-1.5_06_02(45)
PE-1.5_06_01(45)

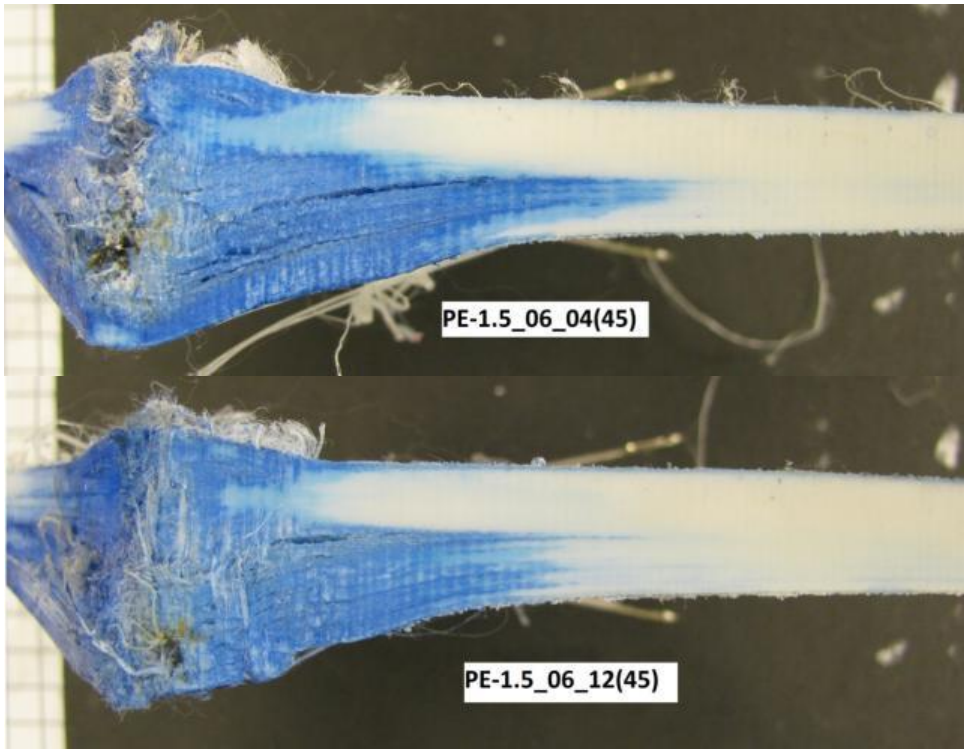
PE-1.5_06_04(45)
PE-1.5_06_12(45)

Profile images of measured witness plates:

PE-1.5_01_09

PE-1.5_01_10

PE-1.5_02_08

PE-1.5_02_10

PE-1.5_03_03

PE-1.5_03_09

PE-1.5_03_10

PE-1.5_03_12

PE-2.5_04_07

PE-2.5_04_08

PE-2.5_04_11

PE-2.5_05_07

PE-2.5_05_09

PE-2.5_05_10

PE-2.5_06_05

PE-2.5_06_09

Appendix C

ADDITIONAL CHARTS

Full list of VI/VR curve data charts:

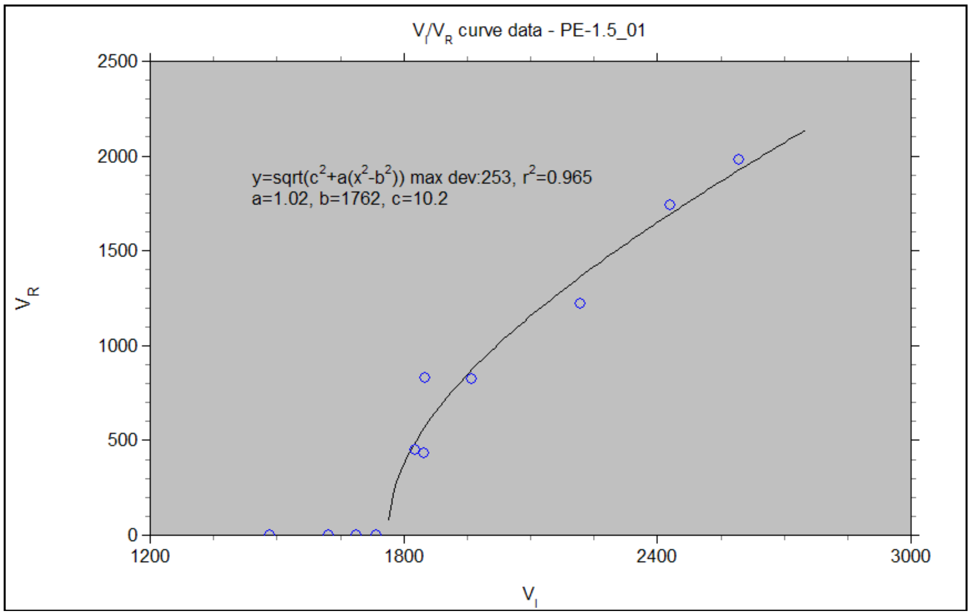

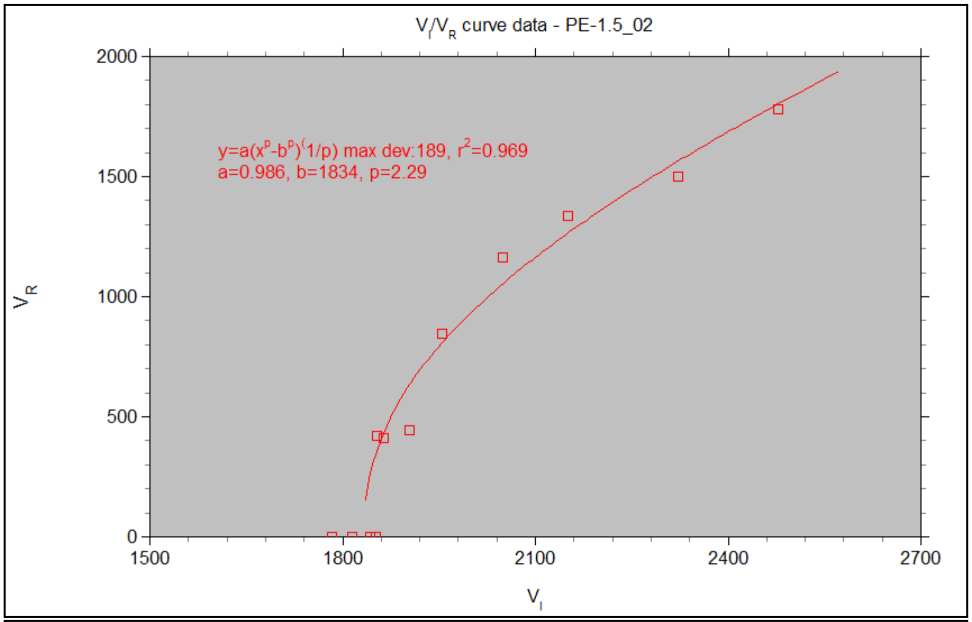
V$_I$/V$_R$ curve data - PE-1.5_02
y=a(x^p-b^p)^(1/p) max dev:189, r^2=0.969
a=0.986, b=1834, p=2.29
V$_R$
V$_I$
2000
1500
1000
500
0
1500
1800
2100
2400
2700

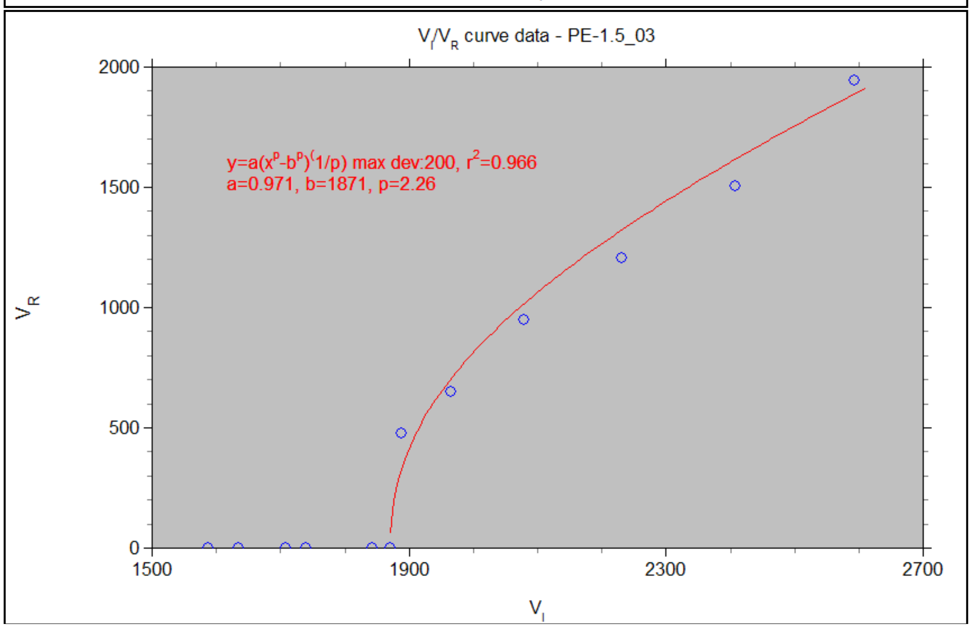
V$_I$/V$_R$ curve data - PE-1.5_03
y=a(x^p-b^p)^(1/p) max dev:200, r^2=0.966
a=0.971, b=1871, p=2.26
V$_R$
V$_I$
2000
1500
1000
500
0
1500
1900
2300
2700

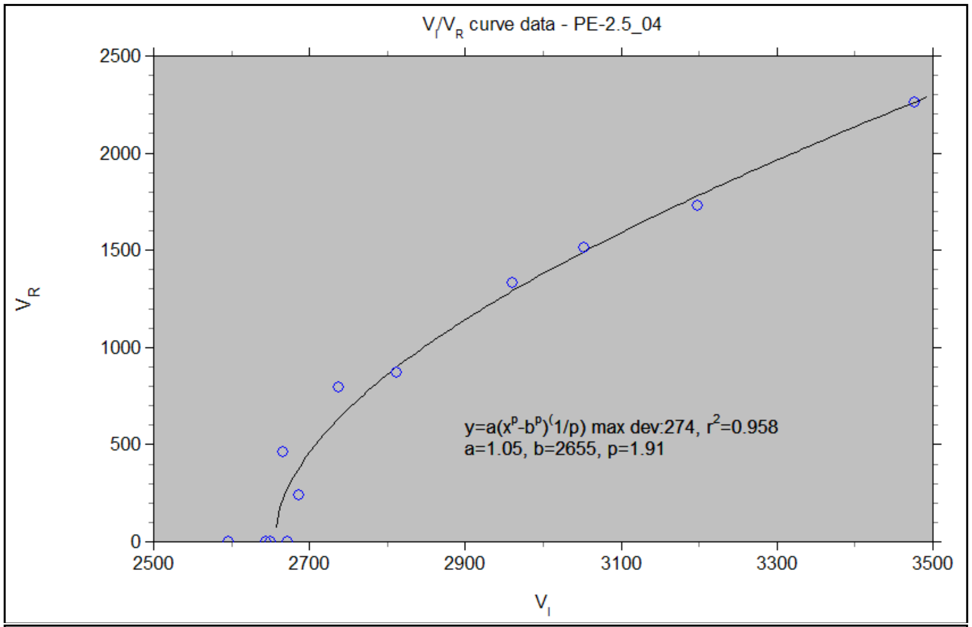
V_I/V_R curve data - PE-2.5_04
y=a(x^p-b^p)^(1/p) max dev:274, r^2=0.958
a=1.05, b=2655, p=1.91
2500
2000
1500
1000
500
0
2500
2700
2900
3100
3300
3500
V_R
V_I

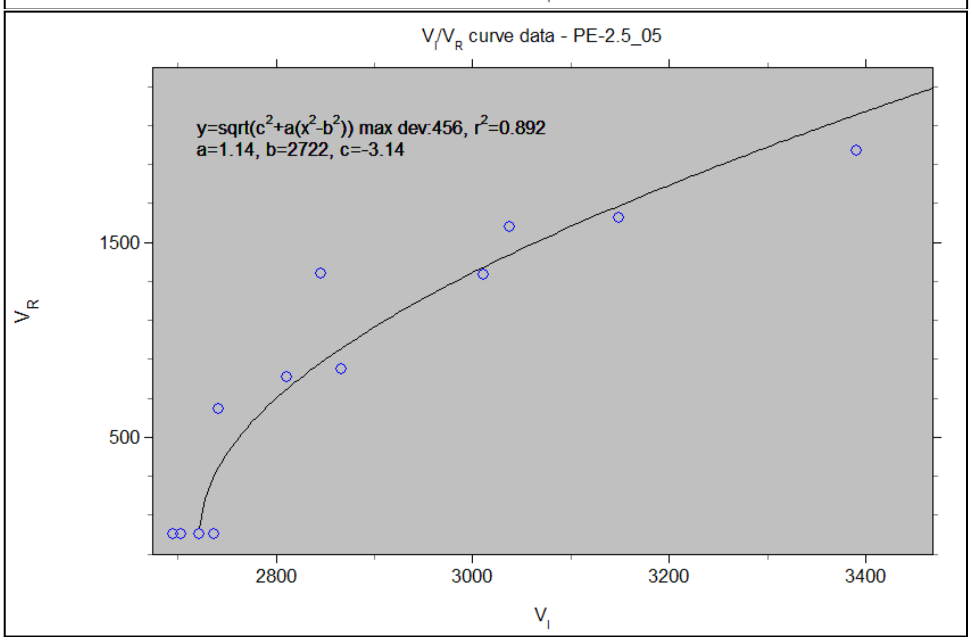
V_I/V_R curve data - PE-2.5_05
y=sqrt(c^2+a(x^2-b^2)) max dev:456, r^2=0.892
a=1.14, b=2722, c=-3.14
1500
500
2800
3000
3200
3400
V_R
V_I

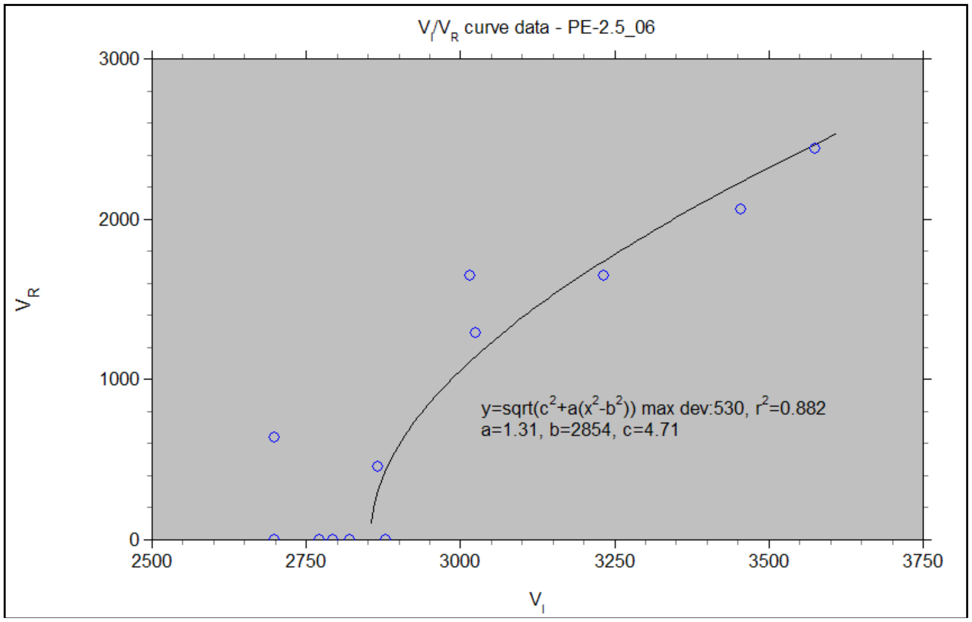

Process for curve fitting using Easy Plot:

After the V_I and V_R data has been collected, this process was used to find a best fit curve for to calculate the V_{50} for that test.

1. Take the values that have positive number for the residual velocity (do not include the values that have a $V_R = 0$) put them in excel and square them
2. Take this new data set and plot the values in another plot
3. Double click on a point and click on "curve fit"
4. Choose a linear equation and click "OK"
5. Take the square root of the first number in the equation, this will later be used as the initial guess for "a"
6. Take the second number in the equation and divide it by the first number, then take the square root of that value, this will later be used as the initial guess for "b"
7. Now plot the actual results from the V50 test
8. Zoom in so that only the values with residual velocities are visible
9. Double click on the data you want to fit a curve to
10. Click on the "curve fit" button
11. Input either of the equations
    a. y=sqrt(c^2+a(x^2-b^2)) (Gama & Gillespie)
    b. y=a(x^p-b^p)^(1/p) (Lambert)
12. Click "OK"

13. Input the initial guess for “a” and “b” you calculated previously
14. “p” or “c”
    a. Initial guess p=2
    b. Initial guess c=50
15. The resulting curve should fit the data
    a. The equation will also be plotted
16. If the curve does not fit, try using the other equation

    By re-fitting the curve using the newly found “b”, a simpler equation can be found. This process can be done a number of times to reach the simplest answer.

Full list of probability of penetration charts:

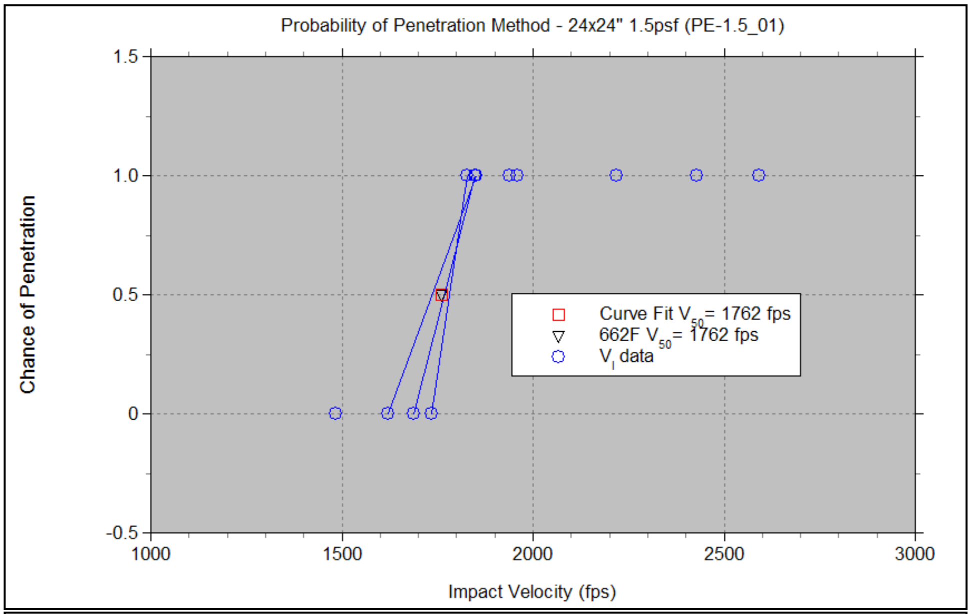

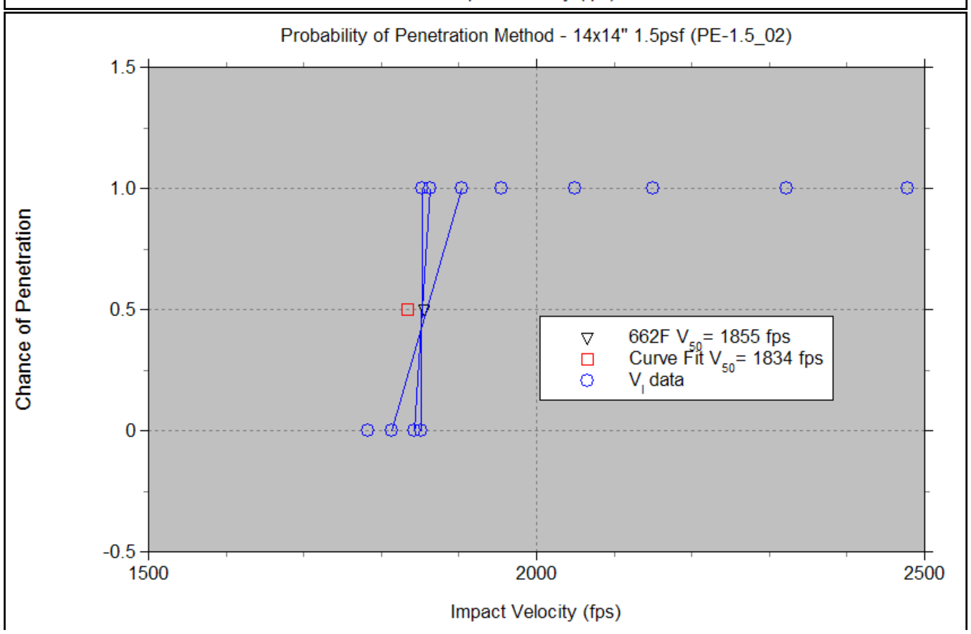

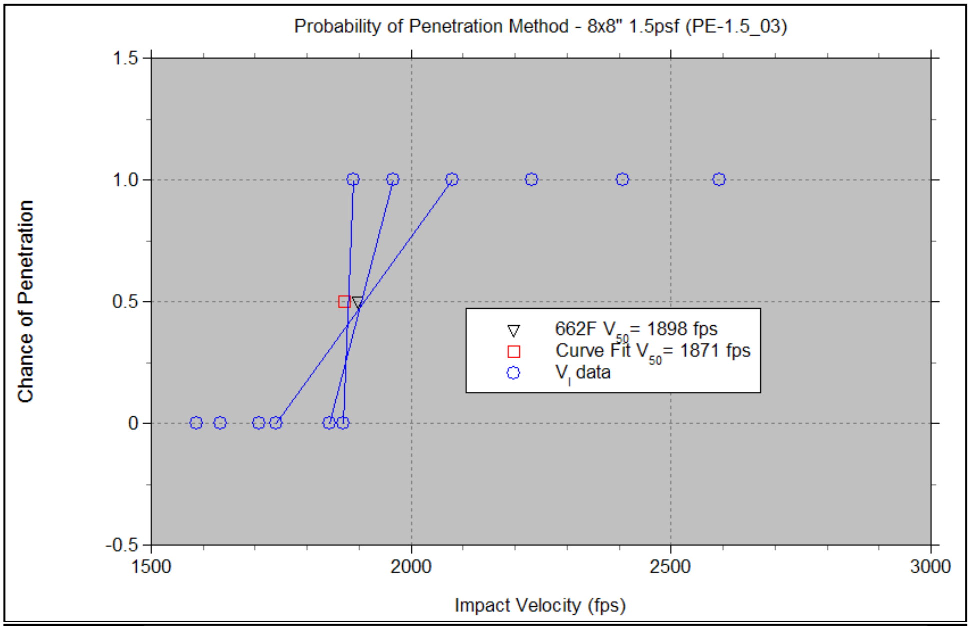
Probability of Penetration Method - 8x8" 1.5psf (PE-1.5_03)
Chance of Penetration
Impact Velocity (fps)
662F V_{50}= 1898 fps
Curve Fit V_{50}= 1871 fps
V_i data
1.5
1.0
0.5
0
-0.5
1500
2000
2500
3000

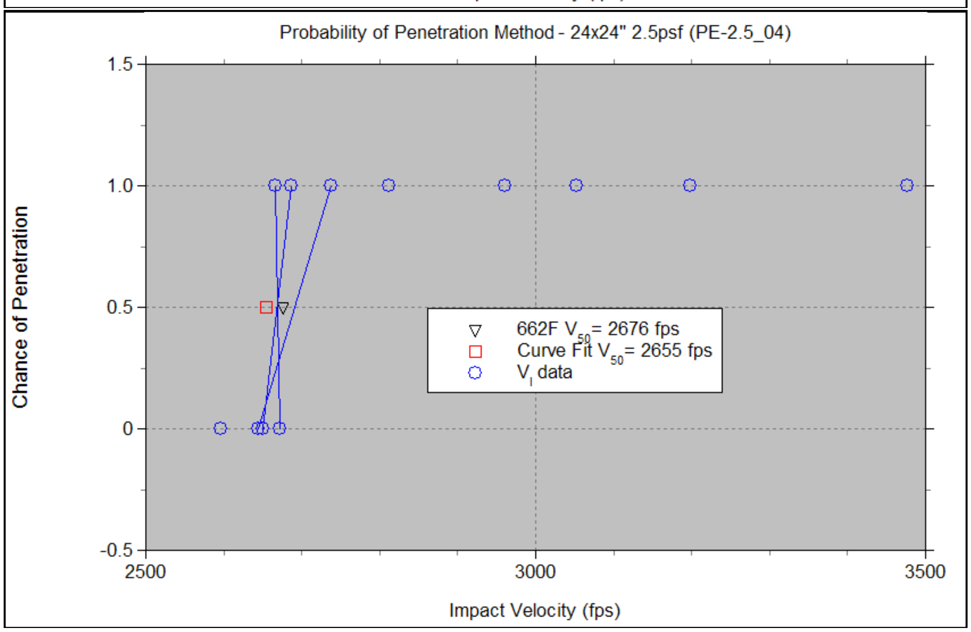
Probability of Penetration Method - 24x24" 2.5psf (PE-2.5_04)
Chance of Penetration
Impact Velocity (fps)
662F V_{50}= 2676 fps
Curve Fit V_{50}= 2655 fps
V_i data
1.5
1.0
0.5
0
-0.5
2500
3000
3500

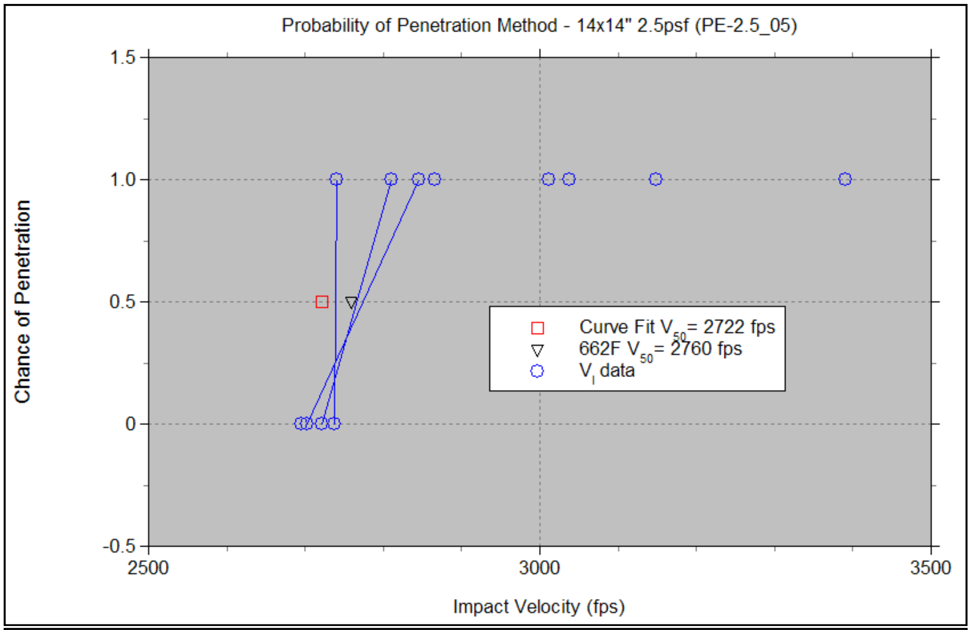

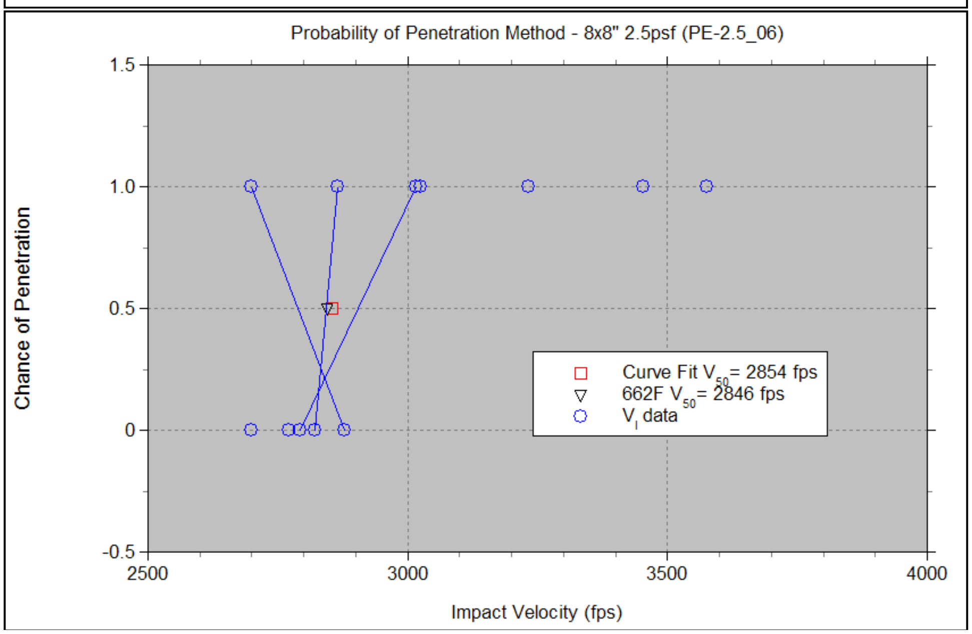

2.5 psf damage area vs. VI/V50 charts:

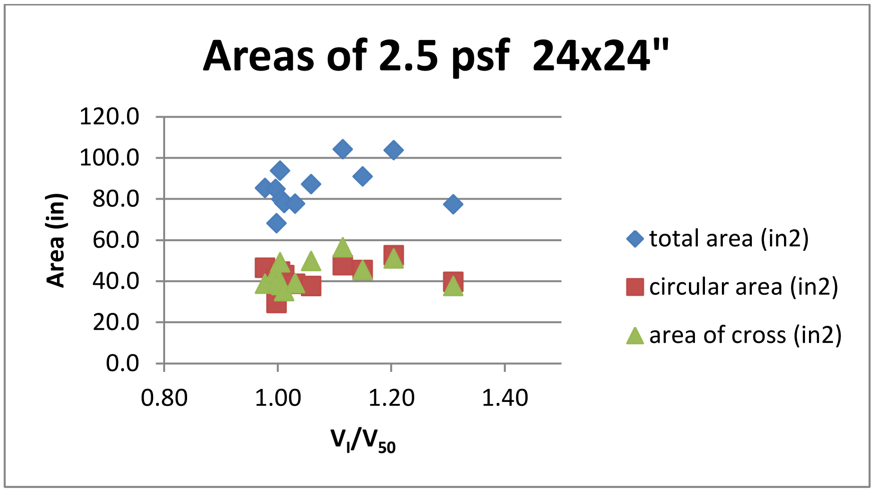
Areas of 2.5 psf 24x24"
120.0
100.0
80.0
60.0
40.0
20.0
0.0
Area (in)
0.80
1.00
1.20
1.40
V_l/V_{50}
total area (in2)
circular area (in2)
area of cross (in2)

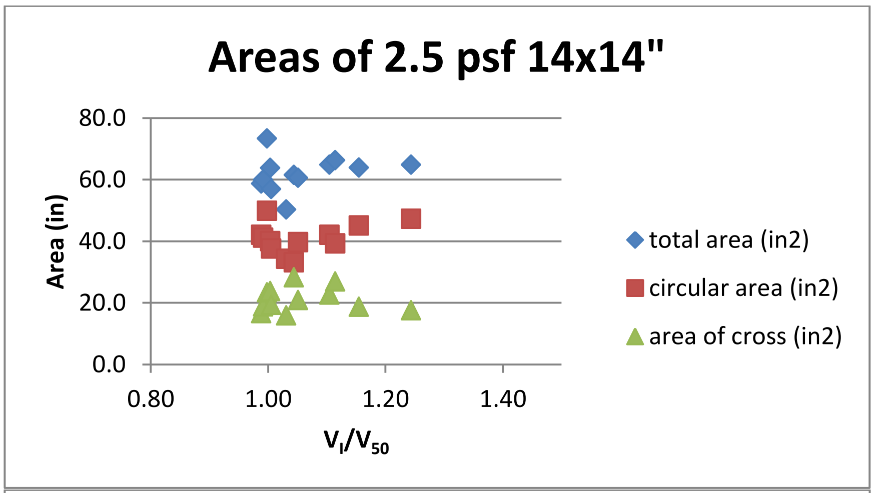
Areas of 2.5 psf 14x14"
80.0
60.0
40.0
20.0
0.0
Area (in)
0.80
1.00
1.20
1.40
V_l/V_{50}
total area (in2)
circular area (in2)
area of cross (in2)

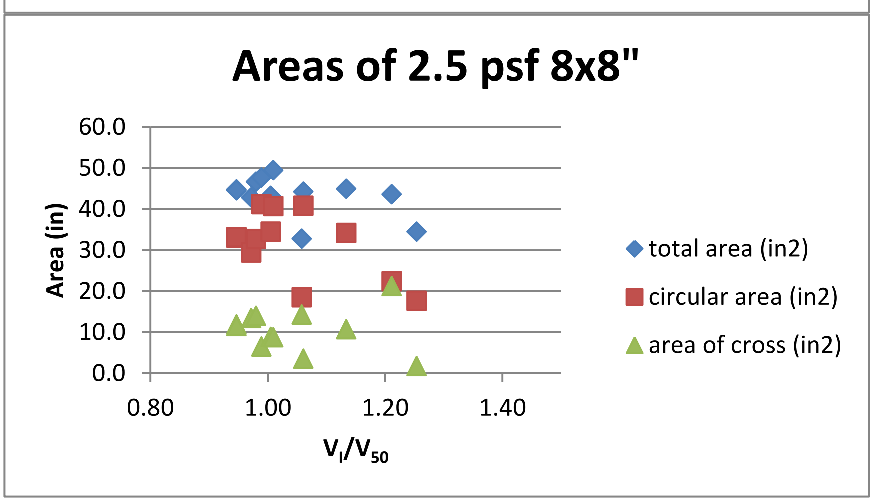
Areas of 2.5 psf 8x8"
60.0
50.0
40.0
30.0
20.0
10.0
0.0
Area (in)
0.80
1.00
1.20
1.40
V_l/V_{50}
total area (in2)
circular area (in2)
area of cross (in2)

2.5 psf damage widths vs. VI/V50 charts: